

STUDY OF ALUMINA IN AUSTENITIC STAINLESS STEELS

A Thesis

by

CHUNG JUIWANG

Submitted to the Office of Graduate and Professional Studies of
Texas A&M University
in partial fulfillment of the requirements for the degree of

MASTER OF SCIENCE

Chair of Committee,	Raymundo Arroyave
Co-Chair of Committee,	Ibrahim Karaman
Committee Member,	Miladin Radovic
Head of Department,	Ibrahim Karaman

December 2014

Major Subject: Materials Science and Engineering

Copyright 2014 Chung Jui Wang

ABSTRACT

The purpose of this work is to optimize the chemical composition as well as heat treatment for the creation and improvement of the mechanical performance in alumina forming austenitic stainless steel. Alumina forming austenitic stainless steel consists of a typical microstructure of austenitic stainless steels, austenitic matrix, with a key exception of an alumina oxide formation on the outer most layer of the alloy.

The contribution of aluminum for oxidation resistance is similar to that of chromium; while in a corrosive environment both form a stable oxide layer to prevent critical loss of mass of the parent material. However, alumina scales have a much higher thermodynamic stability in addition to the orders of magnitude slower in growth rate when compare to chromia scales.

Austenite contributes directly to twinning and the mechanical performance of the alloy due to its transformation to martensite under external stress. In order to stabilize austenite against martensitic transformation through temperature, as opposed to mechanical stresses, the martensite start temperature is calculated through the Ishida model.

The addition of aluminum to an austenitic stainless steel composition can alloy for the growth of alumina oxide; however it also promotes a BCC microstructure and too much aluminum addition allows for the destabilization of the austenitic FCC matrix. In order to create an acceptable balance for alumina forming austenitic stainless steel, thermodynamic and kinetic models are used to predict properties of the steel alloy.

In this work, a theoretical approach is coupled to a Genetic Algorithm based optimization procedure to design and find the optimal chemical composition for an alloy to form the superior alumina oxide while maintaining the properties of austenitic steel. In particular, the effective valence and third element phenomena is used in conjunction in order to accurately map out possible trends and predict alloy oxide behavior. The findings from such a model supports the major conclusion that the combination of third element phenomena, oxide transport properties, material thermodynamics and kinetics can be used to provide accurate insight on the formation of alumina for austenitic stainless steel.

NOMENCLATURE

USC	Ultra-Supercritical Combustion
SS	Stainless Steel
HTUPS	High-Temperature Ultrafine-Precipitation-Strengthened Steel
ORNL	Oak Ridge National Laboratory
AFA	Alumina-Forming Austenitic
BCC	Body-Centered Cubic
FCC	Face-Centered Cubic
GA	Genetic Algorithm
CALPHAD	Calculation of Phase Diagrams

TABLE OF CONTENTS

	Page
ABSTRACT	ii
NOMENCLATURE	iv
TABLE OF CONTENTS	v
LIST OF FIGURES	vii
LIST OF TABLES	x
CHAPTER I INTRODUCTION	1
CHAPTER II LITERATURE REVIEW	4
Chemical Composition of Alumina Forming Austenitic Steel	5
Alloy Modeling and Prediction	10
Genetic Algorithms	15
CHAPTER III ALUMINA OXIDE	16
Typical Alumina Oxide Forming Alloy Systems	16
Formation and Transport Properties of Alumina Oxides	17
Influence of Reactive Elements and Alumina Oxide Growth	19
CHAPTER IV METHODS FOR ALLOY OXIDE MODELING AND PREDICTION	20
Thermodynamic Model	20
Kinetic Model	21
Sato's Contour Model	21
Third Element Phenomena Model	23
CHAPTER V EFFECTIVE VALENCE MODELING	28
Modeling of Effective Valence	28
CHAPTER VI THIRD ELEMENT MODELING	37
Modeling of Third Element Phenomena	38

CHAPTER VII GENETIC ALGORITHM	64
Using GA for Optimization.....	64
Discovery Process for Alumina Forming Austenitic Steels through GA.....	71
Proposed Alloy Optimization by GA	74
CHAPTER VIII SUMMARY	79
REFERENCES	80
APPENDIX	84

LIST OF FIGURES

	Page
Figure 1 Thermodynamic Stability of Aluminum, Chromium, Iron, and Nickel Oxide [7]	2
Figure 2 Recession Map of Chromia and Alumina Volatility in High-Temperature Water Vapor [4]	4
Figure 3 Contour Phase Fraction of FCC for SS-316 with Variable Temperature and Chromium Content	6
Figure 4 Contour Phase Fraction of FCC for SS-316 with Variable Temperature and Nickel Content	7
Figure 5 Contour Phase Fraction of FCC for SS-316 with Variable Temperature and Manganese Content	8
Figure 6 Contour Phase Fraction of FCC for SS-316 with Variable Temperature and Silicon Content	9
Figure 7 Multi-Dimensional Plot with Alumina Oxide Trend	12
Figure 8 Transition to Mixed Stable Layer and Stable Alumina Layer [26-29, 34]	14
Figure 9 Progression of Oxidation for Typical Fe-Al-Cr17	
Figure 10 Crystalline α -Al ₂ O ₃ with Six Coordinated Aluminum Atoms [20, 46, 47]	18
Figure 11 Growth of Alumina Layer through Aluminum and Oxygen Diffusion	19
Figure 12 Interpretive Visualization of the Third Element Graph	26
Figure 13 Free Energies of Sample Alloys with Respect to Temperature	29
Figure 14 Effective Valences of Sample Alloys with Respect to Temperature	30
Figure 15 Combining Effective Valence with Free Energy for K Value	31
Figure 16 Free Energy, Effective Valence and K Value of Experimental Alloys	32

Figure 17	K Value Alumina Formation through Element Control.....	34
Figure 18	Hybrid Alloy Designing Process.....	38
Figure 19	Third Element Effect of AFA Alloy 1 *Forms Stable Oxide Layer [64].....	39
Figure 20	Third Element Effect of AFA Alloy 2 *Forms Unstable Oxide Layer [64].....	40
Figure 21	Third Element Effect of AFA Alloy 3 *Forms Stable Oxide Layer [64].....	41
Figure 22	Third Element Effect of AFA Alloy 4 *Forms Stable Oxide Layer [64].....	43
Figure 23	Third Element Effect of AFA Alloy 5 *Forms Stable Oxide Layer [64].....	44
Figure 24	Third Element Effect of AFA Alloy 6 *Forms Unstable Oxide Layer [64].....	45
Figure 25	Third Element Effect of AFA Alloy 7 *Forms Stable Oxide Layer [64].....	47
Figure 26	Third Element Effect of AFA Alloy 8 *Forms Unstable Oxide Layer [64].....	48
Figure 27	Third Element Effect of AFA Alloy 9 *Forms Unstable Oxide Layer [64].....	49
Figure 28	Third Element Effect of AFA Alloy 10 *Forms Unstable Oxide Layer [64].....	50
Figure 29	Third Element Effect of AFA Alloy 11 *Forms Unstable Oxide Layer [64].....	51
Figure 30	Third Element Effect of AFA Alloy 12 *Forms Unstable Oxide Layer [64].....	52
Figure 31	Third Element Effect of AFA Alloy 13 *Forms Stable Oxide Layer [64]	53
Figure 32	Third Element Effect of AFA Alloy 14 *Forms Stable Oxide Layer [64]	54
Figure 33	Third Element Effect of AFA Base *Forms Stable Oxide Layer [8].....	55
Figure 34	Third Element Effect of Alloy 880-4 *Forms Unstable Oxide Layer [8].....	57

Figure 35	Third Element Effect of 1.5 Al Trip As *Forms Unstable Oxide Layer [8]	58
Figure 36	Third Element Effect of HTUPS 2 *Forms Unstable Oxide Layer [6, 15]....	59
Figure 37	Third Element Effect of HTUPS 3 *Forms Unstable Oxide Layer [6, 15]....	60
Figure 38	Third Element Effect of HTUPS 4 *Forms Stable Oxide Layer [6, 15]	61
Figure 39	Normalized Compiled K and Third Element Value for Experimental Alloys	63
Figure 40	Alloy Design Process Schematic.....	64
Figure 41	Encoding Genetic Traits of an Alloy into GA Simulation	66
Figure 42	Schematic Diagram of (a) Cross-Over and (b) Mutation	68
Figure 43	Schematic Diagram of Genetic Algorithm	70
Figure 44	Genetic Algorithm Alloy Design Path	73
Figure 45	Free Energy, Effective Valence and K Value of Experimental Alloys	76
Figure 46	Third Element Effect of PGAA1	77
Figure 47	Third Element Effect of PGAA 2.....	78

LIST OF TABLES

	Page
Table 1 Domain in GA Search for Element Optimization	74
Table 2 Optimized Genetic Algorithm Alloys Proposed by GA.....	75
Table 3 Experimental Alumina Forming Alloys	84
Table 4 Proposed GA Alloy List.....	85

CHAPTER I

INTRODUCTION

As the motivation of increasing cost efficiency for power plants is continued to be investigated, modern technological advancements have allowed the development of ultra-supercritical combustion, USC, high-efficiency coal-fired power plant as a viable option. The advanced USC coal-fired power plants is designed to increase the efficiency of current generation plants, from 35% to 50%, while mitigating the potential environmental impacts of societal consumption. [1, 2] With the increase of efficiency, a notable cost of higher operating pressure and temperature is also observed. This presents a rather significant materials challenge to handle the increased required operating parameters. In particular, it becomes much more difficult for conventional stainless steels to handle the oxidation from a corrosive environment at higher than the norm pressure and temperature.

Stainless steels are a family of metal alloys that are used when corrosion or oxidation may be a problem. This critical niche filled by stainless steels is extremely hard to be replaced by any other materials with their extremely low cost. The typical definition of a stainless steel is a ferrous alloy that contains a minimum of 12% chromium for the excellent corrosion and oxidation properties that is imparted. The formation of a stable, passivating chromium oxide layer insulates the bulk alloy from oxidation and other damaging reactions from the environment. [3, 4] Current austenitic stainless steel standards are typically the nonmagnetic 300 series, such as the SS-316. These steels are mainly composed of iron, nickel, and chromium; of which are less effective in aggressive

high temperature oxidizing environments of around 600-900C. [3, 5, 6] As a potential alternative for handling this new problem alumina oxide scales are examined.

The contribution of aluminum for oxidation resistance is similar to that of chromium; while in a corrosive environment both form a stable oxide layer to prevent critical loss of mass of the parent material. However, alumina scales are two orders of magnitude slower in growth rate than that of chromia scales as well as having a lower free energy for more thermodynamic stability. These traits result in better performance at higher temperatures as well as having immunity to water vapor effects at the said temperatures. [5]

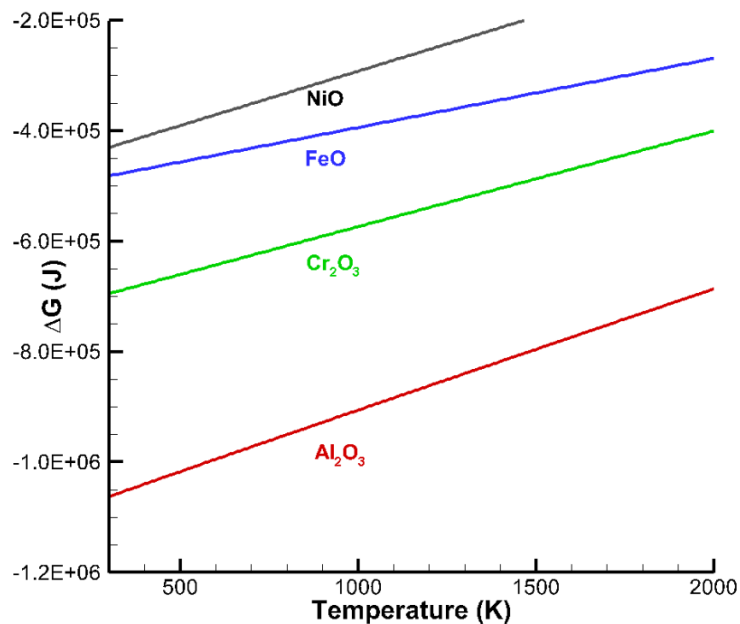


Figure 1 Thermodynamic Stability of Aluminum, Chromium, Iron, and Nickel Oxide [7]

Although the concept of replacing chromium with aluminum has been discussed many decades before, many previous experiments do not efficiently address the issue of creating a good balance between oxidation resistance and the alloy's mechanical properties. [5, 6, 8-17] To minimize the costs and efforts of addressing this issue this work examines multiple austenitic stainless steel alloys to find a visible trend and determine a minimum standard needed to be fulfilled to form an alumina oxide scale in austenitic steels.

CHAPTER II

LITERATURE REVIEW

Alumina scales provides unique oxidation properties because of its slower growth rate a lower free energy for a more thermodynamically stable oxide scale, Figure 1. Previous research has indicated that, in addition to stable oxide layer growth, alumina scales are extremely wear resistant and stable in water vapor at high temperatures. [3, 4, 18-20] The traditional oxide layer of chromia performs poorly in atmospheres containing water vapor due to the formation of volatile hydroxide species which remove the surface oxide. The alumina system, unlike the chromia system, is much less sensitive to recession by volatility at high temperatures below 1200C, as seen in Figure 2.[4]

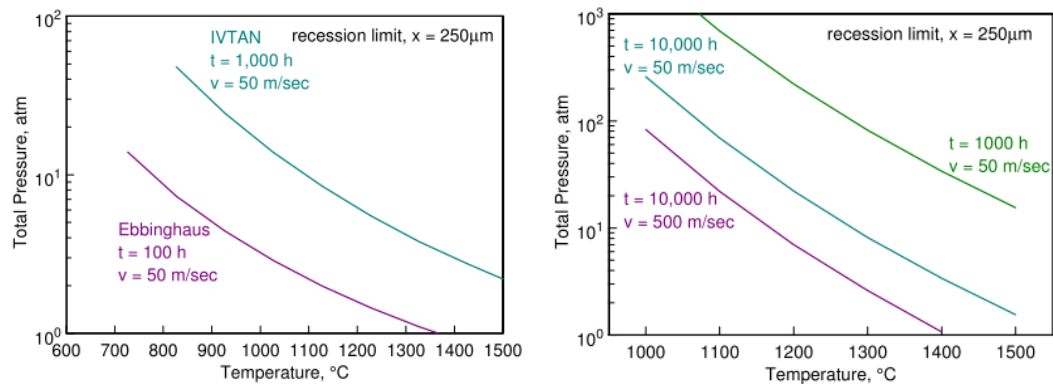


Figure 2 Recession Map of Chromia and Alumina Volatility in High-Temperature Water Vapor [4]

In order to form a stable, continuous alumina layer for oxidation resistance, the control on diffusion of aluminum, chromium, and oxygen is important. There are many different alloys that have been developed through the trial and error of altering each element in the alloy composition for the formation of a usable oxide layer. An example of the broadly investigated alumina stainless steel can be seen by the Oak-Ridge National Laboratory's alumina-forming austenitic stainless steels. [8, 11] The Oak Ridge National Laboratory Alumina-Forming Austenitic, ORNL-AFA, alloy studies uses a standard base composition of Fe-Ni-Cr-Al-Si-Mn-Mo-Nb-C-B and multiple single element modification to the base alloy for a thorough study of the intricate dynamics for alumina formation and oxidation resistance between each particular element.

Chemical Composition of Alumina Forming Austenitic Steel

The conventional austenitic stainless steel usually contains the base chemical composition of: Fe-(18)Cr-(10)Ni-(0.75)Si-(2)Mn-(0.08)C (wt%); however, for alumina formation, the proposed chemical composition becomes: Fe-(12-15)Cr-(20-30)Ni-(2.5-4)Al-(1-3)Nb (wt%). [5, 6, 8-17]. A key factor for alumina forming austenitic steel is achieving alumina formation while having the balance of Al, Cr, and Ni levels to maintain a single phase FCC austenitic alloy matrix structure from the composition. [13-15] Typical alloying levels of aluminum and chromium for stainless steel applications are around (4-6)Al and (10-25)Cr (wt%). A few of major element values in conventional stainless steel that can destabilize the parent austenitic matrix structure can be seen in Figure 3, Figure 4, Figure 5, and Figure 6.

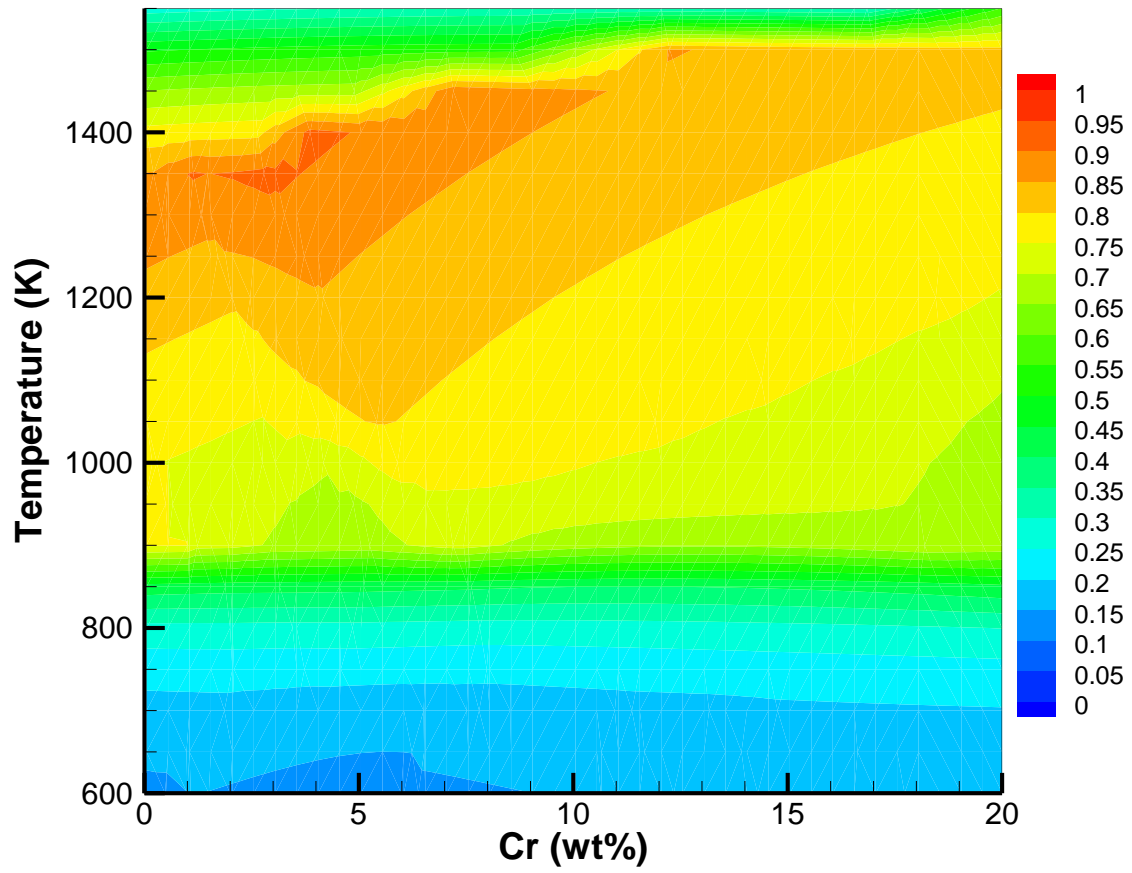


Figure 3 Contour Phase Fraction of FCC for SS-316 with Variable Temperature and Chromium Content

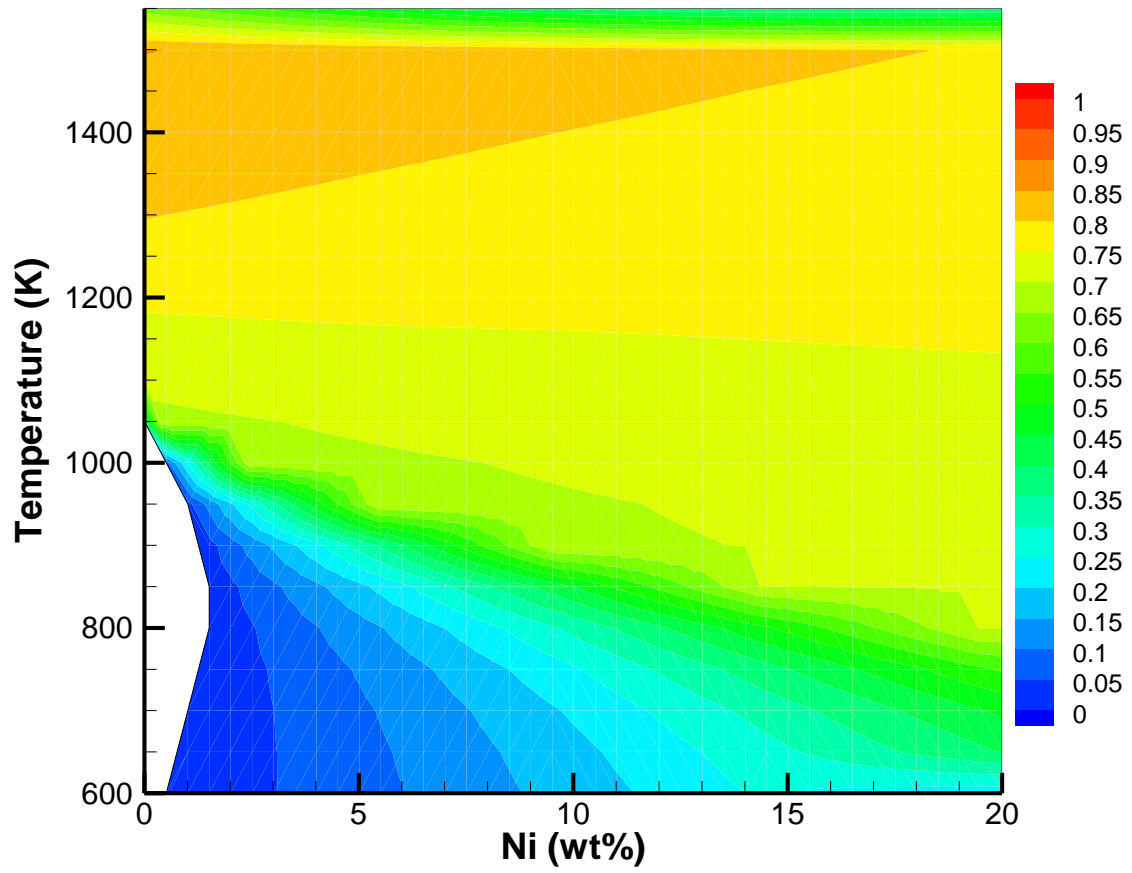


Figure 4 Contour Phase Fraction of FCC for SS-316 with Variable Temperature and Nickel Content

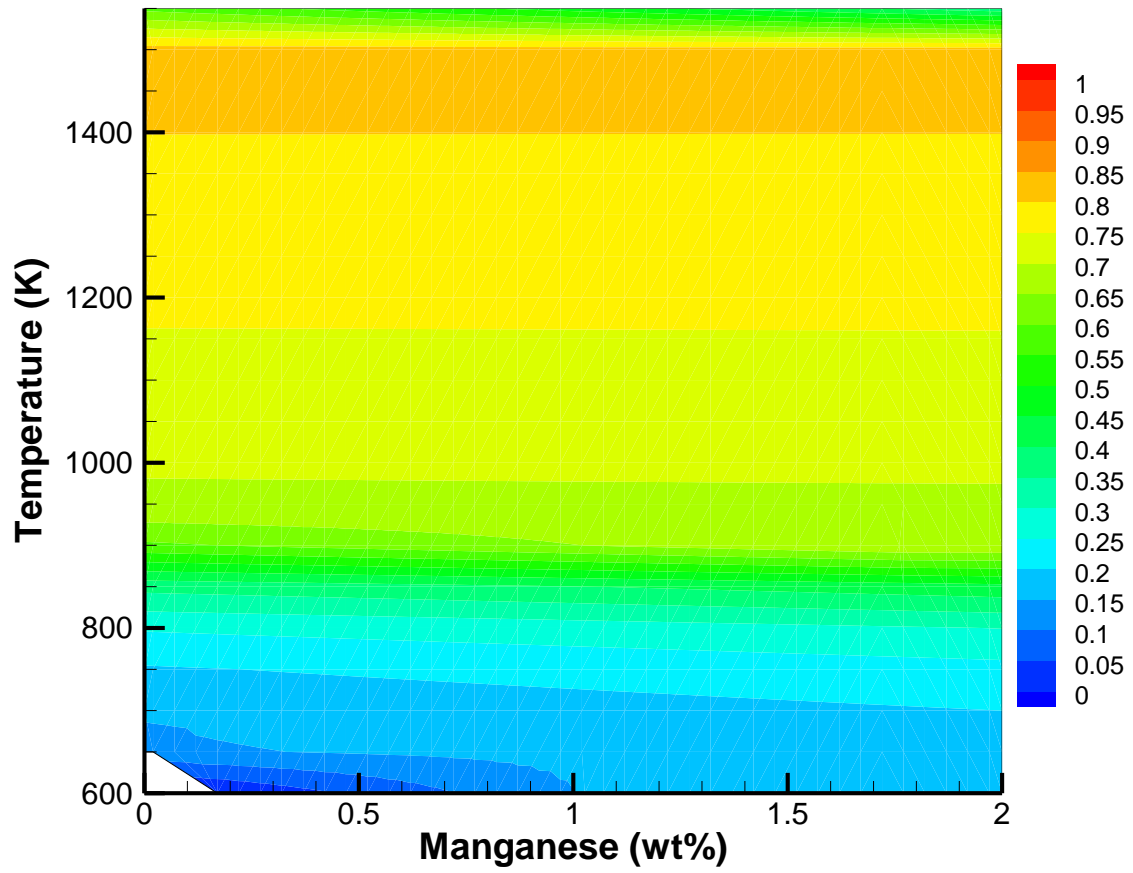


Figure 5 Contour Phase Fraction of FCC for SS-316 with Variable Temperature and Manganese Content

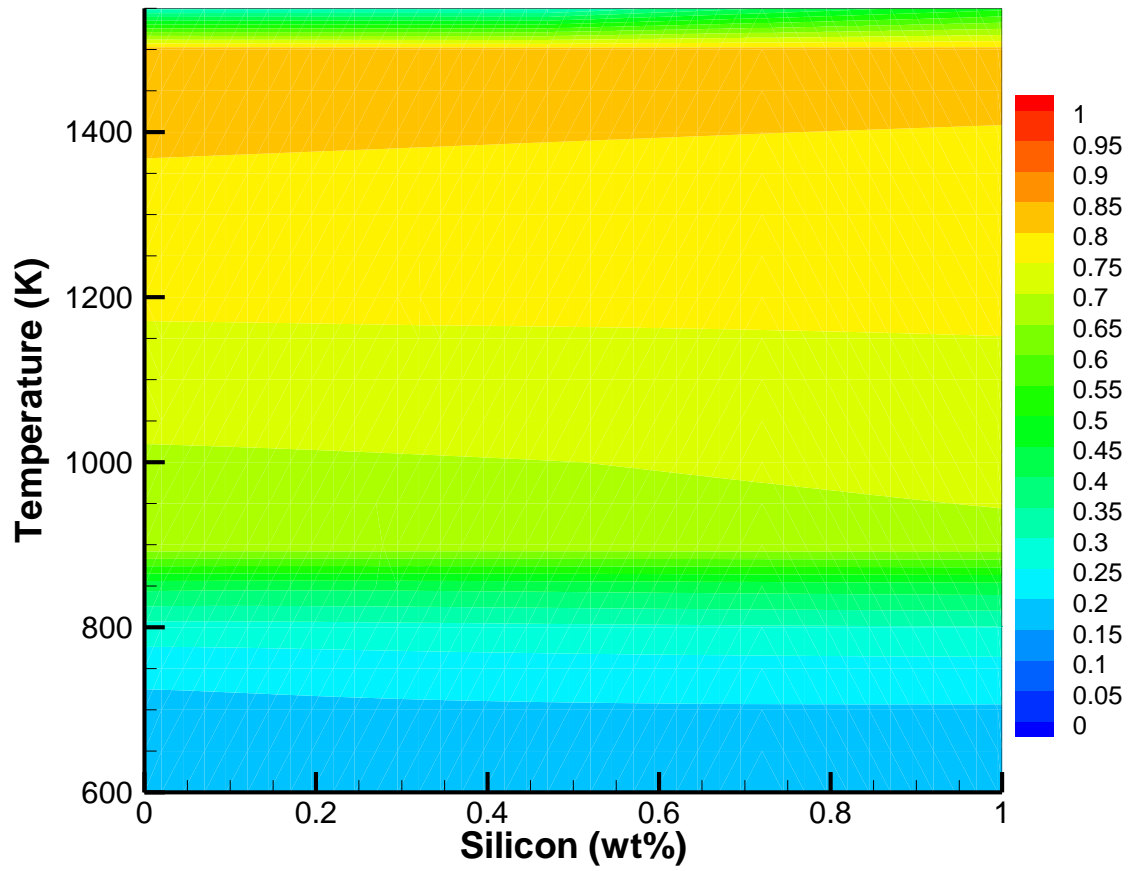


Figure 6 Contour Phase Fraction of FCC for SS-316 with Variable Temperature and Silicon Content

As it can be seen in the figures above, the stability of FCC austenite can be easily influenced by relatively small changes to the alloy composition or temperature. To prevent destabilization of the austenitic matrix in alumina forming steels, many previously proposed alloys have an extremely high nickel content of ~20 (wt%) to offset the increased BCC forming elements; however, the proposed cost advantage would suffer for the large increase of nickel needed. [5, 6, 8-17] Additional minor elements typical to austenitic stainless steel, such as SS-316, to be considered in the formation of a FCC matrix are molybdenum and silicon. Molybdenum promotes ferrite formation and retention while silicon is a ferrite stabilizer. [21] Another key factor for alumina forming austenitic steel is the interaction of aluminum and alumina oxide with other environmental and alloying elements. One such example is seen in the High-Temperature Ultrafine-Precipitation-Strengthened Steel, HTUPS, alloys in which multiple alloys with nearly identical compositions were tested. [6, 15] An interesting point from the outcome of the experiment is that the conditions for alumina scale formation was found to be extremely sensitive to titanium; being unable to develop on virtually identical alloys with the sole exception of titanium and vanadium. The proposed hypothesis for such the phenomena was that the addition of titanium and vanadium may be expected to promote internal oxidation due to increased oxygen permeability. [15]

Alloy Modeling and Prediction

Although thermodynamics are necessary to predict whether an oxide surface is feasible, it is not the only factor to be considered. In addition to the thermodynamic Gibbs free energy of formation, ΔG , the kinetics of alumina scale formation should also be taken

into account. According to the Wagner-Hauffle theory, when the valence of an impurity ion is greater than that of the parent cation Al^{3+} in the oxide, the formation of alumina oxide is decelerated; however, when the valence is lower the dominant defect concentration increases and the rate of alumina oxide formation is increased, allowing for a more stable oxide formation. [22] Therefore it is necessary to determine the transport properties of the alumina oxide. [23]

From previous experimental results and analysis applied, it is determined that alumina oxide is an n-type conductor orders of magnitude more stable than either iron or chromium oxide. [5] With the transport properties defined for alumina oxide, and the assumption of that there is sufficient flux of aluminum at the metal-scale interface, it was reported that the migration of oxygen through the alumina scale is rate-controlling. [24] Consequently, the total effective valence was then found and utilized to construct an illustration of the oxidation diagram concept where the alumina scale oxidation trend could be clearly defined in the multi-dimensional plot seen in Figure 7.[24]

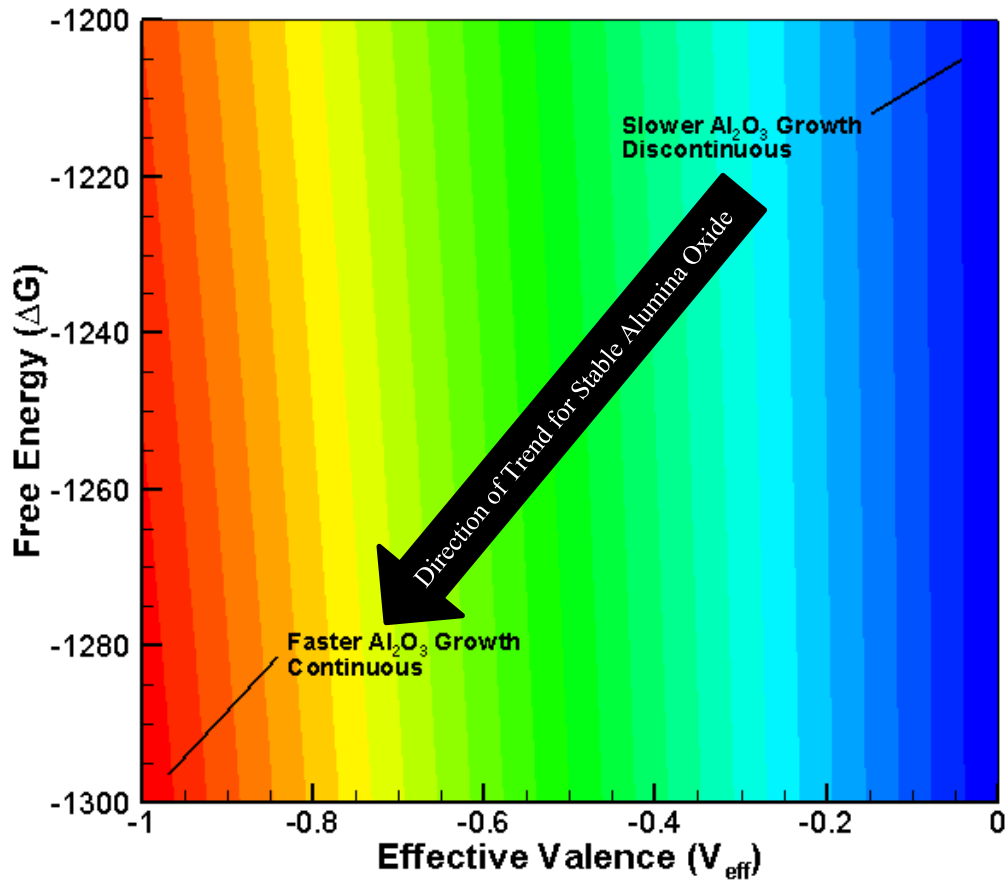


Figure 7 Multi-Dimensional Plot with Alumina Oxide Trend

As previously mentioned, the matrix of the alloy must be FCC; however, aluminum destabilizes austenite and is considered a ferrite promoter. [3, 4, 18-20, 22] As such, it becomes necessary to minimize the aluminum content for alumina scale formation in order to preserve the equilibrium for austenite retention. Therefore, another consideration of considerable practical importance is element optimization which will be done through the third element effect of alumina formation, by which the presence of a

third element with a reactivity intermediate to the components of the given binary alloy can decrease the content of the more reactive element needed to form its external oxide scale. In ternary alloy systems, it can be seen that the required aluminum for stable alumina oxide formation can be directly influenced through chromium content. [3, 25-31] It is reported that the addition of Cr in binary Fe–Al alloys has been shown to reduce the minimum required aluminum. [32, 33] In other words, the addition of B to an A–B–C alloy can reduce the critical C concentration to establish an external scale of the C oxide; where A is the most noble, C is the most reactive component, and B has an oxygen affinity intermediate between those of A and C. [32] It is suggested that the element B in the ternary alloy system acts as an oxygen getter, or third element, during the initial stage of oxidation; limiting oxygen diffusion into the alloy so that internal oxidation of C is minimized. [22] This type of process in the alloy system does not involve a prevention of the internal oxidation of aluminum but instead promotes the growth and transition of mixed iron and aluminum rich external scales directly into an external Al_2O_3 scale formation. [26-29, 34] A graphical view of this can be seen in Figure 8

Unstable Oxide Layer → Mixed Stable Layer → Stable Alumina Layer

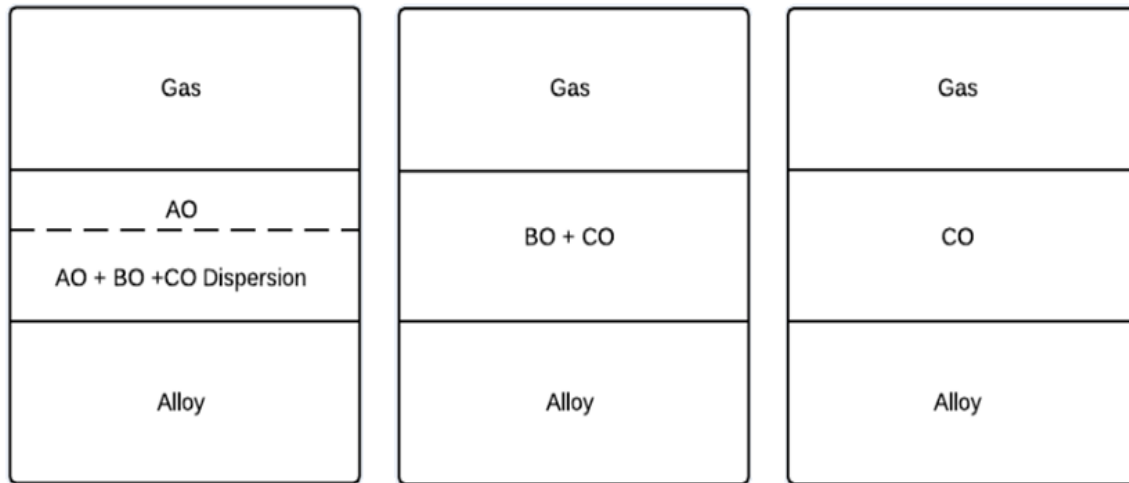


Figure 8 Transition to Mixed Stable Layer and Stable Alumina Layer [26-29, 34]

Genetic Algorithms

Even though the theoretical models can accurately predict oxide formation with a given composition set, the computational cost for alloy design using a guess and check design process is extremely high and impractical. Therefore computational algorithms are a necessity to streamline the overall alloy design process. In order to decrease the time and cost of discovery and refinement of new alloys Genetic Algorithms are a potential method to couple to the physical calculations.

The definition of Genetic Algorithm, GA, is a computer based system that imitates the theory of survival of the fittest leading to the natural selection of a superior species, Darwinism. [35, 36] This type of evolution based search concept for alloy design has been previously utilized in many various alloy design researches, including steel. [21, 37-40] General design through GA utilizes multiple variables and objectives where the GA program performs an efficient wild domain search.

CHAPTER III

ALUMINA OXIDE

There have been considerable amounts of research in the development of alumina oxide scales within metal alloy systems. [20, 41, 42] In this paper, the mechanisms for the development of protective alumina oxide scales are discussed.

Typical Alumina Oxide Forming Alloy Systems

Regarding binary Fe-Al alloys one of the crucial elements for high temperature oxidation resistance is the dependence on the growth of a protective oxide; for a good protective layer, the oxide layer should be stable, continuous, and have a slow growth rate. [20] The importance of a slow growth rate is primarily because it governs the transport process of oxidation, determining the rate of oxidation as well as the penetration of aggressive species. Another critical factor with alumina formation is having sufficient aluminum content to develop and maintain an alumina layer to prevent subsequent breakaway oxidation. [20] However, the increase of aluminum content may severely decrease the alloy ductility and other mechanical properties. It is also necessary for the formation of alumina oxide to be $\alpha\text{-Al}_2\text{O}_3$ rather than the metastable $\gamma\text{-Al}_2\text{O}_3$. A common solution to increasing aluminum is the addition of chromium to M-Al alloys; where the chromium acts as a getter to prevent internal oxidation of aluminum and allow for stable formation of alumina oxide. [3, 20, 25-31] The addition of a third element, chromium, to the iron-aluminum system for favorable oxide formation is typically referred to as the third element effect. Although iron based binary alloys readily form $\alpha\text{-Al}_2\text{O}_3$ due to high rates

of inter-diffusion of aluminum and low oxygen solubility, the presence of chromium is also found to stabilize α - Al_2O_3 in preference to γ - Al_2O_3 . [20, 43, 44]

Formation and Transport Properties of Alumina Oxides

When oxidation occurs at high temperatures, transitional alumina may be observed during the initial formation of alumina oxide. The first phase to form is typically FeO and Cr_2O_3 . Although the FeO grows rapidly, Cr_2O_3 forms underneath as a stable, continuous layer. The next phase to form is the metastable Al_2O_3 , below the Cr_2O_3 layer. The metastable alumina oxide layer transforms into α - Al_2O_3 when it becomes incorporated into the external scale of the alloy. [20, 22] Figure 9 shows this typical oxidation progression for the Fe-Al-Cr system.

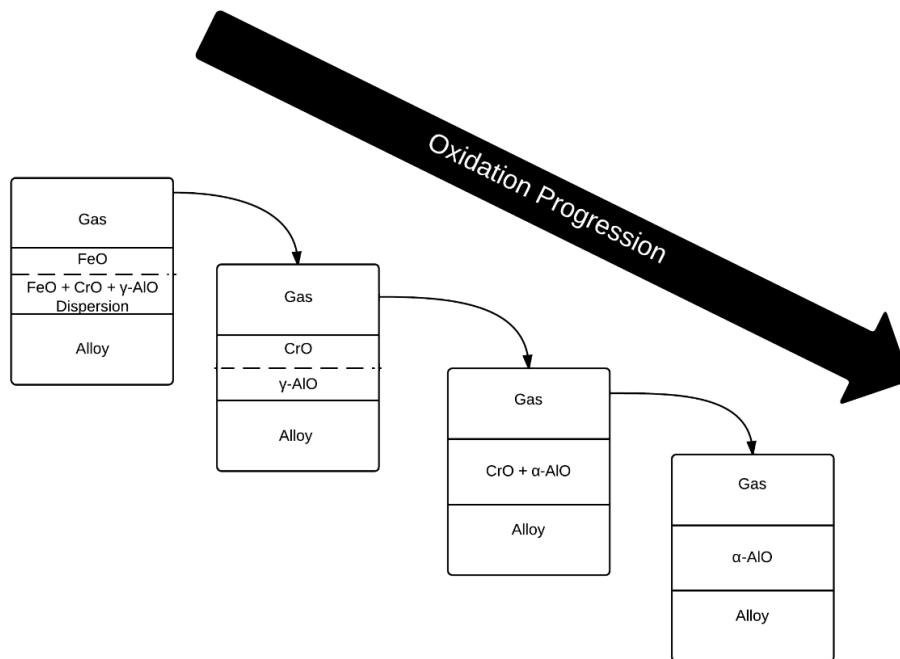


Figure 9 Progression of Oxidation for Typical Fe-Al-Cr

When a continuous film of oxide has formed on a metal surface, the metal and gaseous reactants can be considered two separated regions with a barrier in between. In order to continue reaction with the bulk alloy, cations, anions, and electrons must be able to diffuse through the oxide layer. In other words, the rate determining step for the oxidation reaction is determined by the properties of the oxide layer. [45] α - Al_2O_3 is the most stable form of alumina oxide at high temperatures. The crystal structure of α - Al_2O_3 , Figure 10, constitutes a hexagonally close packed oxygen ions and octahedral interstices filled by trivalent cations [20, 46, 47]

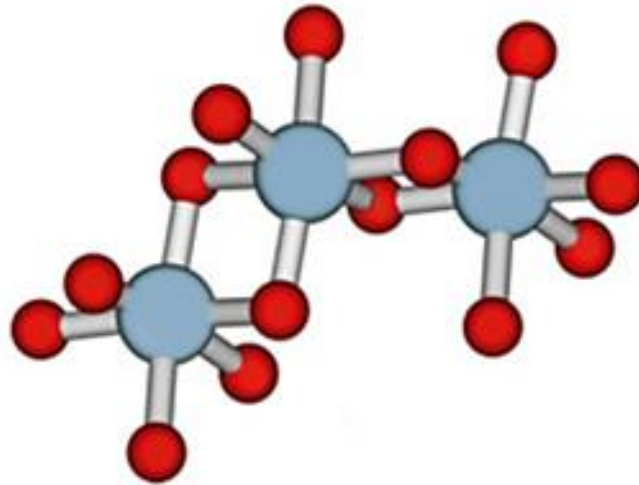


Figure 10 Crystalline α - Al_2O_3 with Six Coordinated Aluminum Atoms [20, 46, 47]

Influence of Reactive Elements and Alumina Oxide Growth

Reactive elements are often known to influence and dictate the early stages of alumina oxide growth. In the literature, there is general agreement that active elements influence the transport processes in Al_2O_3 scales. One of the main effects of active elements is the influence on increasing or decreasing either oxygen or aluminum diffusion, Figure 11. [48] Based on calculations of diffusion coefficients from parabolic rate constants, the alumina layer growth is controlled by grain boundary diffusion of aluminum and oxygen.[48, 49] Typically, low levels of active element decrease grain boundary diffusion of aluminum and high levels of active element increase grain boundary diffusion of oxygen.[50]

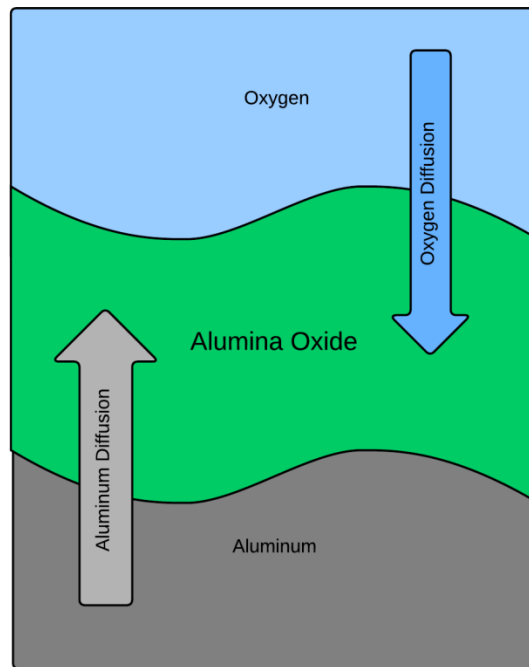


Figure 11 Growth of Alumina Layer through Aluminum and Oxygen Diffusion

CHAPTER IV

METHODS FOR ALLOY OXIDE MODELING AND PREDICTION

As mentioned, in order to map out the trends for alumina formation in austenitic stainless steel, multiple concepts and models are combined to predict alumina formation. In this chapter, the model discussed by Sato is applied to combine both thermodynamic and kinetic influences on the oxidation of an alloy.

Thermodynamic Model

CALPHAD, Calculation of Phase Diagrams, is the computer coupling of phase diagrams and thermochemistry and provides useful, consistent phase predictions. In the CALPHAD method, the total free energy for a binary system is expressed as

$$G = \sum_1^2 x_k G_k^{srf} - T \cdot S^{con} + G^E \quad (1)$$

where x is the mole fraction of the composition, G_k^{srf} is the free energy of the ideal mixture of the species, S^{con} is the configuration entropy for the possible arrangement of the species, and G^E is the excess Gibbs free energy which is from the results of non-ideal mixing of the solution. [51]

The study and creation of a thermodynamic model for the alloys in this work is done with the commercial program Thermocalc through its TQ Interface. The TQ Interface code is utilized in order to access the databases TCFE7 and MOBFE1 for the prediction and understanding of each phase in the alloys.

Kinetic Model

To form a stable oxide layer, there is a need for a balance between the diffusion of oxygen from the environment and the diffusion of the reactant from the bulk material in addition to the more apparent need for thermodynamic stability. To simulate the reaction of the alloy to corrosion, the diffusion of each element within the alloy needs to be known. According to Fick's first and second law, the species k diffusing in phase i can be described as

$$J_k^i = -D_k^i \frac{\partial w_k^i}{\partial x} \quad (2)$$

$$\frac{\partial w_k^i}{\partial t} = \frac{\partial}{\partial x} \left(D_k^i \frac{\partial w_k^i}{\partial x} \right) \quad (3)$$

where the diffusion coefficient D_k^i can be calculated by the driving force and the phenomenological parameter obtained from the TCFE7 and MOBFE1 database. [52, 53]

In this work, the commercial code Dictra is used in conjunction with the TCFE7, MOBFE1, and NIST database to accurately predict and model diffusion behavior. The kinetic model developed through Dictra is used concurrently with the thermodynamic created with Thermocalc's TQ Interface to generate precise and consistent data values for use in the oxide prediction models used in this work.

Sato's Contour Model

The oxidation phenomenological framework established by Wagner [22] can be explained by the diffusion of aluminum, chromium, and oxygen; all of which are influenced a number of ways as well. The fundamental equation governing the oxidation phenomena of an alloying element can be represented as



so that the thermodynamic equilibrium equation [54] can be used as follows

$$\Delta G = \Delta G^0 + RT \ln Q \quad (2)$$

where $\Delta G = 0$ and $Q = K$ so the equation can be combined and redefined into

$$\Delta G = RT \ln \frac{Q}{K} \quad (3)$$

where K and Q can be defined as

$$K = \exp\left(\frac{-\Delta G^0}{RT}\right) \quad (4)$$

and

$$Q = \frac{a_{Al_2O_3}}{[a_{Al}]^2 [a_o]^3} \quad (5)$$

where K represents the equilibrium constant and Q defines the reaction's quotient. Thus oxidation can be thermodynamically determined to take place if K is greater than Q .

While a thermodynamic model can be used to roughly determine if alumina formation is favorable, contributions from kinetic properties needs to be acknowledged as well. Using a combination of Wagner's theory and consideration for all factors known to influence alumina scale growth rate, Sato's contour model combines both thermodynamic and kinetic influence on the oxide formation. [22, 24] The model utilizes the basic equilibrium equation Eq. (2) and adds a kinetic equation

$$Val_t^{eff} = \sum_{n=i} (z_i - z_{al}) \bar{c}_i = \Delta e' \quad (6)$$

where Val_t^{eff} is the total effective valence of Al_2O_3 , z_i is the effective valence of the element i , \bar{c} indicates the atomic fraction of element i and z_{al} is the effective valence of aluminum. Eq. (6) is then tied into the thermodynamic equation to give the parabolic oxidation constant k_t as follows

$$k_t \propto \left[\sum_{n=i} (z_i - z_{al}) \bar{c}_i \right] \cdot [\Delta G^0 + RT \ln Q] \quad (7)$$

Using substitution, the Eq. (7) can be simplified and rewritten as

$$k_t \propto Val_t^{eff} \Delta G \quad (8)$$

With equations (2), (6), and (8) a contour graph can be constructed, allowing for the stable alumina trend to be easily identified as a better chance of alumina formation the lower the free energy and effective valence. [24]

Third Element Phenomena Model

As previously mentioned, the matrix of the alloy must be FCC; however, aluminum destabilizes austenite and is considered a ferrite promoter. [3, 4, 18-20, 22] As such, it becomes necessary to minimize the aluminum content for alumina scale formation in order to preserve the equilibrium for austenite retention. Therefore, another consideration of considerable practical importance is element optimization. This optimization will be done through the third element effect of alumina formation, by which the presence of a third element with a reactivity intermediate to the components of the given binary alloy can decrease the content of the more reactive element needed to form its external oxide scale. [3, 26-31]

In ternary alloy systems, it can be seen that the required aluminum for stable alumina oxide formation can be directly influenced through chromium content. [3, 25-31] It is reported that the addition of Cr in binary Fe–Al alloys has been shown to reduce the minimum required aluminum. [32, 33] In other words, the addition of B to an A–B–C alloy can reduce the critical C concentration to establish an external scale of the C oxide; where A is the most noble, C is the most reactive component, and B has an oxygen affinity intermediate between those of A and C. [32] It is often suggested that element B in the ternary alloy system acts as an oxygen absorber, or third element catalyst, during the initial stage of oxidation; limiting oxygen diffusion into the alloy so that internal oxidation of C is minimized. [22] This type of process in the alloy system does not involve a prevention of the internal oxidation of aluminum but instead promotes the growth and transition of mixed iron and aluminum rich external scales directly into an external Al_2O_3 scale formation.

$$f_v^* = \frac{N_B^{O*} \rho(\text{BO}_v)}{F(h_B)} + \frac{N_C^{O*} \rho(\text{CO}_\mu)}{F(h_C)} \quad (9)$$

where $\rho(\text{BO}_v)$ is the ratio of the molar volumes of the alloy and the oxide BO_v , f_v^* is the critical value for the volume fraction of internal oxide, and h_B is defined as $\gamma\phi_B^{1/2}$, with $\phi_B = D_O/D_B$ where D_O and D_B are the diffusion coefficient for oxygen and element B in element A, respectively. The variable h_C is defined as $\gamma\phi_C^{1/2}$, with $\phi_C = D_O/D_C$ where D_O and D_C are the diffusion coefficient for oxygen and element C in element A, respectively. $F(r)$ is an auxiliary function defined as [25]

$$F(r) = \pi^{1/2} r \exp(r^2) [1 - \text{erfc}(r)] \quad (10)$$

Typically, the critical value for the volume fraction of internal oxide, f_v^* , is empirically determined and is often times set equal to 0.3. [30] The internal oxidation kinetic parameter γ , can be found through the equation

$$N_o^{so} = G(\gamma) \left[v \frac{N_B^o}{F(h_B)} + \mu \frac{N_C^o}{F(h_C)} \right] \cdot \left[\frac{\text{erf}(\gamma) - \text{erf}(u_o)}{\text{erf}(\gamma)} \right] \quad (11)$$

with another auxiliary function defined as [25]

$$G(r) = \pi^{1/2} r \exp(r^2) \text{erfc}(r) \quad (12)$$

For an iron, aluminum, and chromium system the third element effect assumes that the internal oxides are Cr_2O_3 and Al_2O_3 in a Fe matrix allowing for $v = \mu = 1.5$. [29, 34]

Using the systems of Eq. (9) and (11), the critical concentration can be solved by using the bulk concentration of the other reactive component as an independent variable, N_B^{O*} .

The minimum chromium value required for the third element effect can be redefined, simplified, and calculated through the following equations

$$N_{Cr}^{O*} = N_{Cr}^{eq} (1 - N_{Cr}^{eq}) F \left(\frac{1}{2} [k_c (\text{Cr}_2\text{O}_3) / D_{Cr}] \right)^{1/2} \quad (13)$$

where k_c is the parabolic rate constant for the growth of Cr_2O_3 scales while D_{Cr} is the diffusion coefficient of chromium in iron and N_{Cr}^{eq} is the chromium content in simultaneous equilibrium with iron and chromium oxides. However, since Cr_2O_3 is much more stable than iron oxides, N_{Cr}^{eq} is very small and may be neglected thus giving the equation [29, 34]

$$N_{Cr}^{O*} = F \left(\frac{1}{2} [k_c (\text{Cr}_2\text{O}_3) / D_{Cr}] \right)^{1/2} \quad (14)$$

Similarly, the minimum aluminum value required for the third element effect can be calculated through

$$N_{Al}^{O*} = F \left(\frac{1}{2} [k_c (Al_2O_3) / D_{Al}] \right)^{1/2} \quad (15)$$

Calculating Eq. (9), (11), (12), and (13) will allow for the visualization of the third element plot seen in Figure 12,

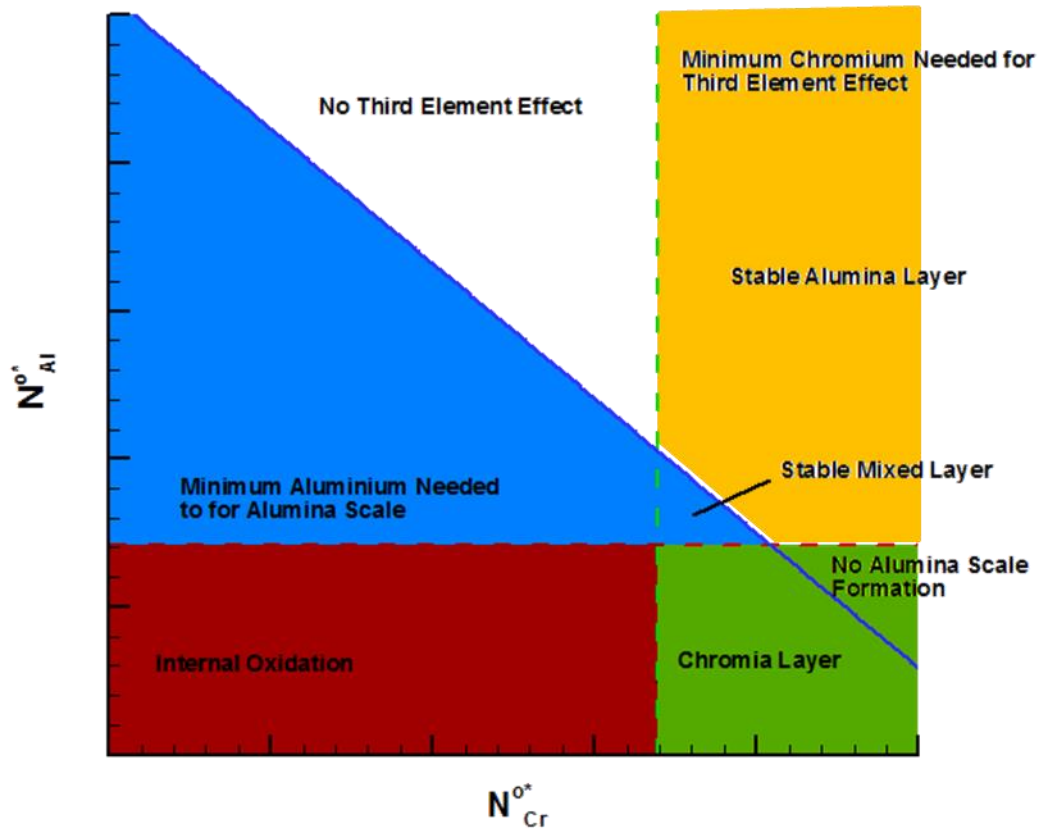


Figure 12 Interpretive Visualization of the Third Element Graph

where $N_{\text{Al}}^{\text{O}^*}$ is the molar fraction of aluminum in the alloy and $N_{\text{Cr}}^{\text{O}^*}$ is the molar fraction of chromium in the alloy. As detailed in Figure 12 if there is insufficient aluminum or chromium in the system then there will most likely be no third element effect.

CHAPTER V

EFFECTIVE VALENCE MODELING

As mentioned above, in order to map out the trends for alumina formation in austenitic stainless steel, multiple concepts and models are combined to predict alumina formation. In this chapter, the model discussed by Sato is applied; combining both thermodynamic and kinetic concepts to a multitude of previously explored experimental alloy, see Appendix, for accuracy and trend discovery.

Modeling of Effective Valence

To determine if alumina formation can indeed be modeled and predicted through thermodynamic equations, it is necessary to take previous experimental works and map them accordingly to the development of alumina scales. [5, 6, 8, 9, 11, 15, 16] In order to generate a diagram based on the thermodynamic variables of Gibbs free energy, total effective valence of Al_2O_3 , and K value the first variable, Gibbs free energy, was calculated through the use of the TCFE6 Thermocalc database. As seen in Figure 13, the free energies of most of the alloys are extremely close in value, with no distinguishable characteristics to determine for the formation of alumina oxide. This again demonstrates the need for an additional variable, effective valence. [24]

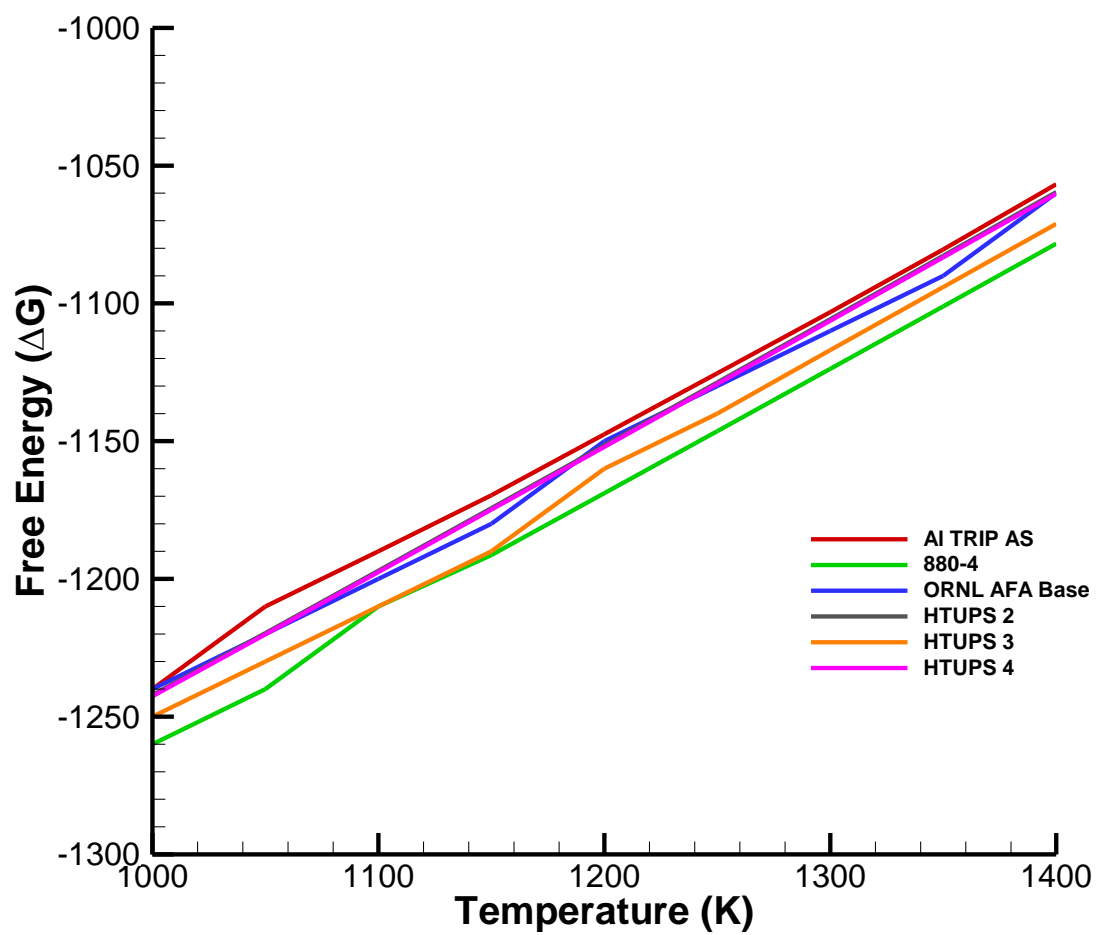


Figure 13 Free Energies of Sample Alloys with Respect to Temperature

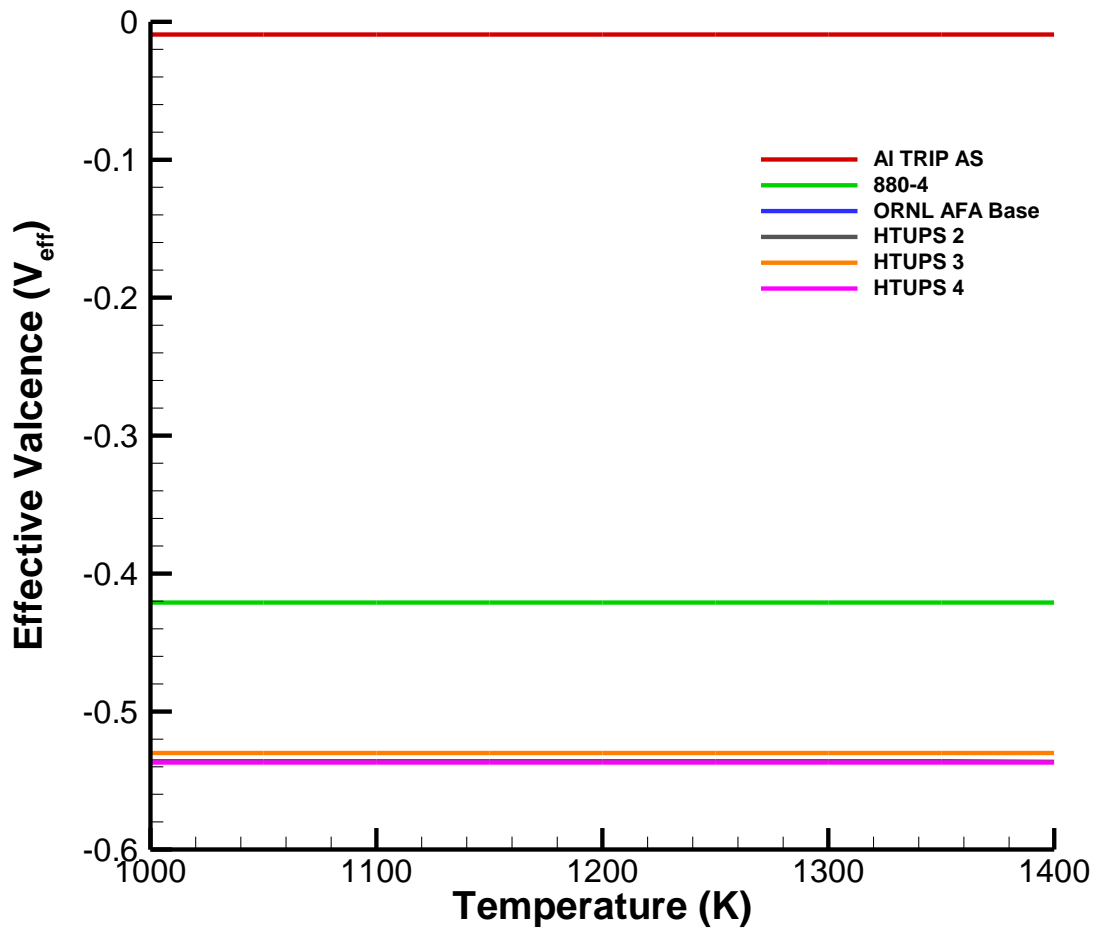


Figure 14 Effective Valences of Sample Alloys with Respect to Temperature

Calculating the effective valence, Figure 14, it can be seen that despite the free energy similarities, a larger disparity can be seen from the effective valence of each alloy. Using the free energy and effective valence calculated, the K value can be determined for each alloy. The free energy, effective valence, and K value was taken for each alloy at 1000 K to create a contour map, Figure 15. With the contour map, it can be seen that,

despite the close similarities of free energy, when effective valence electron is also considered there are extremely notable differences between alloys.

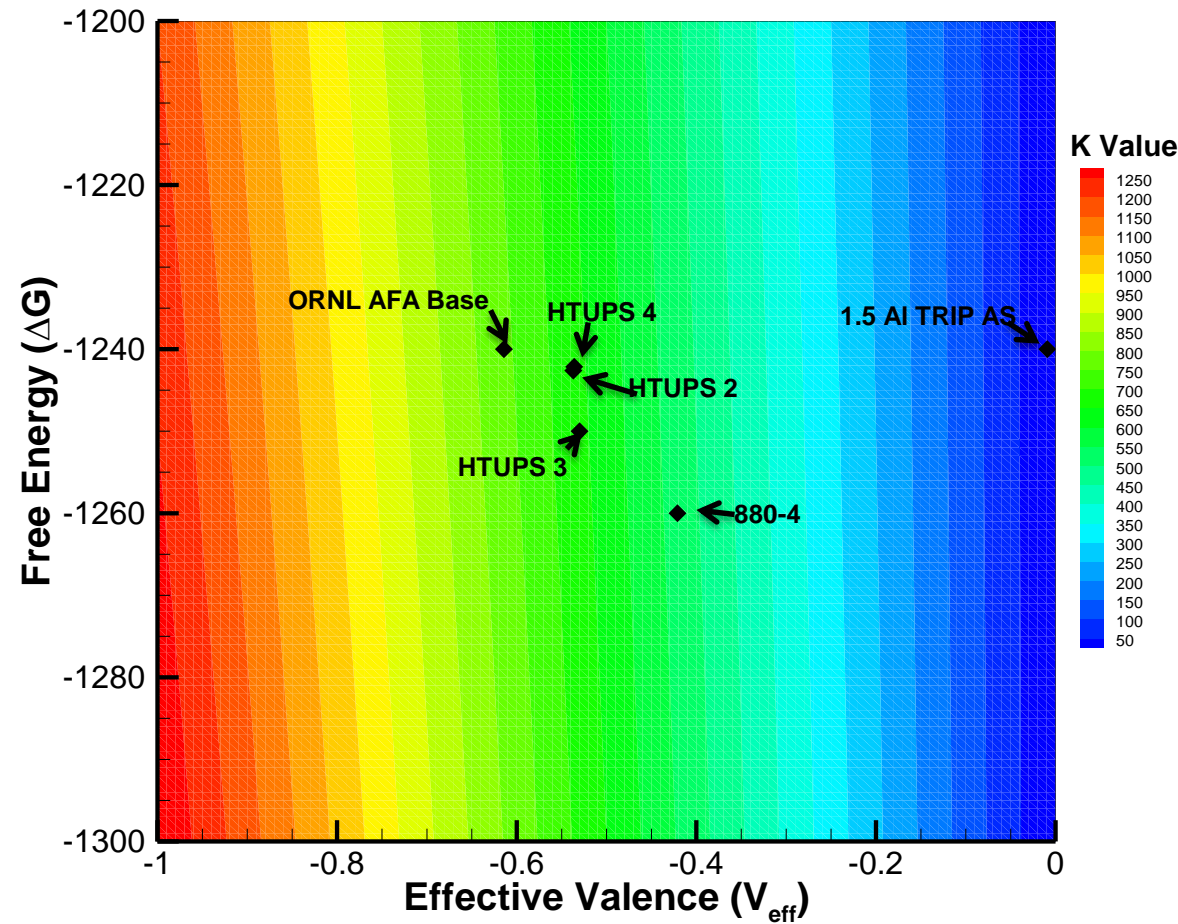


Figure 15 Combining Effective Valence with Free Energy for K Value

With the utility of the effective valence graph clearly visible in Figure 15, the trend prediction accuracy for alumina formation is tested on twenty different experimental alloys from previous works.

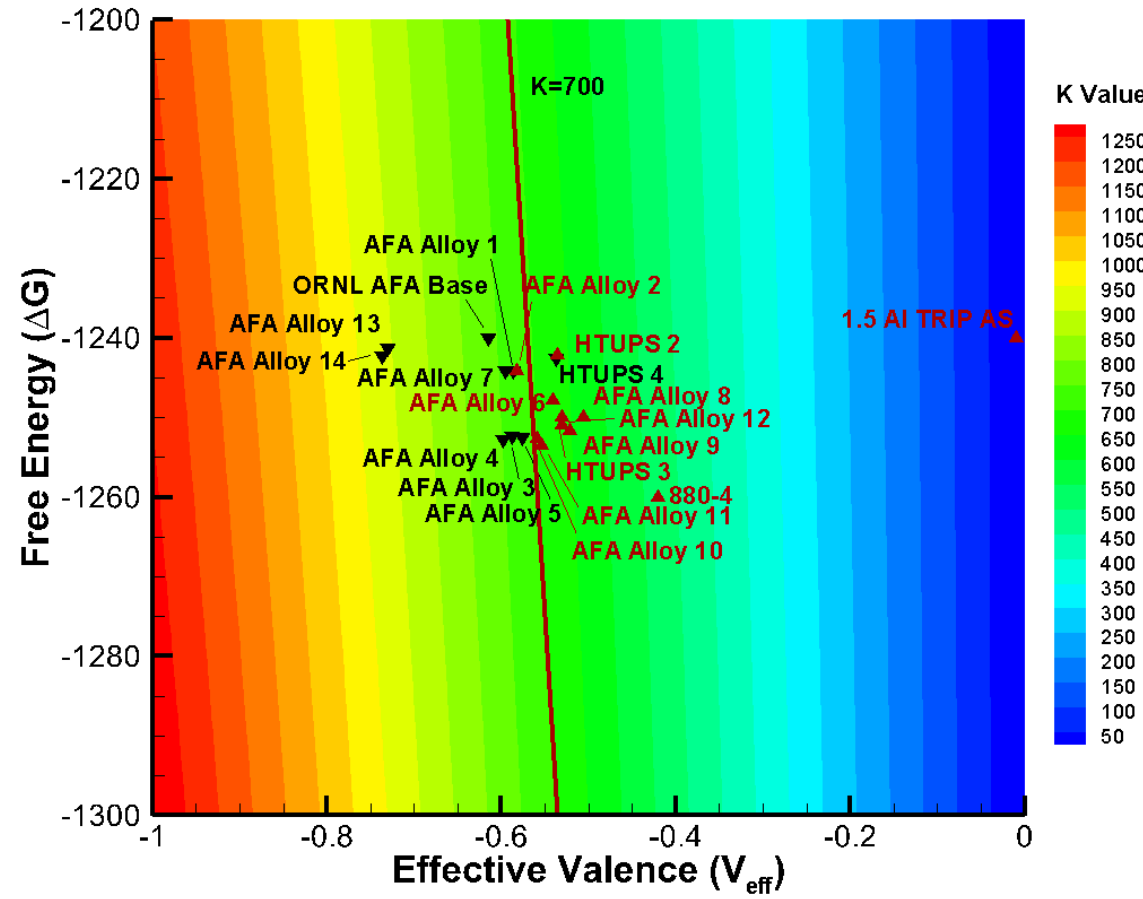


Figure 16 Free Energy, Effective Valence, and K Value of Experimental Alloys

The contour map above, Figure 16, shows where each experimental composition lies in terms of its K value, effective energy valence, and free energy relative to each other alloy. Alloys designated with a black gradient symbol, ▼, have demonstrated a stable alumina oxide layer in experiments while those with a red triangle symbol, ▲, does not display a stable alumina oxide layer in experiments. With the contour map populated with alloys of various compositions, it can be seen that those with stable alumina formation mainly occupies areas of K values that are greater than 700, with the exception of the HTUPS 4 alloy.

A further in-depth analysis of the role each element in an alloy for this model can be seen in Figure 17. The alloy in this model, Fe - 19.95Ni - 14.19Cr - 2.48Al - 0.15Si - 1.95Mn - 2.46Mo - 0.86Nb - 0.075C, had each individual element changed by 10% of the element's weight percent. It should be noted that the axis of the contour map has been altered to magnify the changes of each element. It is shown that the most weighted elements in controlling the increase or decrease of the K value is the weight percent of chromium and aluminum. This can be explained by both the thermodynamic and kinetic properties of chromium and aluminum in addition to the role played by the third element effect. In other words, the increase or decrease of aluminum would obviously alter the diffusivity and activity of oxygen and aluminum for alumina formation; however chromium alters alumina formation from a rather ambiguous role of oxygen grabber, allowing for alumina to form while oxygen diffusivity is immensely decreased through chromia formation.

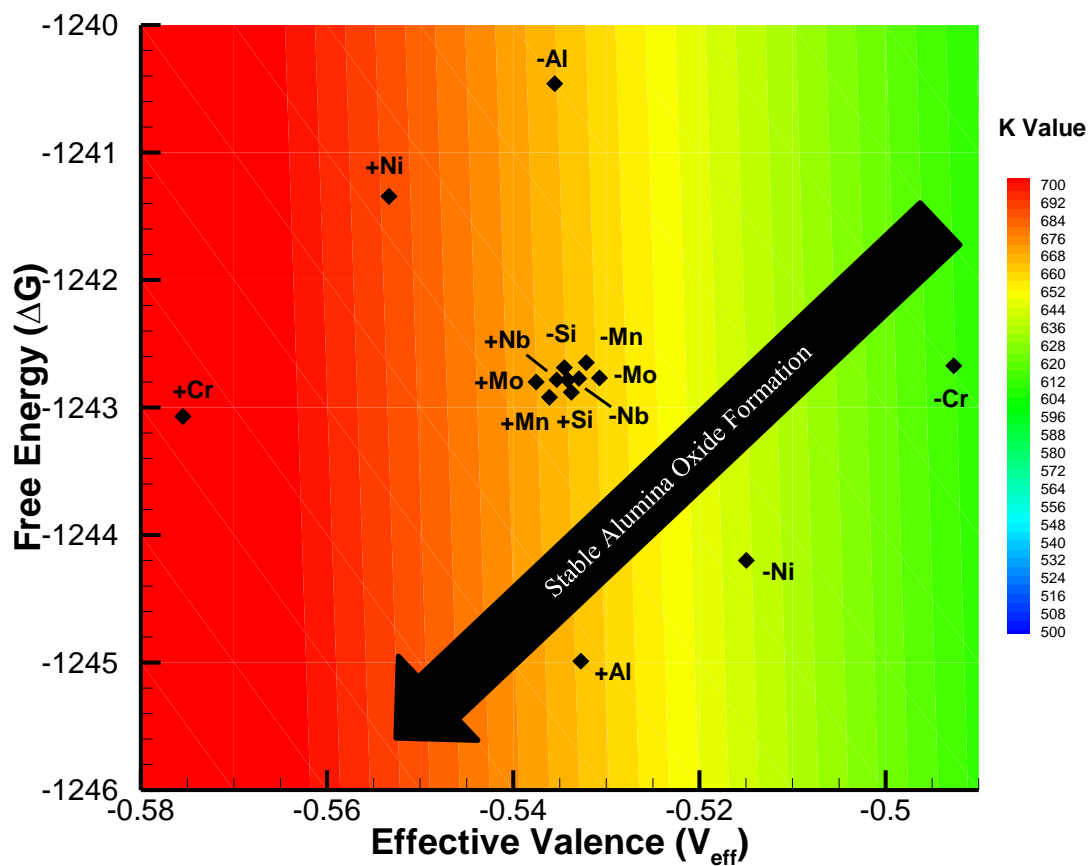


Figure 17 K Value Alumina Formation through Element Control

Aside from the major elements of aluminum and chromium in the composition, nickel, manganese, molybdenum, silicon, and niobium also play an extremely important role in alumina formation. Although these elements do not hold as much dominance in changing the K value as aluminum and chromium, they play a major factor in the austenite stability, element diffusivity, and the overall strength and stability of the alloy. [21, 55-62]

Nickel is an extremely important element that plays a major role in both austenite stability and the K value of the alloy. Although nickel increases the free energy, it counteracts the impediment to alumina scale formation by decreasing the effective valence. The primary purpose of nickel addition is to encourage sufficient stable austenitic phase field to form within the alloy. [56-58, 60, 61]

The original purpose of manganese addition was to prevent solidification cracking usually associated with iron and sulfur. In austenitic stainless steels, the effect of manganese on the mechanical properties of the alloy itself is minimal; however, the element plays an important role in austenite stability as a powerful deoxidizer. [21, 55, 59]

In commercial steels such as 304 L and 316 L, alloying molybdenum produces a powerful effect on pitting and crevice corrosion. Molybdenum also reduces the necessary intensity of oxidizing effects in alloys for forming a passive film as well as decreases the tendency of oxide film break down. [21, 61]

As a ferrite stabilizer, silicon is added during melting for its deoxidizing properties. In correct amounts, within austenitic stainless steels silicon prevents carburizing and

improves oxidation resistance. This directly helps the formation alumina by allowing time for the slower alumina to develop through decreasing oxygen diffusivity. [21, 63]

Although some elements may not play a direct role in alumina formation, it is certain that each element within an alloy composition are intricately linked to determining the alumina scale stability as well as the other structural properties of the alloy.

CHAPTER VI

THIRD ELEMENT MODELING

Although effective valence modeling provides a powerful instrument in alumina formation for austenitic steel, it is not infallible. As such, it is necessary to supplement this tool with an additional set of variables and criteria. In this chapter, the model utilizing the third element effect will be discussed and applied to combine both thermodynamic and kinetic third element phenomena to the existing effective valence model in order to form a more accurate and efficient trend and model prediction. The resulting model will be applied to a multitude of previously explored experimental alloy, see Appendix, for accuracy and trend discovery.

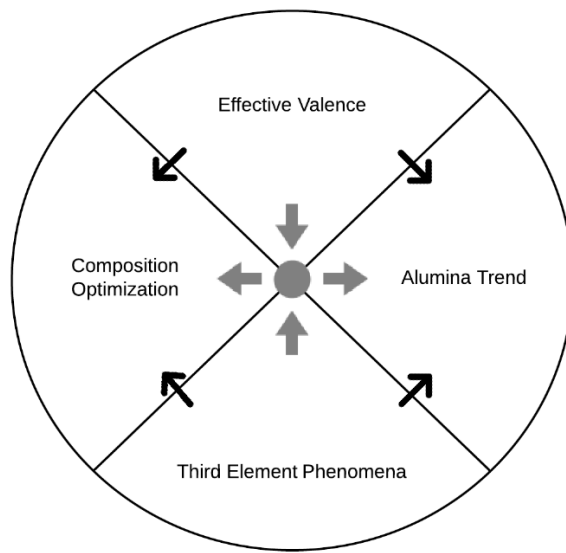


Figure 18 Hybrid Alloy Designing Process

Modeling of Third Element Phenomena

With a general trend of elements established using Sato's contour model, the next step is to optimize the composition with the third element effect. Using the thermodynamic and kinetic values obtained from the TQ interface in Thermocalc to calculate Eq. (9), (11), (12), and (13), a graphical representation of the third element effect could be generated for experimental works completed by other groups. [5, 6, 8-17, 64] It should be noted that given the method of creating a third element graph, each curve generated is unique and can shift if calculated under slightly different conditions. This curve shift is extremely apparent in Figure 35. As such, each curve for the third element model that was generated was done so at 1atm, 1000K, and the exact given composition seen from the experimental works.

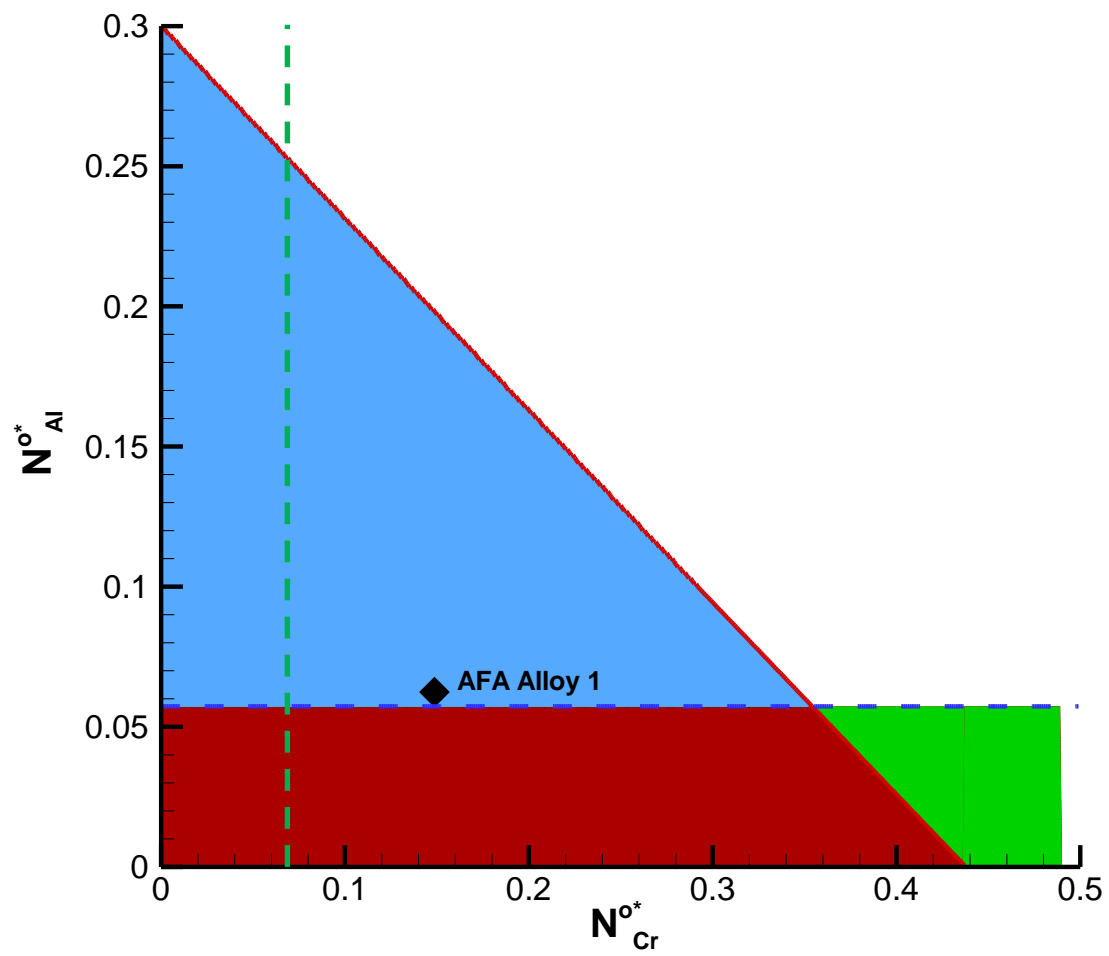


Figure 19 Third Element Effect of AFA Alloy 1 *Forms Stable Oxide Layer [64]

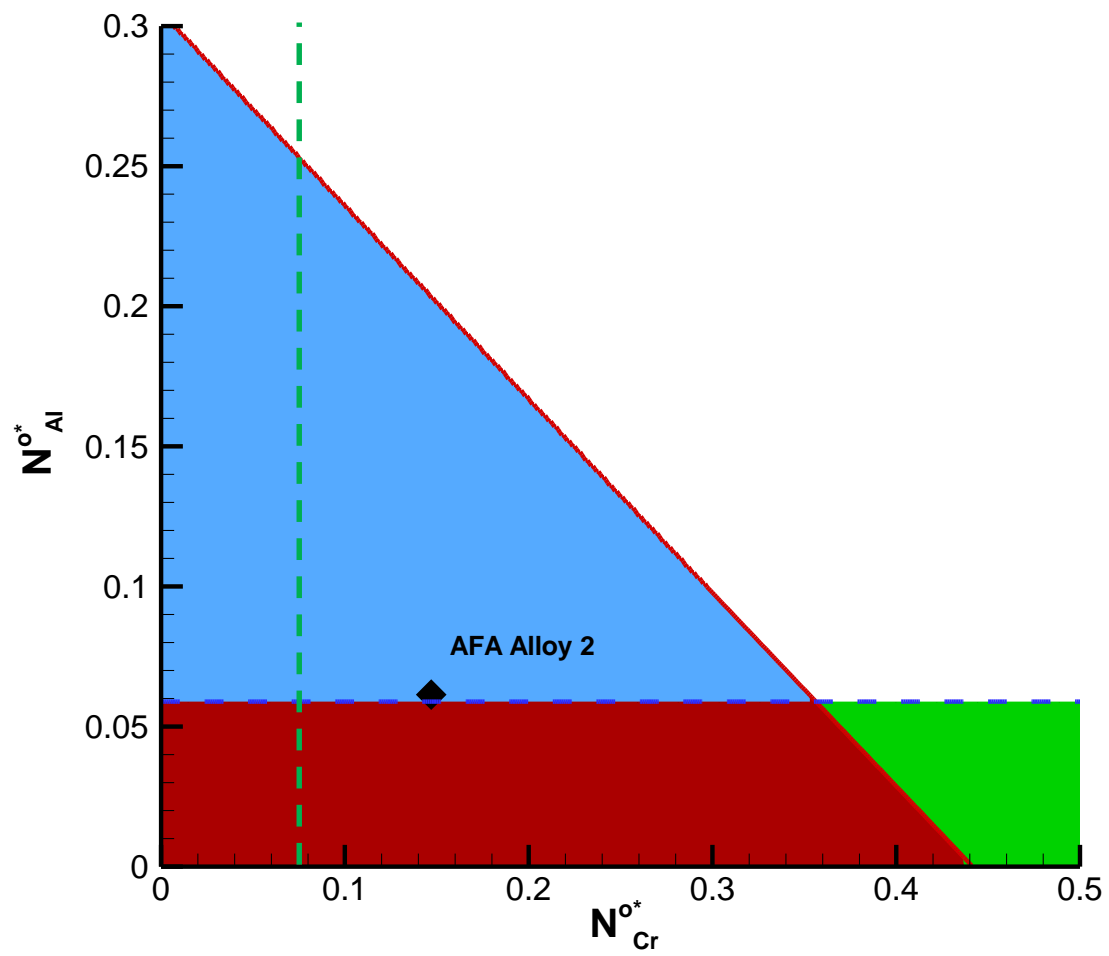


Figure 20 Third Element Effect of AFA Alloy 2 *Forms Unstable Oxide Layer [64]

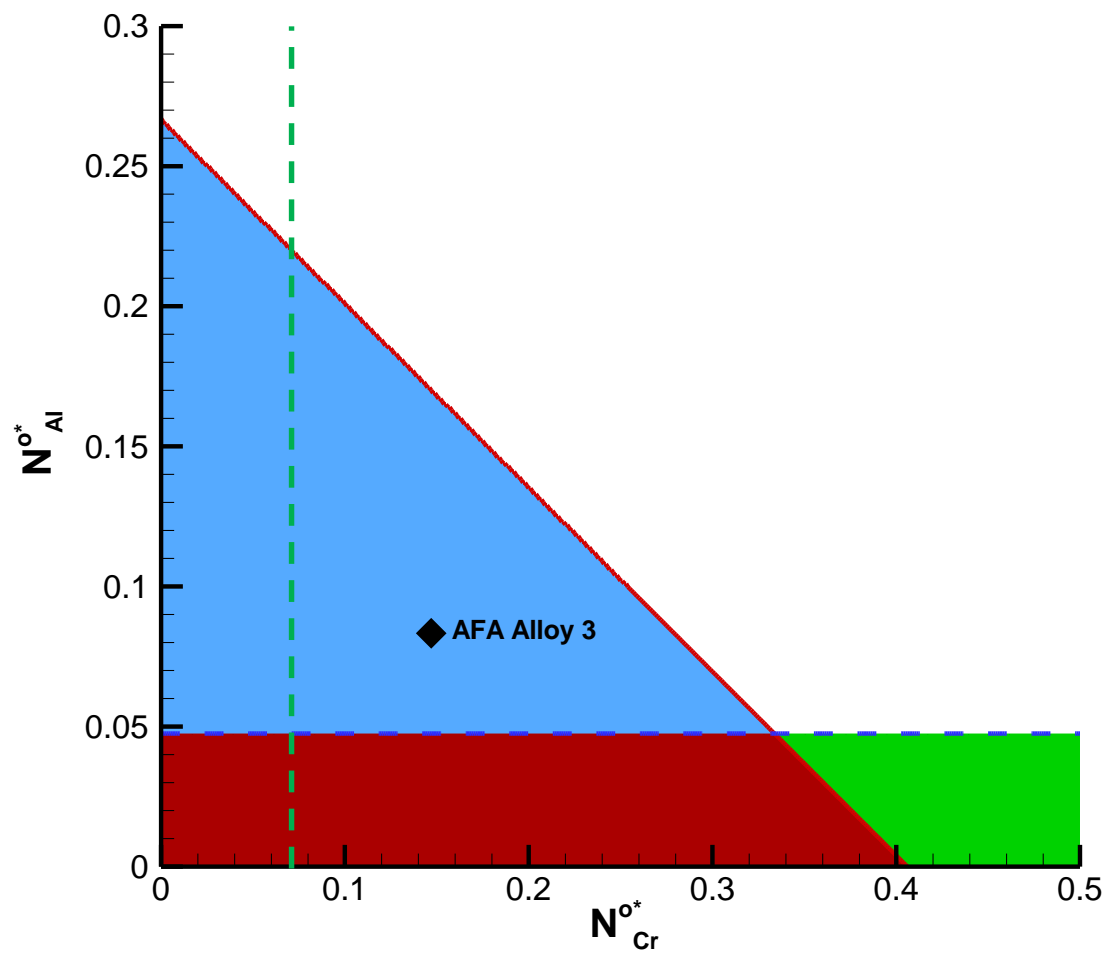


Figure 21 Third Element Effect of AFA Alloy 3 *Forms Stable Oxide Layer [64]

In the third element models of Figure 19, Figure 20, and Figure 21, the AFA Alloys 1-3 meets the necessary requirements in the composition for the third element to be a factor in favor of alumina formation. For both AFA Alloy 1 and 3, the experimental data obtained from the results demonstrated an agreement with the model as there was stable alumina scales observed. [16] In AFA Alloy 2, however, it can be seen that there were no observable stable alumina oxide layer to protect the alloy. Although AFA Alloy 2 is slightly over the boundary in meeting the minimum necessity for encouraging alumina formation through third element, it can be observed in Figure 16 that its K value is lower than the majority of compositions that indicate successful alumina formation. Thus with the combination of both effective valence and third element models, it is shown that AFA Alloy 2 has a much lower chance of alumina formation than if only a single model is used.

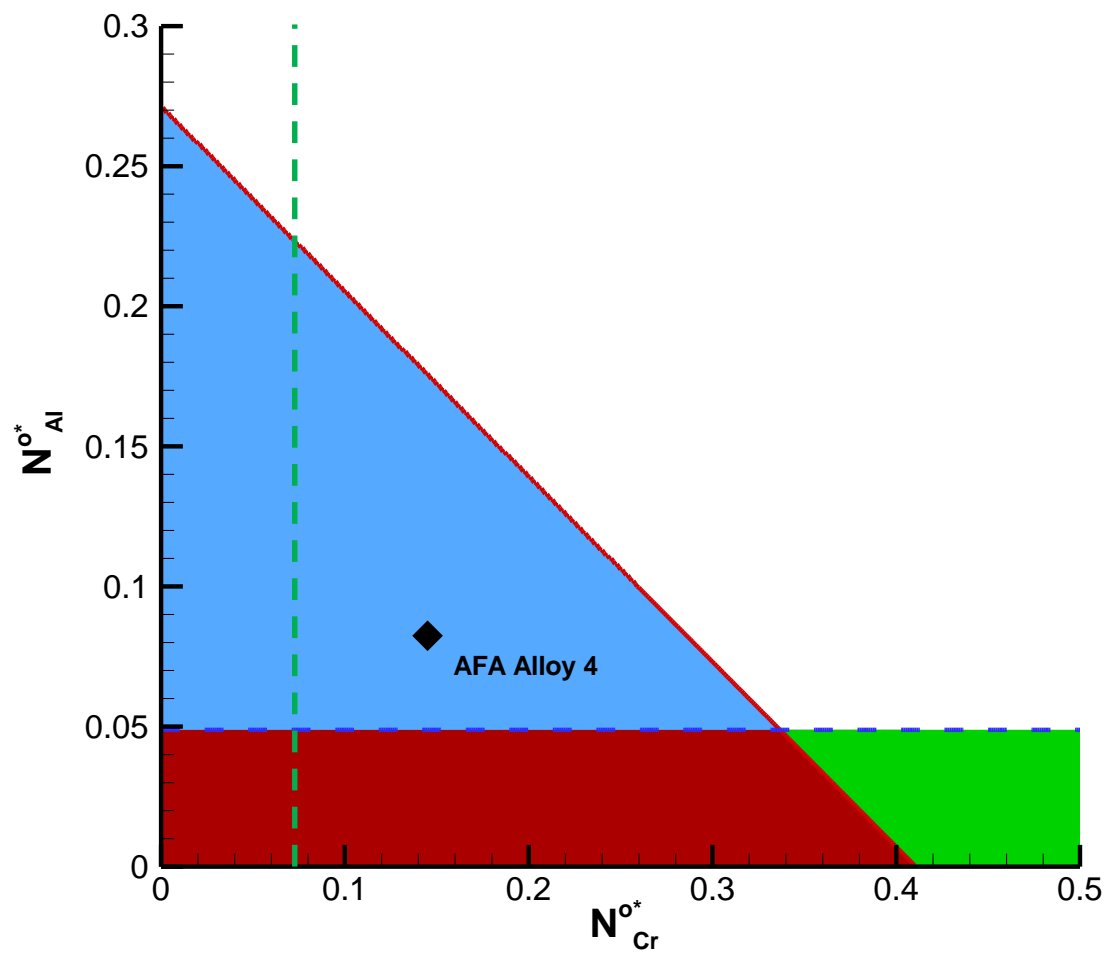


Figure 22 Third Element Effect of AFA Alloy 4 *Forms Stable Oxide Layer [64]

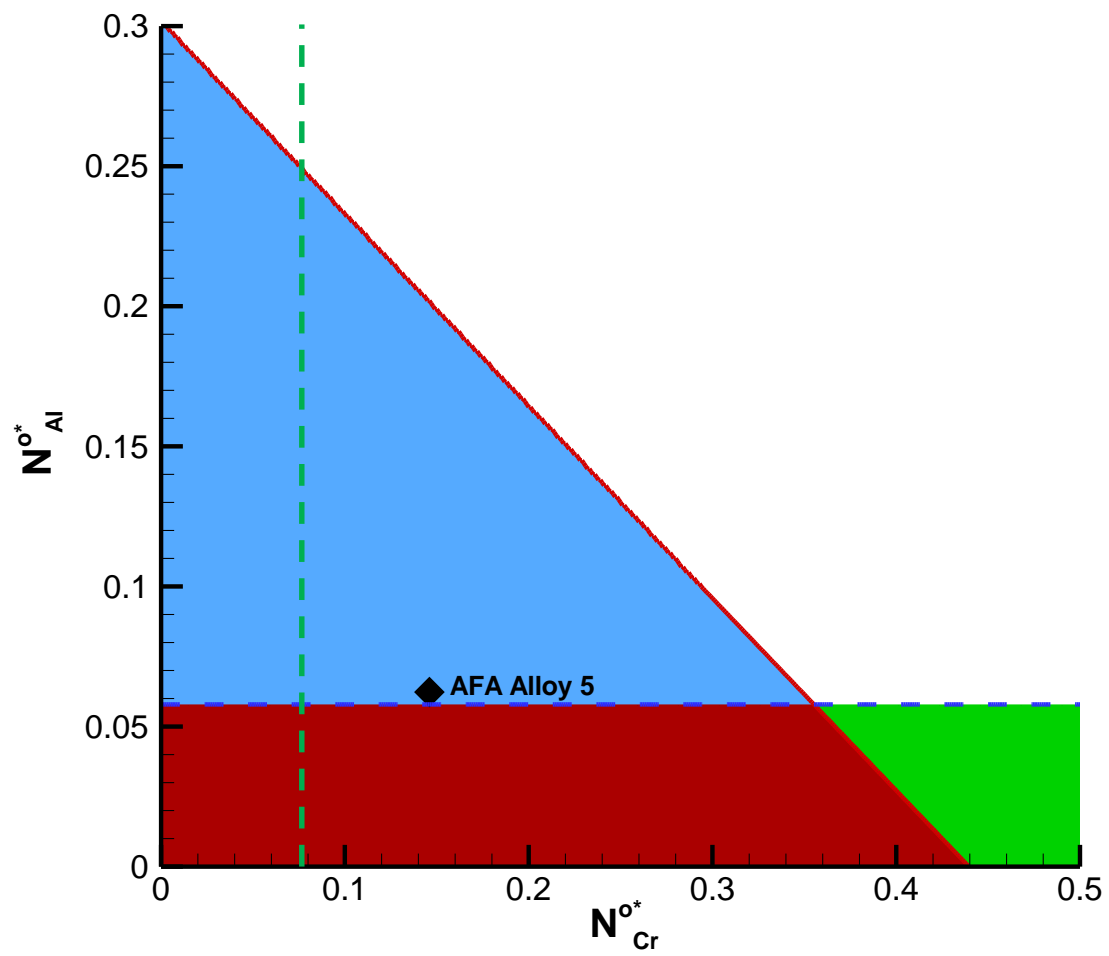


Figure 23 Third Element Effect of AFA Alloy 5 *Forms Stable Oxide Layer [64]

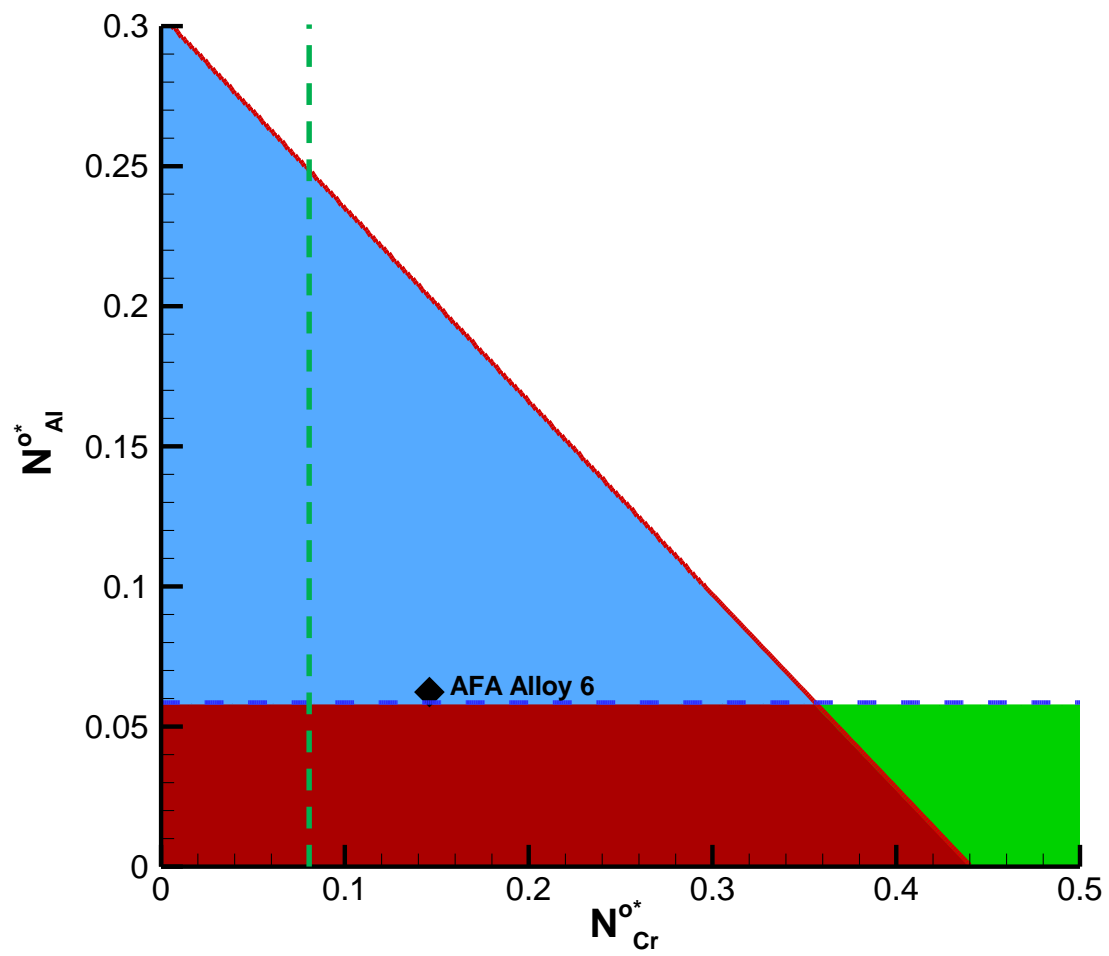


Figure 24 Third Element Effect of AFA Alloy 6 *Forms Unstable Oxide Layer [64]

In the third element models of Figure 22, Figure 23, and Figure 24, the AFA Alloys 4-6 demonstrates the needed requirements in their composition for the third element to be a factor in favor of alumina formation. For both AFA Alloy 4 and 5, the experimental data obtained from the results demonstrated a good agreement with the model simulated. In AFA Alloy 6, however, it should be noted that within the experimental data there were no observable stable alumina oxide layer to protect the alloy. Although AFA Alloy 6 is slightly over the boundary in meeting the minimum necessity for encouraging alumina formation through third element, it can be observed in Figure 16 that its K value is lower than the majority of compositions that indicate successful alumina formation. Thus with the combination of both effective valence and third element models, it is shown that AFA Alloy 6 has a much lower chance of alumina formation than if only a single model is used.

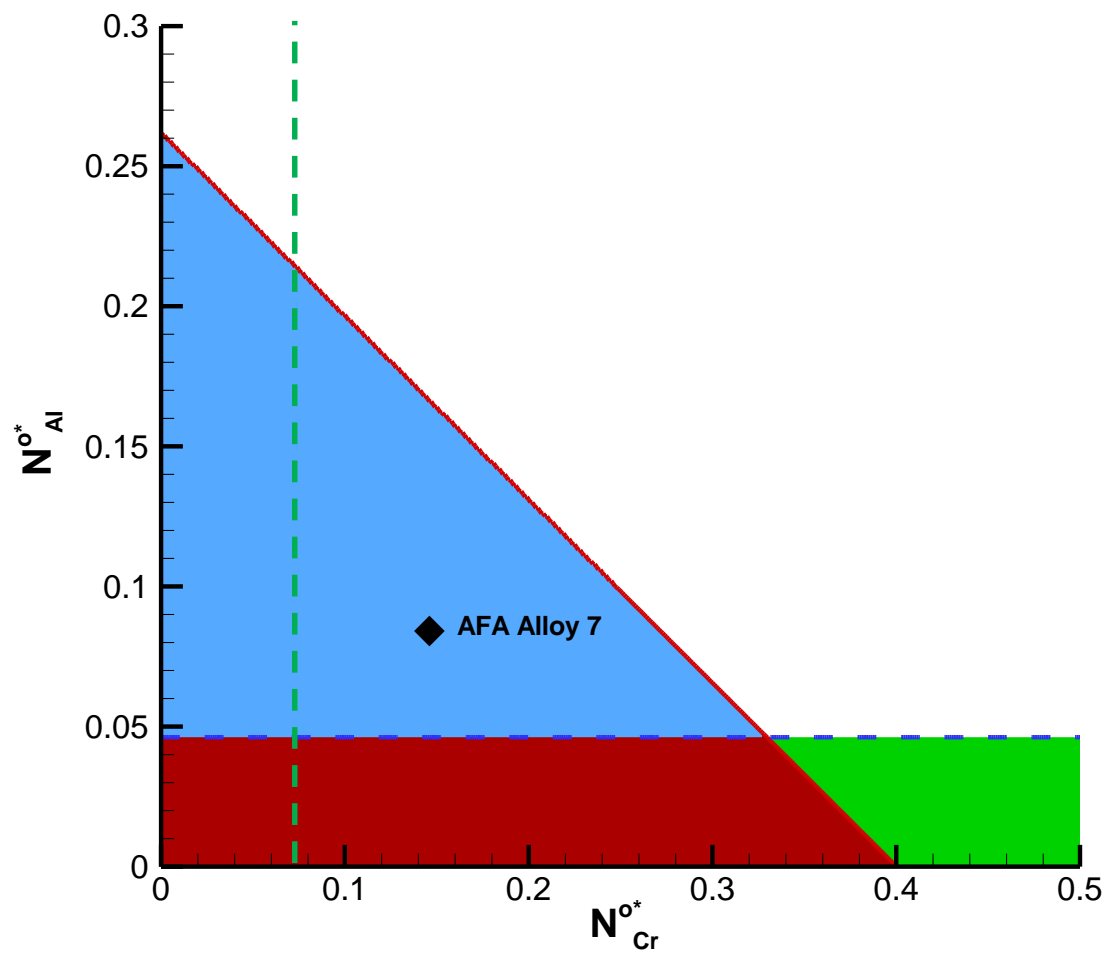


Figure 25 Third Element Effect of AFA Alloy 7 *Forms Stable Oxide Layer [64]

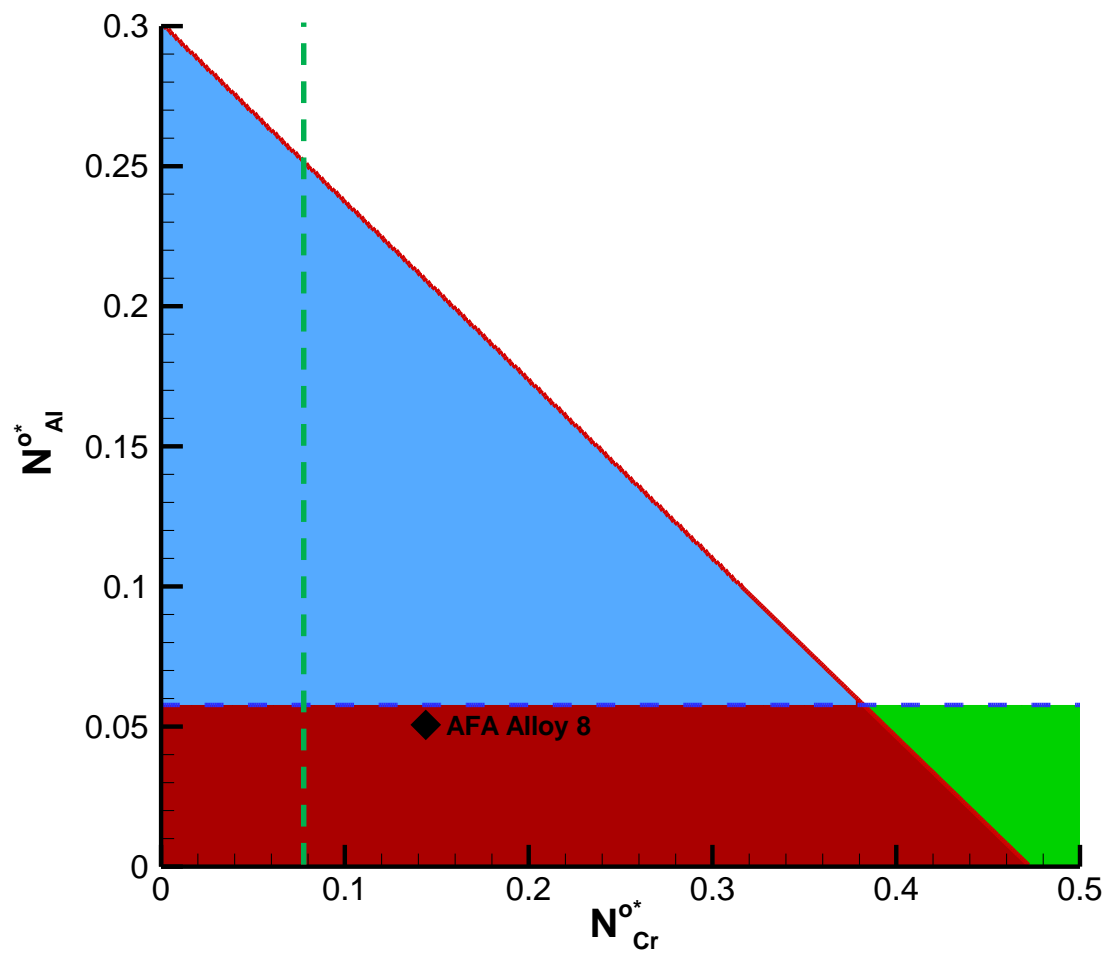


Figure 26 Third Element Effect of AFA Alloy 8 *Forms Unstable Oxide Layer [64]

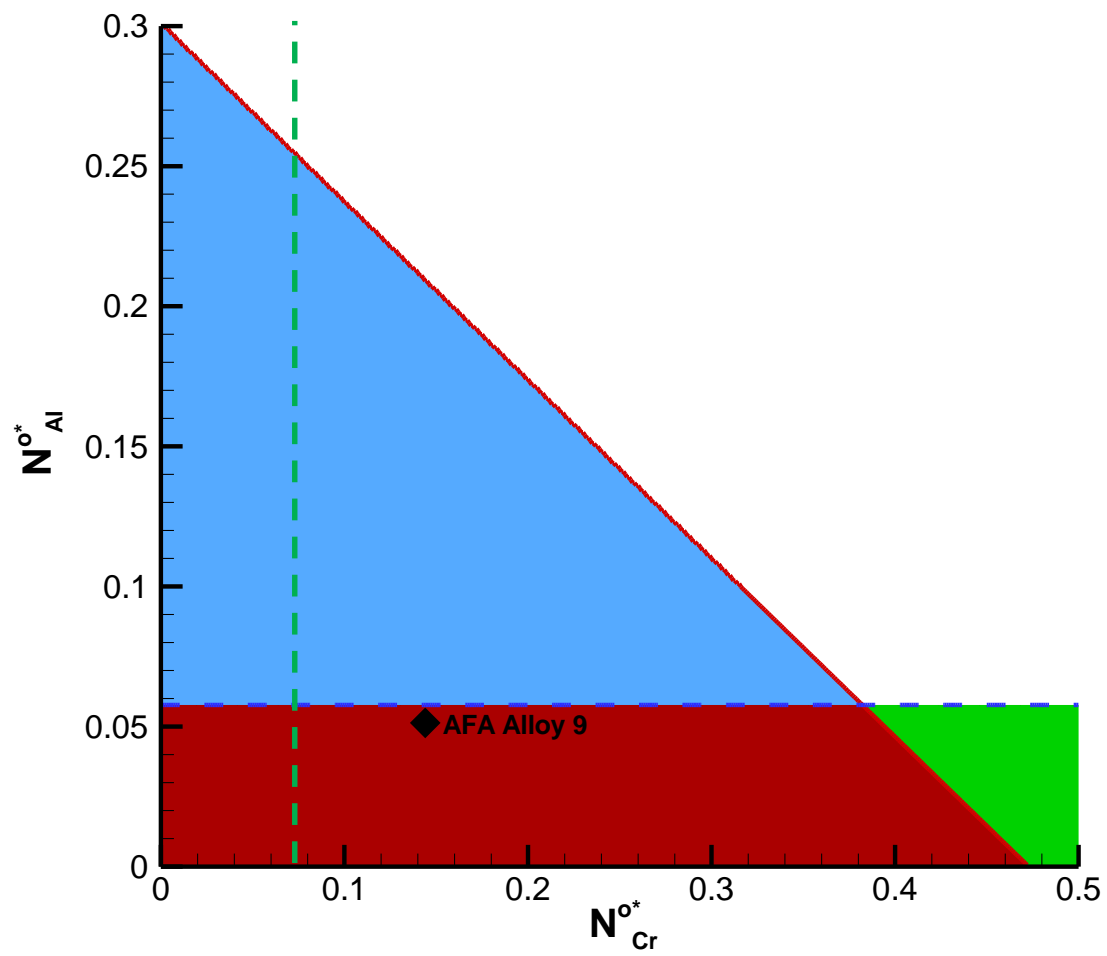


Figure 27 Third Element Effect of AFA Alloy 9 *Forms Unstable Oxide Layer [64]

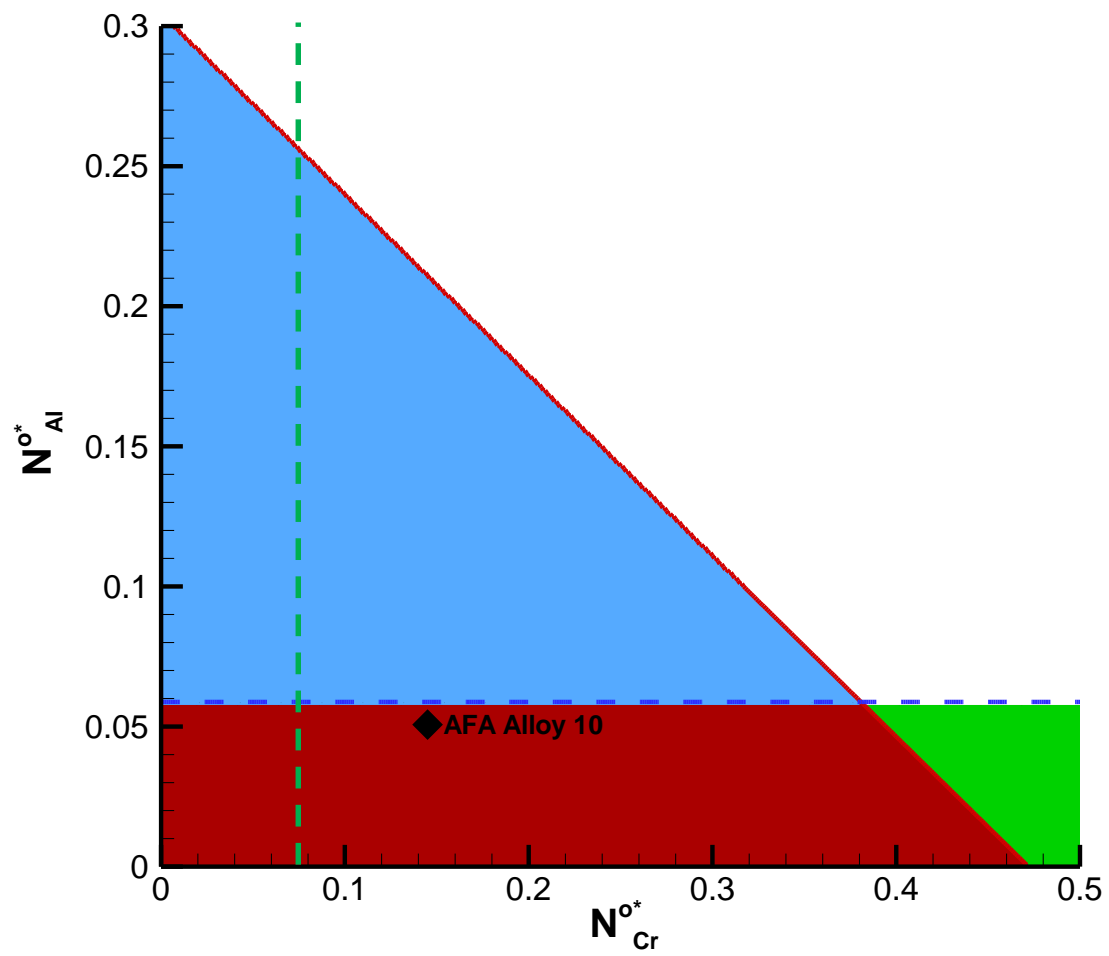


Figure 28 Third Element Effect of AFA Alloy 10 *Forms Unstable Oxide Layer [64]

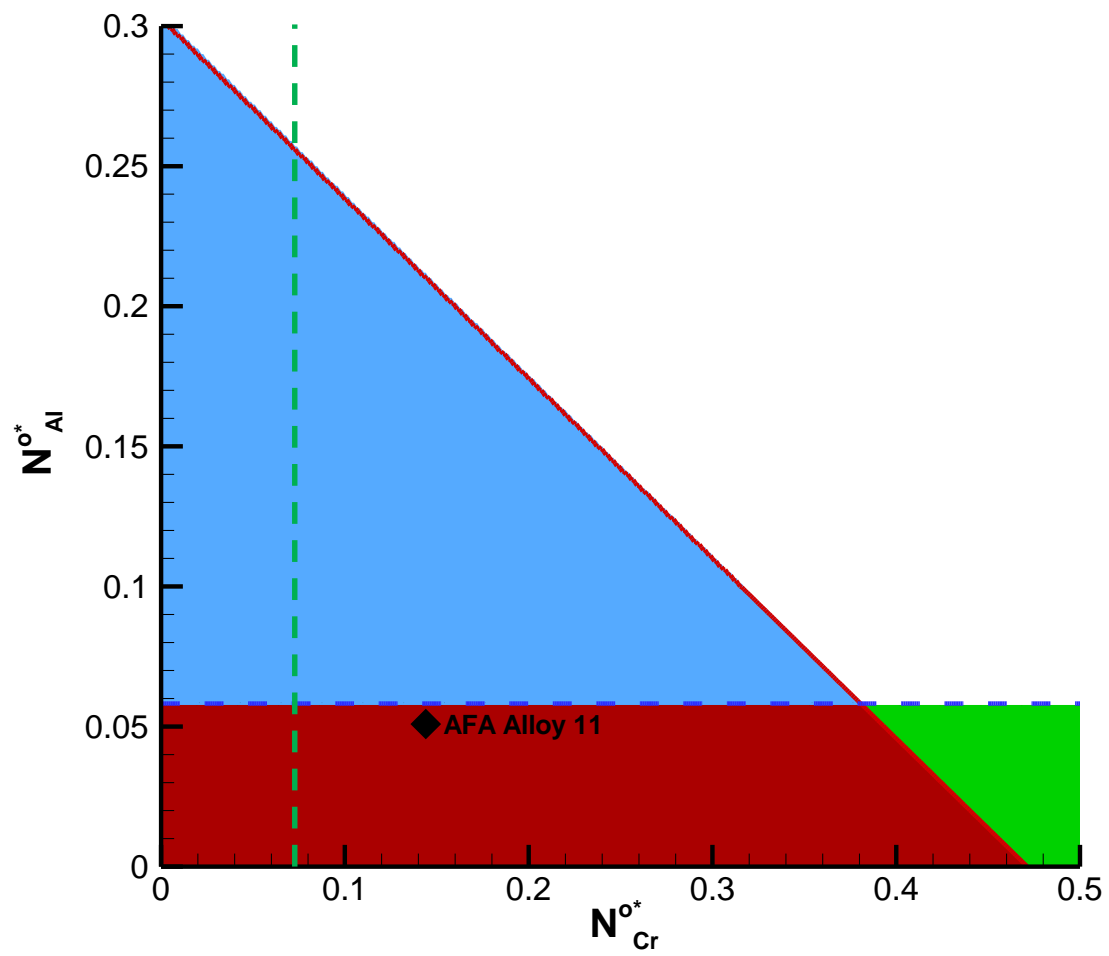


Figure 29 Third Element Effect of AFA Alloy 11 *Forms Unstable Oxide Layer [64]

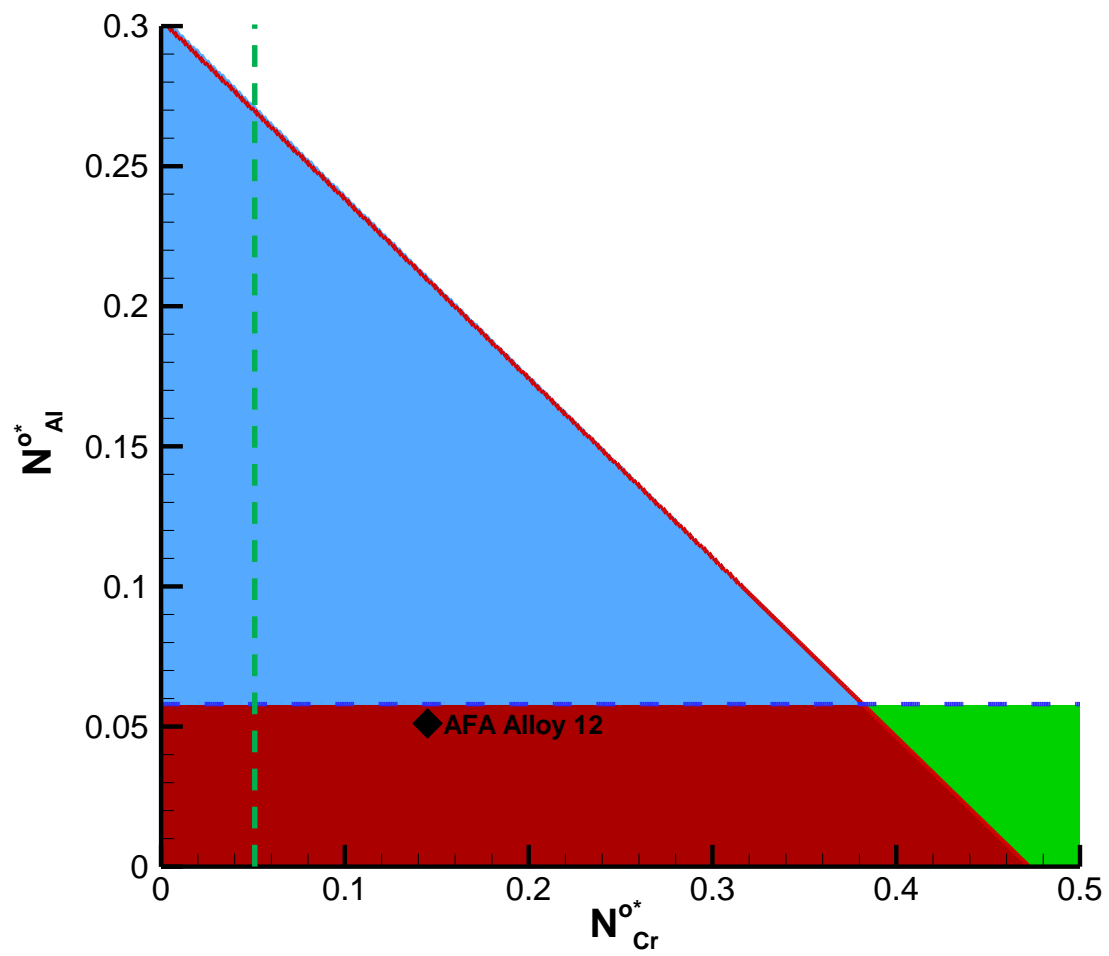


Figure 30 Third Element Effect of AFA Alloy 12 *Forms Unstable Oxide Layer [64]

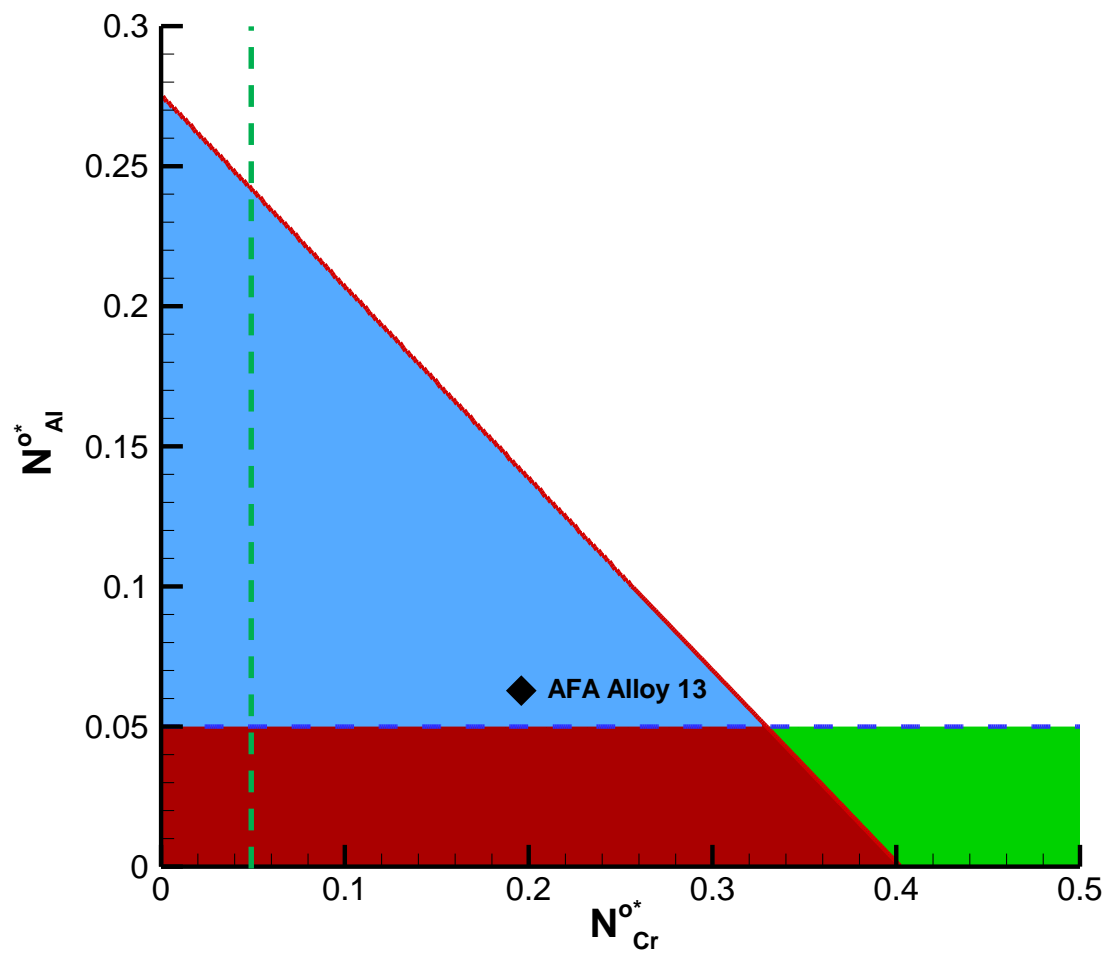


Figure 31 Third Element Effect of AFA Alloy 13 *Forms Stable Oxide Layer [64]

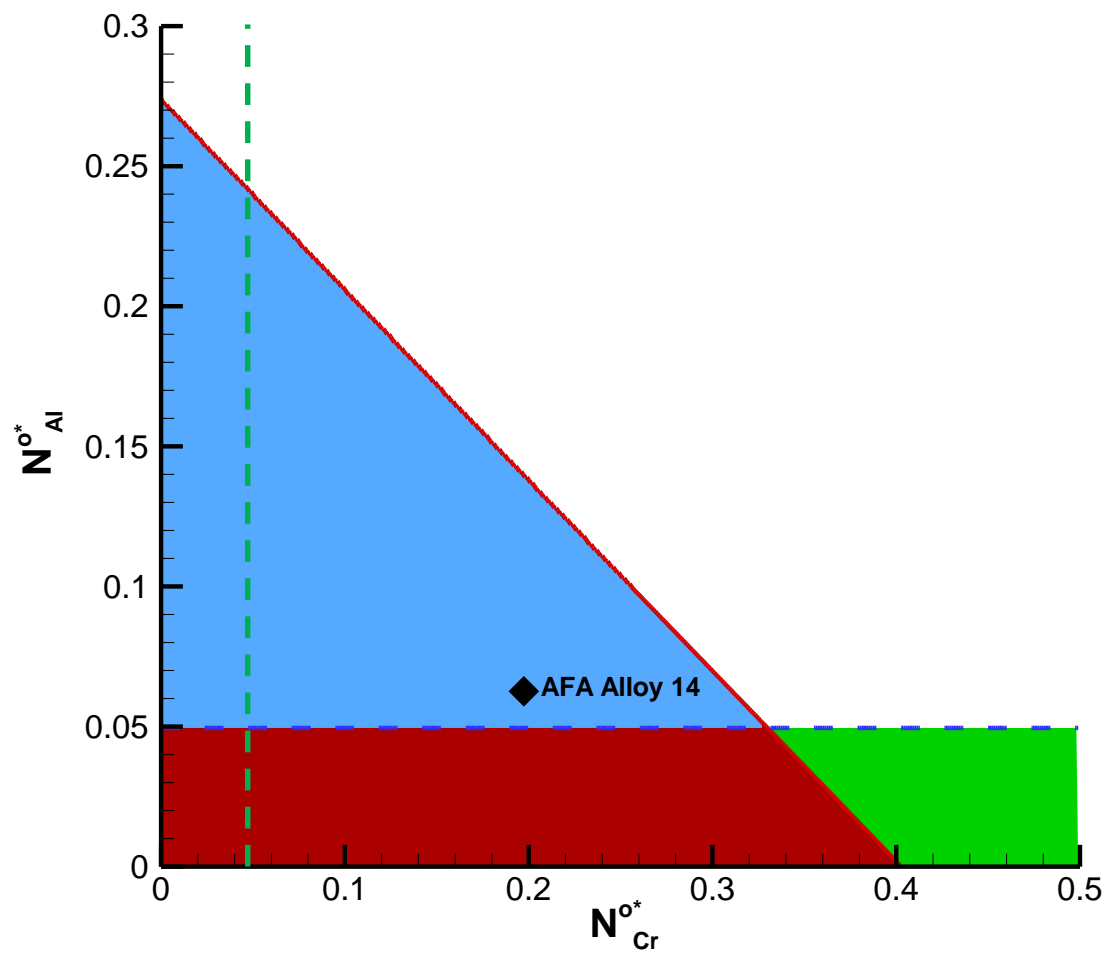


Figure 32 Third Element Effect of AFA Alloy 14 *Forms Stable Oxide Layer [64]

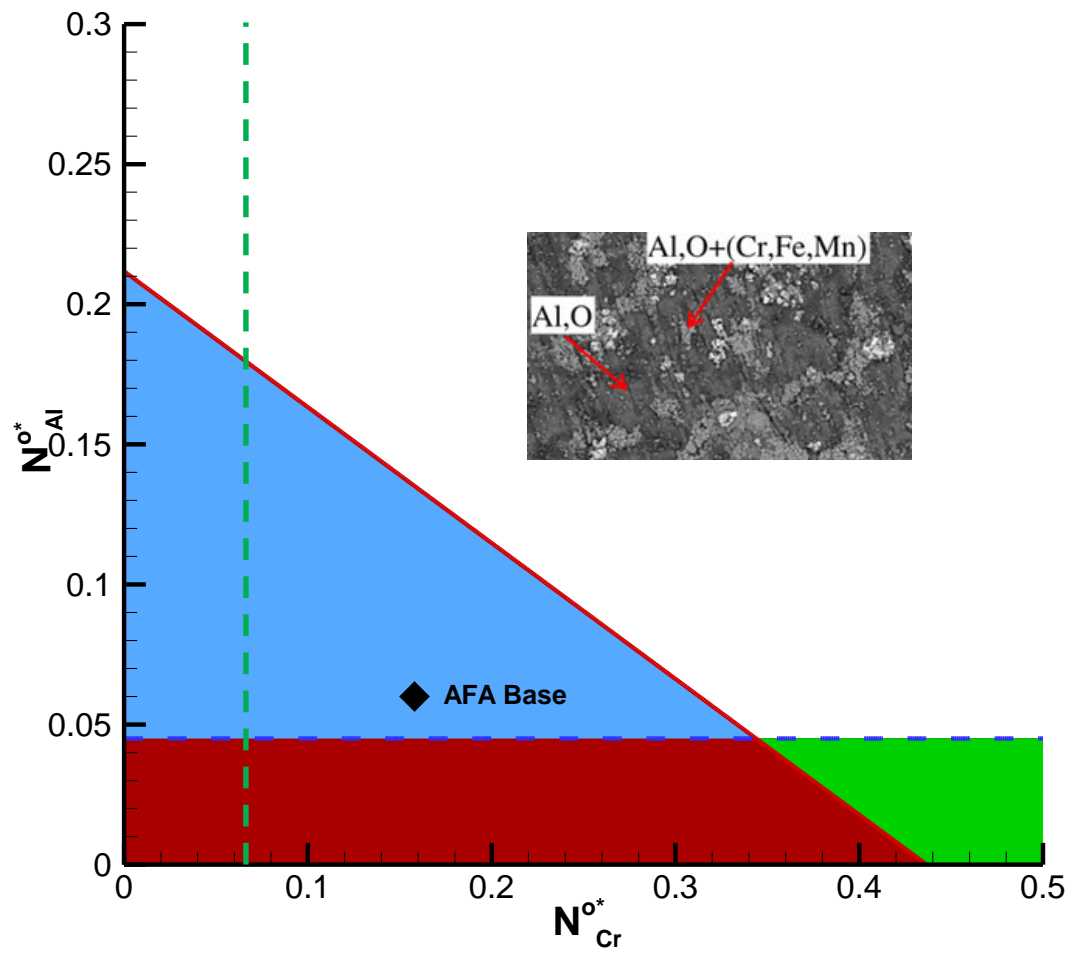


Figure 33 Third Element Effect of AFA Base *Forms Stable Oxide Layer [8]

The remaining AFA Alloys show that in their third element models, seen in Figure 25, Figure 26, Figure 27, Figure 28, Figure 29, Figure 30, Figure 31, Figure 32, and Figure 33, these alloys demonstrate a good agreement with the effective valence model, seen in Figure 16. For both the effective valence and third element model, the AFA Alloys modeled above predicts the same results that have been demonstrated in experiments.

For AFA Alloys 7, 13, 14, and Base, the third element model complies with the necessary requirements for the third element phenomena to be in favor of alumina formation; as does the effective valence model. Likewise, the experimental data obtained from previous works also demonstrates an agreement with the results projected from the models simulated; showing that there was indeed stable alumina scales observed.

For the AFA Alloys 8-12, it can be seen that there were no observable stable alumina oxide layer to protect the alloy. These alloys are well below the necessary requirements set by the third element model. It should also be noted that this comes in agreement with the effective valence model observed in Figure 16, where the K values are lower than the majority of compositions indicating successful alumina formation.

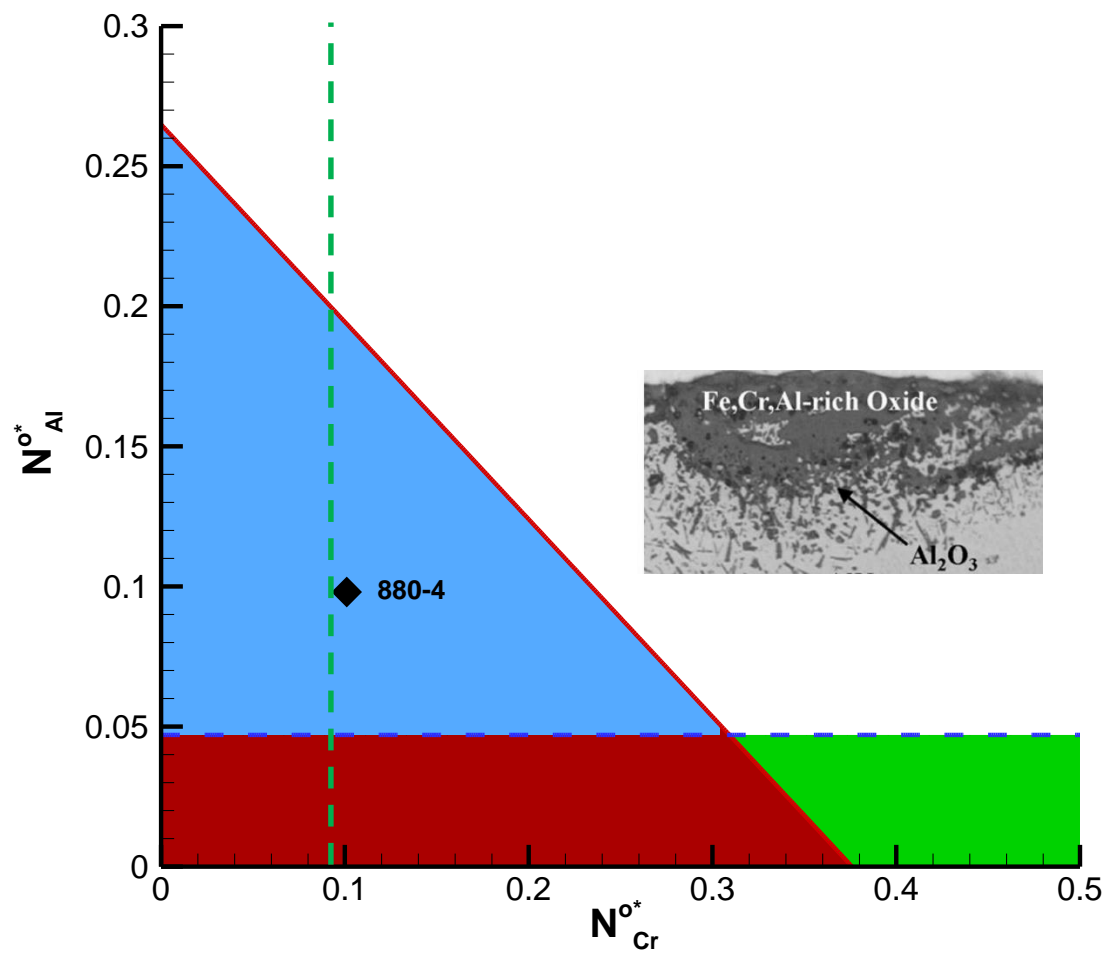


Figure 34 Third Element Effect of Alloy 880-4 *Forms Unstable Oxide Layer [8]

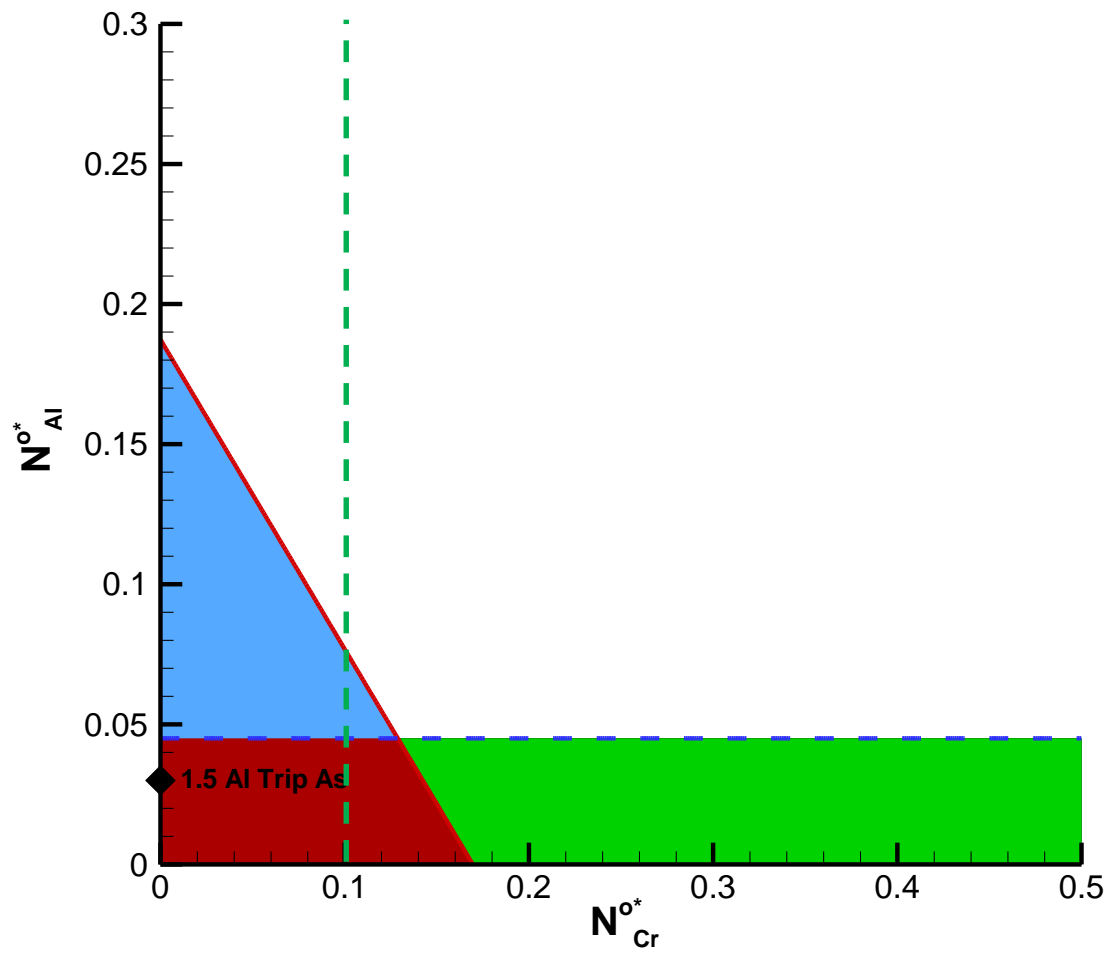


Figure 35 Third Element Effect of 1.5 Al Trip As *Forms Unstable Oxide Layer [8]

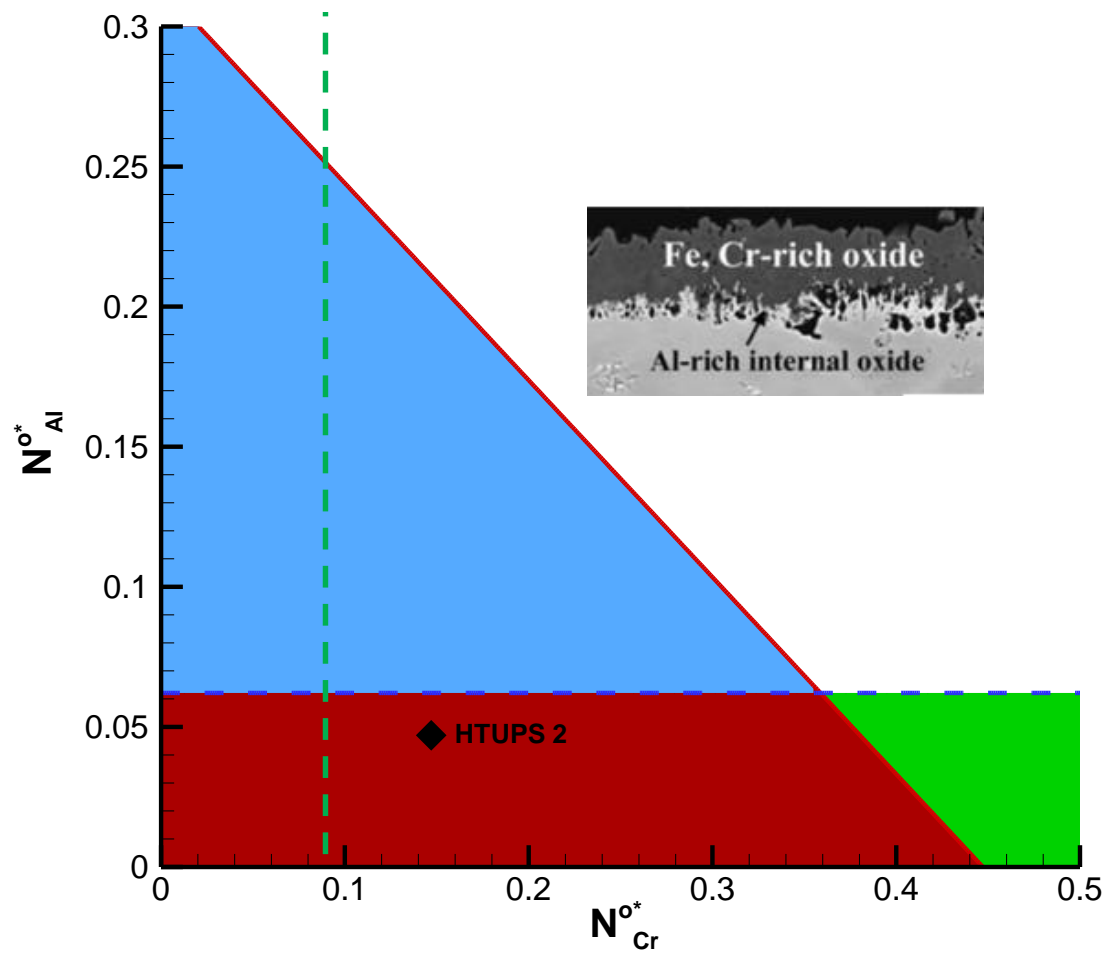


Figure 36 Third Element Effect of HTUPS 2 *Forms Unstable Oxide Layer [6, 15]

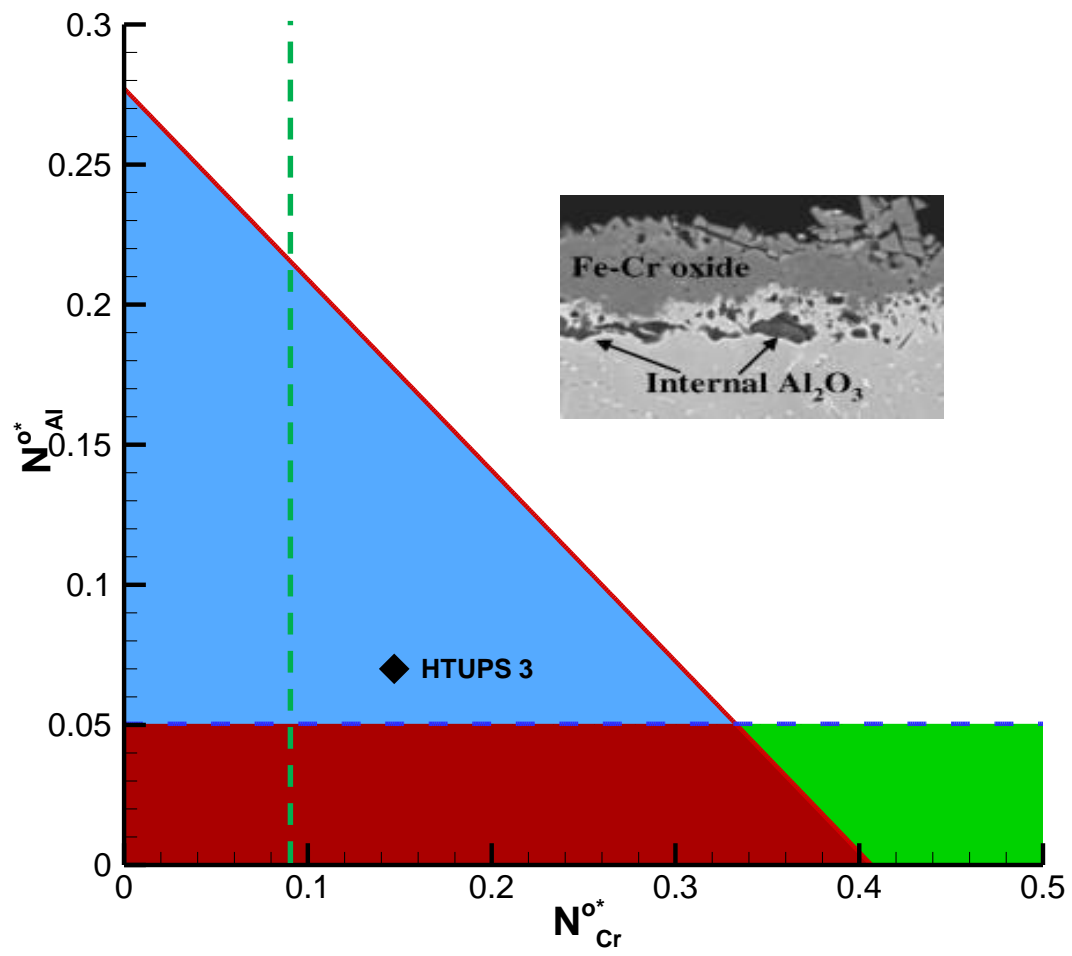


Figure 37 Third Element Effect of HTUPS 3 *Forms Unstable Oxide Layer [6, 15]

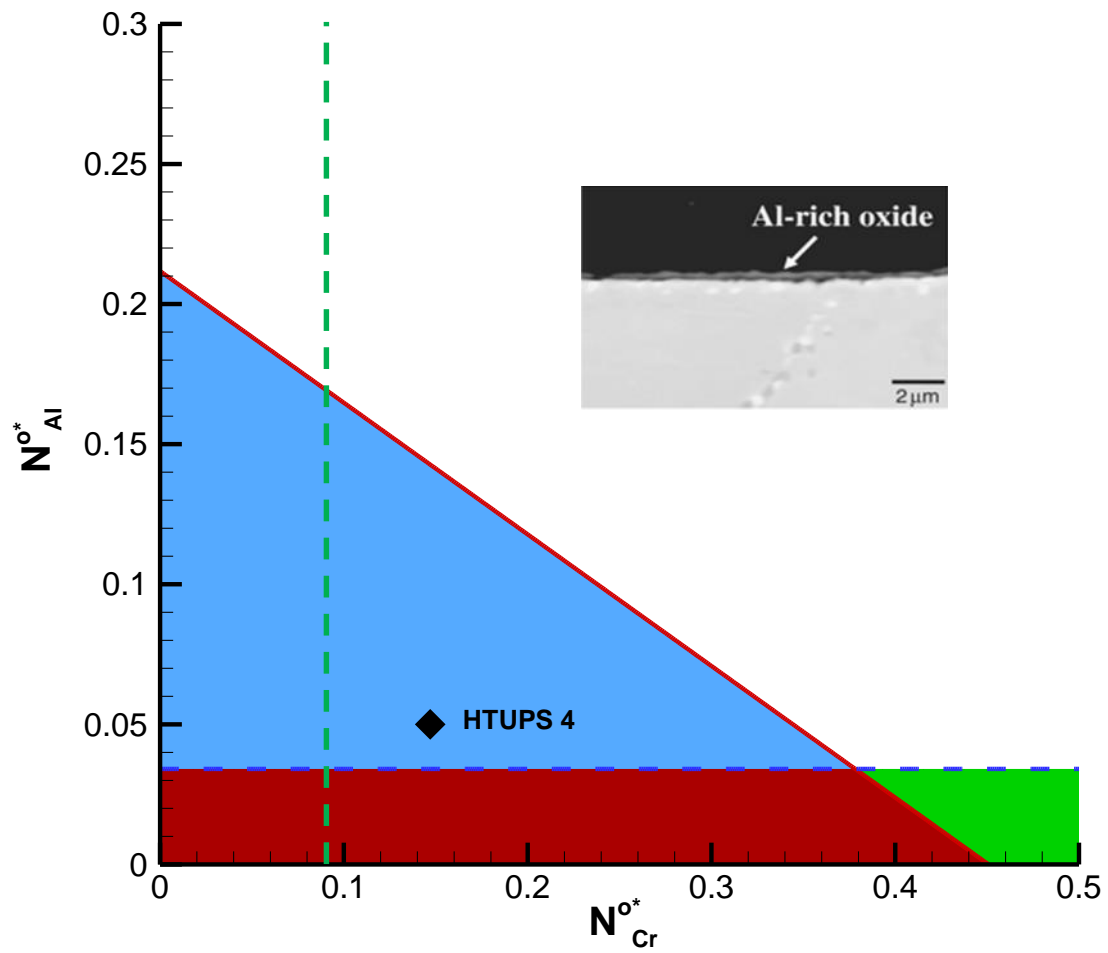


Figure 38 Third Element Effect of HTUPS 4 *Forms Stable Oxide Layer [6, 15]

In the other alloys seen above, Figure 34, Figure 35, Figure 36, Figure 37, Figure 38, the third element models show that, with an exception from the alloy HTUPS 4 where the alloy is experimentally shown to have obtained a stable alumina passive layer, alloys need to show favorable conditions for both the third element model and effective valence model in order to have a high chance of a stable alumina layer to form. If an alloy only shows favorable conditions in one of the models but not the other, as seen in Figure 34 and Figure 37, where the alumina formation trend contrasted the effective valence contour model in Figure 16, that particular alloy composition will most likely be unable to form a stable alumina layer.

In order to better understand the relationship between the third element effect phenomena, free energy, effective valence, and stable alumina scale formation, Figure 39 is used as a graphical simplification. The third element phenomena is assigned a value of either 1 or 0, where 1 is favorable conditions for third element and 0 is unfavorable conditions. The effective valence value is combined with the alloy's free energy value as the K value, as discussed in previous chapters. The K value is then normalized with the previously determined optimal K value line for alumina formation, 700. The two values of K and third element are then combined for an overall view of probability of alumina formation. With a value of two or above required for stable alumina formation in an alloy, it becomes much more obvious which alloys pass the rigorous conditions for alumina formation. With very few exceptions, such as HTUPS 4, the combined effective valence and third element model establishes a very good trend for stable alumina oxide formation

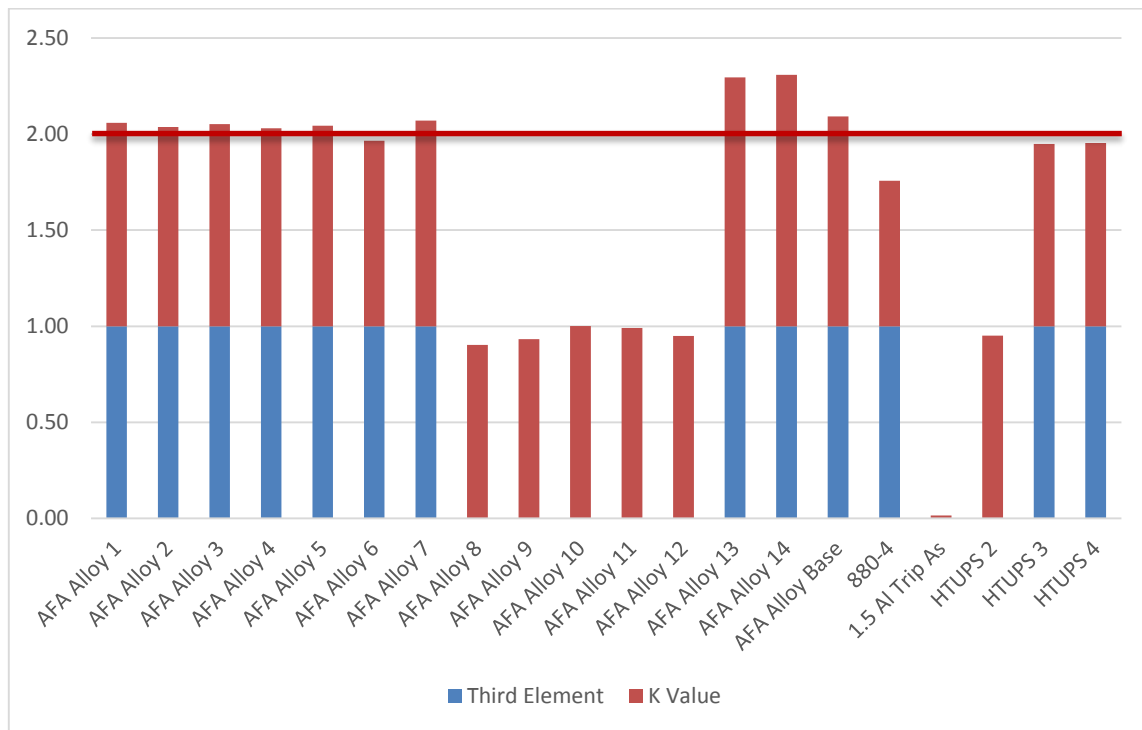


Figure 39 Normalized Compiled K and Third Element Value for Experimental Alloys

CHAPTER VII

GENETIC ALGORITHM

Steel alloy in the material science field is an extremely complicated system that contains many nonlinear relationships between composition and alloy properties. A typical austenitic stainless steel, for example, contains at least eight variables that need to be taken into account. Therefore, although steels have been the subject to a plethora of experimental and theoretical studies, optimization is still extremely relevant.

Using GA for Optimization

To improve both corrosive and mechanical performances, the designing process can be simply divided into four distinct steps seen below: material selection, alloy oxide design, performance, and cost evaluation.

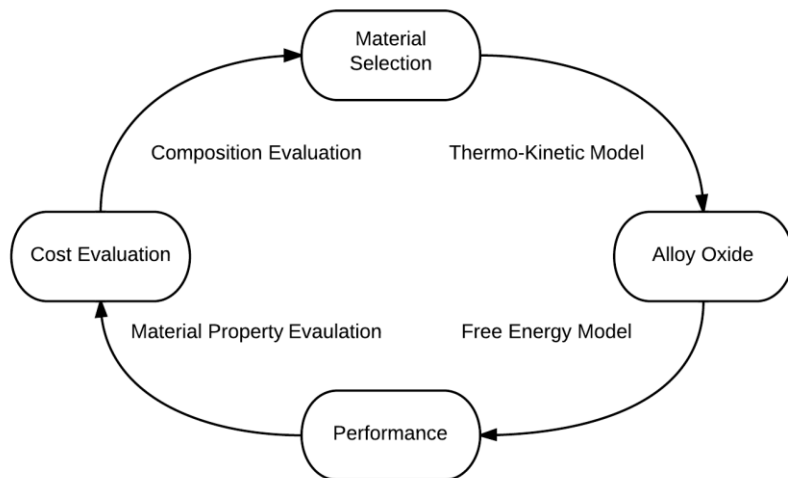


Figure 40 Alloy Design Process Schematic

In this work, once the material is selected, GA is implemented as a computer simulation in which a population of abstract representations of alloy solutions evolves to develop a solution to the optimization problem. The thermodynamic and kinetic models from the effective valence and third element models, which are utilized to predict alumina formation as described in previous chapters, are linked to GA to create a composition landscape that indicates the trend of alumina formation. To evaluate the alloy performance, the alloy matrix is evaluated through Thermocalc where it must have a minimum of phase composition of 99% austenite. The martensitic start temperature is also used through the implementation of Ishida's empirical equation. [65, 66] Cost evaluation is then done through a fitness function that minimizes the element composition based on the costs of alloying for each element. Through this alloy design process, GA can imitate the evolutionary nature of Darwinism, survival of the fittest, purely through binary encoding of each major alloy trait into the alloy's "genes".

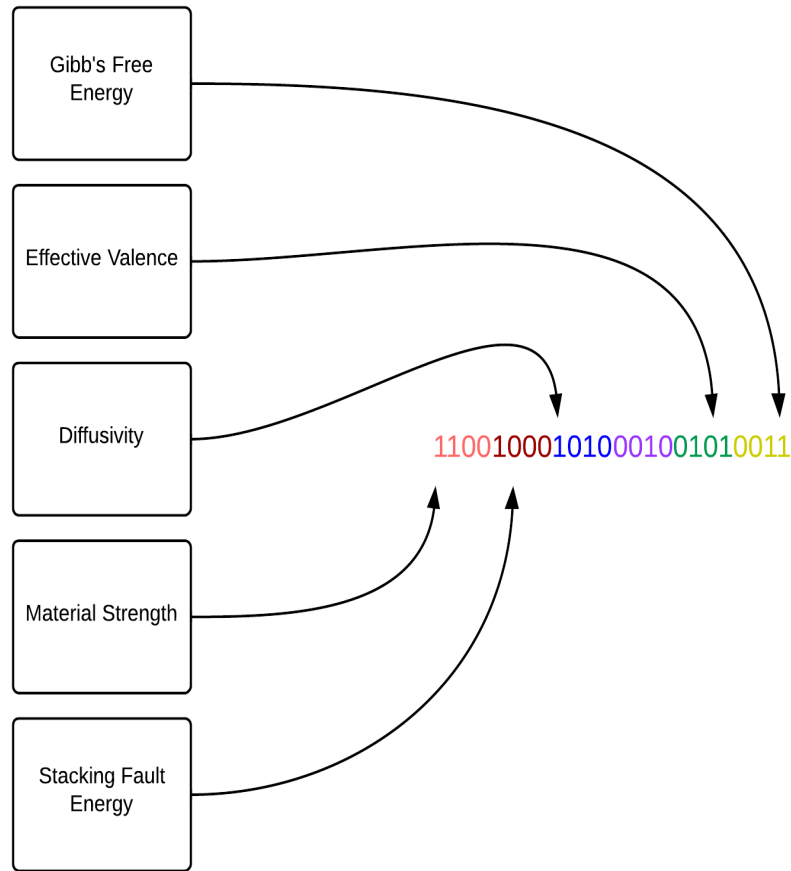


Figure 41 Encoding *Genetic Traits of an Alloy* into GA Simulation

The traits in any given alloy can either be theoretically or experimentally determined and defined; such as free energy, yield strength, diffusivity, hardness, etc. These defined traits are then represented and stored as a numerical value. It is illustrated in Figure 41 that the majority of GA is in the genotype domain due to numerical convenience. The first generation is randomly selected as an initial seed and created as a string. The choice selection then assigns a fitness value in accordance to the physical

properties stored in the strings. The selection and evaluation process is done by eliminating individuals with poor performance and storing the best two in the current generation group. In order to maintain a consistent group size, the surviving individuals are bred together to preserve the dimensions of the cluster. The reproduction process involves cross-overs and mutations to create population diversity. The strings are first randomly paired and have a random chance of exchanging chromosomes, which has been set to fifty percent as seen in Figure 43. After the cross-over process has been completed, the mutation rate equation

$$P = C / (x \cdot A) \quad (16)$$

is used to determine the final changes to the string; the equation of which C represents the chromosome of each string, x is the number of variables in a string, and A is the number strings in the generation. [35-37, 67, 68] Both cross-overs and mutations examples are demonstrated in Figure 42.

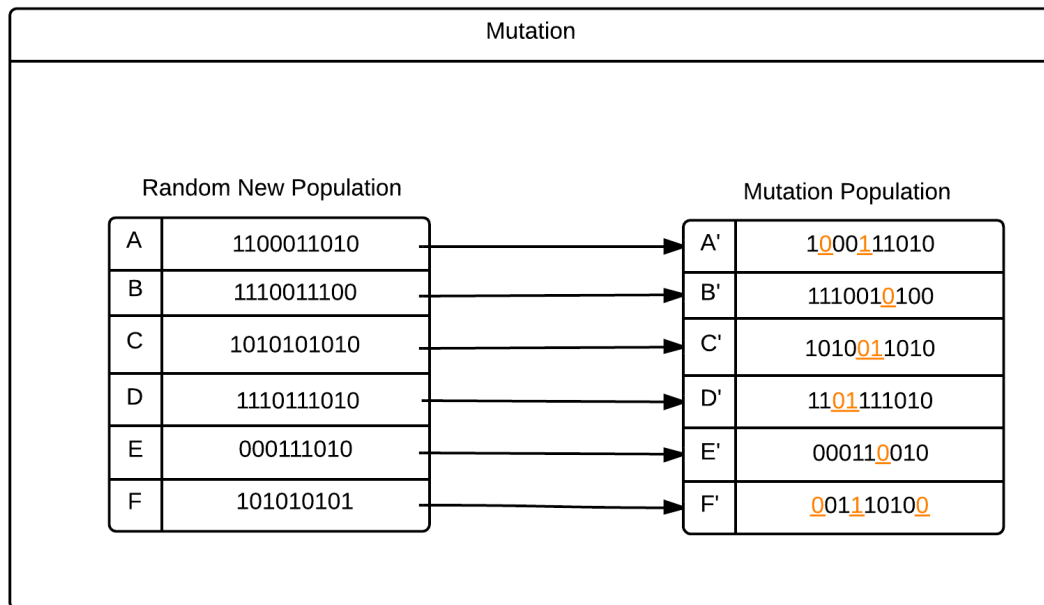
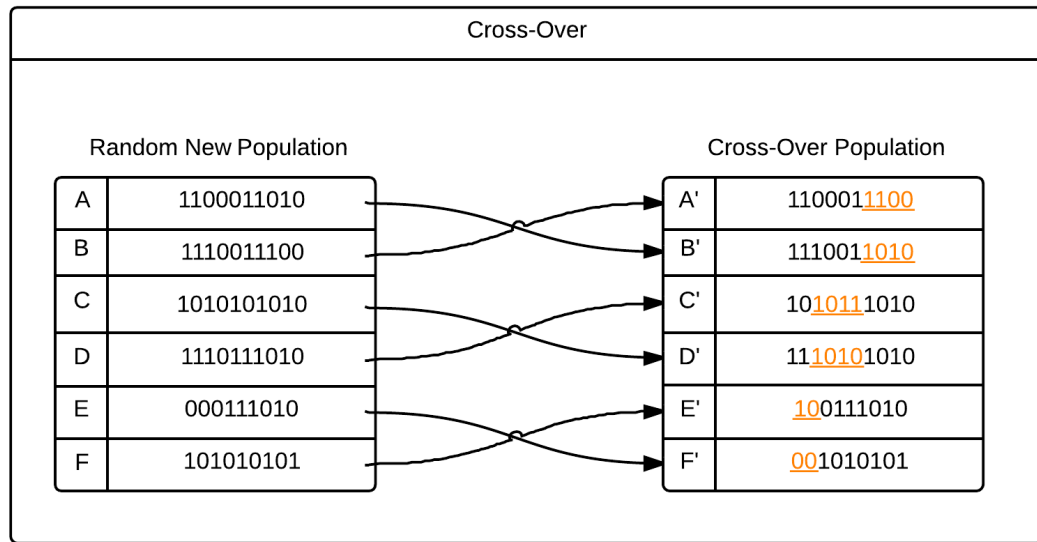


Figure 42 Schematic Diagram of (a) Cross-Over and (b) Mutation

The first step in the GA programming is to generate a random population of alloys within a given composition range. Each individual within the population is analyzed with a number of go/no-go criteria. For any particular individual to be considered, the composition in question needs to be suitable for the given environment; in other words, survival of the fittest. [35] After filtering through the population, the surviving individuals are then randomly selected for reproduction of offspring, whether through cross-overs or mutations, which are then utilized to repopulate the alloy population list. A graphical representation of this process can be seen in Figure 43.

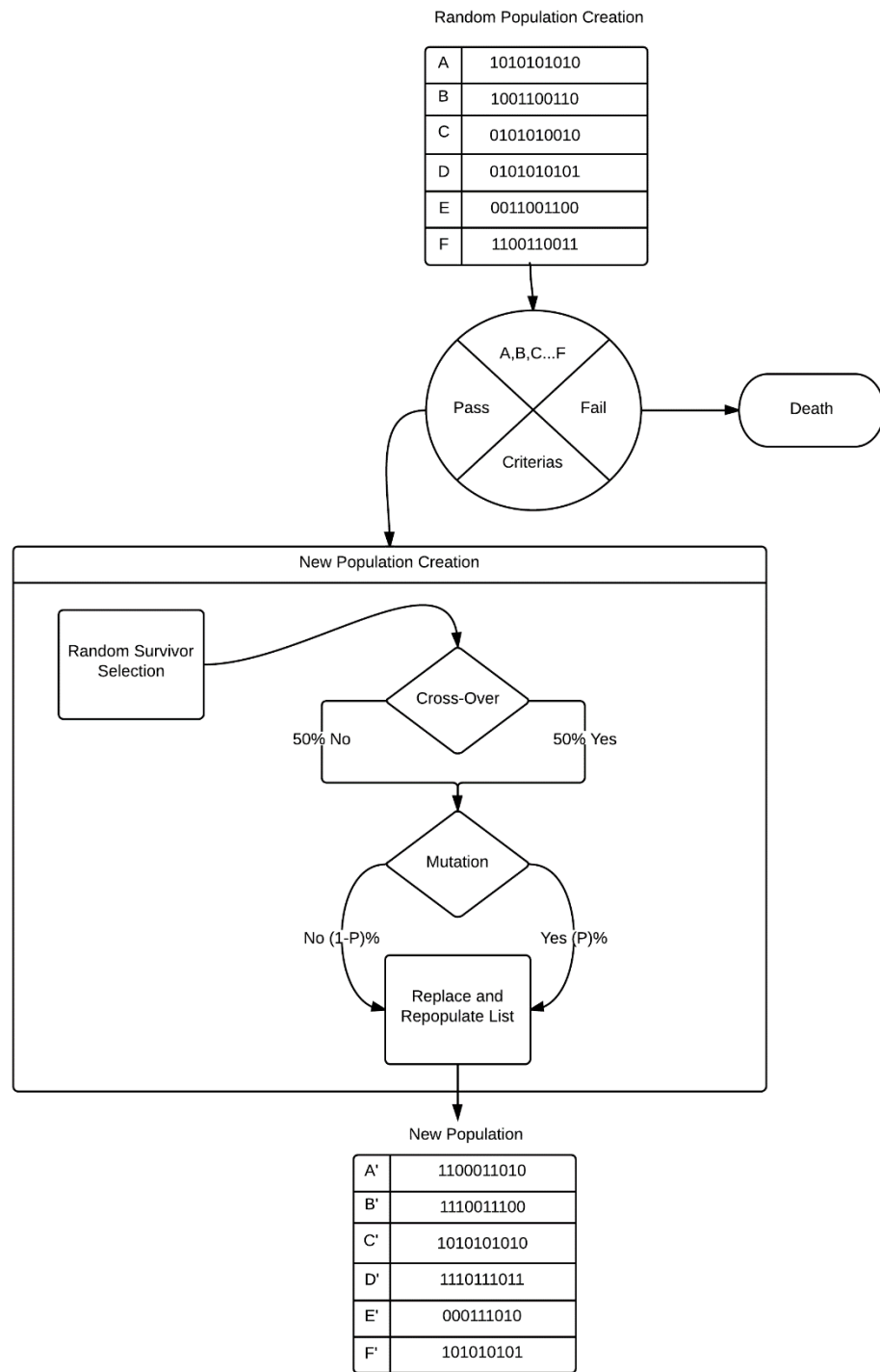


Figure 43 Schematic Diagram of Genetic Algorithm

Discovery Process for Alumina Forming Austenitic Steels through GA

The limitation of GA programming lies in the extremely large search space that a GA has to search through; which is essentially an infinite number of equations and permutations that are possible. Therefore, it is generally required to create a numerical range and criteria for GA to search under.

When GA is first initialized, a random population of alloys is generated along with a set of go/no-go criteria. These criteria are arranged as go/no-go in order to minimize computation time. The creation of the random population is, as mentioned previously, done within a set range of variables which are the elements contained in the alloy composition. The first assessment is the volume fraction maximization of retained austenite; the thermodynamic properties calculated for this alloy criterion are calculated through Thermocalc. To pass the requirement for survival the alloy must contain at least 99% austenite with the matrix. This leads to the next criterion which involves the stability of the austenite within the matrix. In order to appraise the stability of the alloy's structure, the stability of the austenite is evaluated through the martensitic start temperature, T_{ms} , as well as the examination for sigma phase.

With the stability of the alloy established, the next objective is the development of the alumina oxide layer. This criterion is set up as a Boolean pass/fail due to the double-edged benefits of alumina formation. For instance, if the conditions for a stable alumina oxide layer are unfavorable, the structural properties of the material become compromised due to possible formation of undesirables such as aluminum nitride or internal alumina oxide. The development of alumina formation assessment is completed by cross-checking

the information given between the effective valence and third element model discussed earlier in this work. As a further precaution, a small factor of safety is implemented within the alumina formation models; the K value requested of the effective valence model is set to 750 and the required minimum aluminum composition, NAI , is increased by 0.005.

Once a random composition acquiesces to all of the go/no-go criteria, it is given a score through a user-defined function value. The function value consists of the K value, Tms , and alloy composition cost. Using the user defined function value, the alloys that pass the set criteria is recorded into a list of candidate solutions, containing the necessary alumina formation and alloy stability information needed for making an informed alloy design decision.

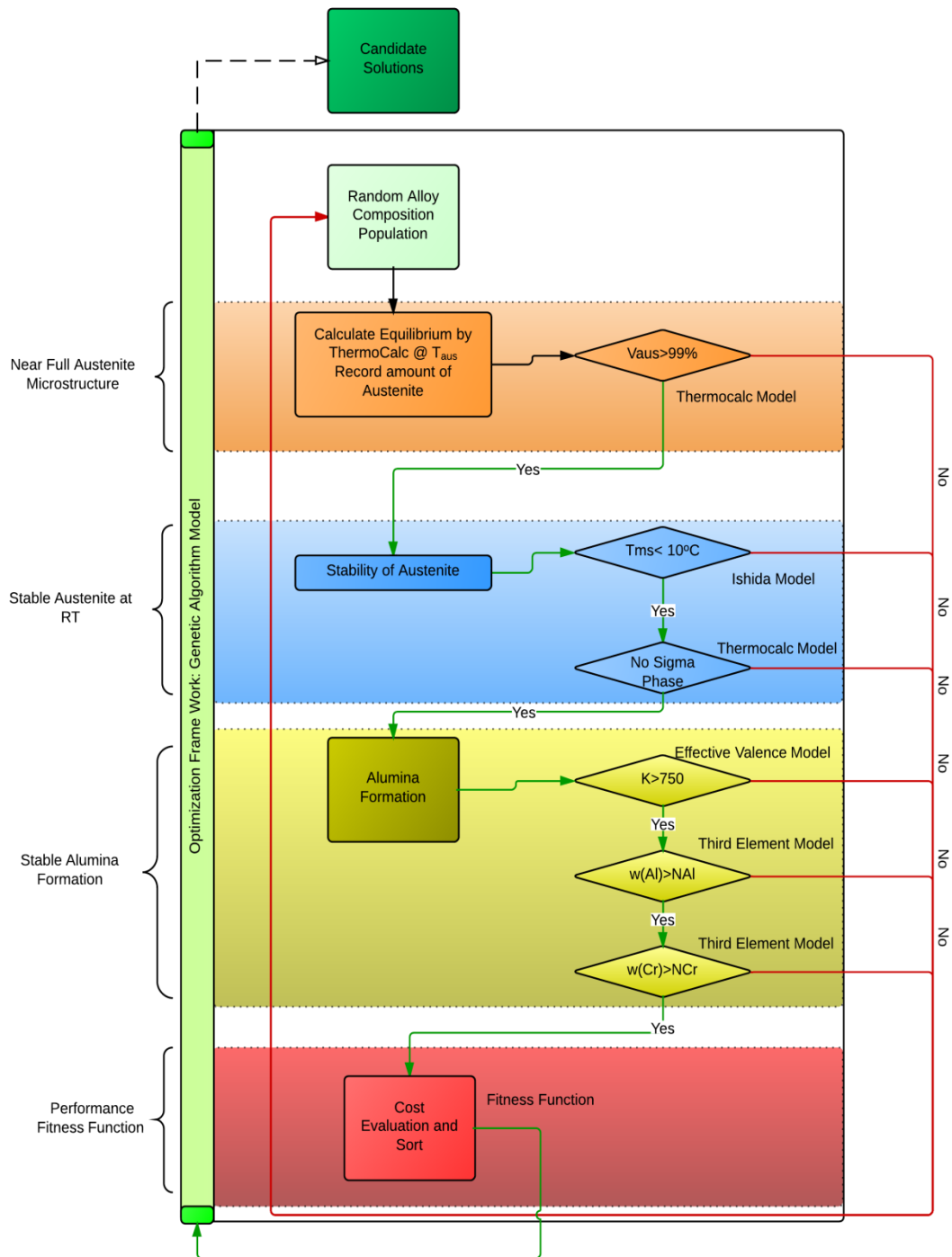


Figure 44 Genetic Algorithm Alloy Design Path

Proposed Alloy Optimization by GA

As mentioned, in order to improve the performance of alumina forming austenitic stainless steel, a properly selected element composition within a reasonable range is needed. Following the study from previous chapters, the domain required for the alloy can be found in Table 1

Table 1 Domain in GA Search for Element Optimization

Domain for Alloying Elements	Min	Max
Volume Fraction of Austenite	90%	100%
Martensitic Start Temperature	~	10°C
K Value (Effective Valence x Free Energy)	750	~
Aluminum	As low as possible	~
Chromium	As low as possible	~

Using the previously discussed criteria, GA was utilized to generate a list of unique alumina forming austenitic stainless steel alloys, see Appendix. As the constraints for the alloy's matrix, mechanical property, and alumina forming are extremely strict, it can be

seen that the alloy generated through GA contain rather similar values for each element. Despite such similarities between some alloys there are no repeated alloys within the generated alloy list by GA.

Although all of the alloy compositions are extremely similar to each other, the GA generated alloys can fall into two distinct groups, high and low manganese content coupled with low and high nickel content, respectively. This interesting trend can be explained by the role each of the elements play in stabilizing austenite and the optimization process of GA. Two example alloys can be seen below in Table 2, where one has 3.8 wt% manganese and the other has 8.9 wt%.

Table 2 Optimized Genetic Algorithm Alloys Proposed by GA

PGAA	Fe	C	Mn	Ni	Mo	Al	Cr	Si
1	Bal.	0.073	3.893	11.000	2.026	2.994	19.820	0.382
2	Bal.	0.088	8.993	17.140	2.242	3.112	15.300	0.194

While both manganese and nickel content both promote austenite stability in the alloy, it is not optimal for both to be maximized. As can be seen in Figure 44 it is only necessary to maintain a 99% phase fraction of austenite; instead of increasing either nickel or manganese content for austenite stability, GA instead uses the newfound leeway for another criteria, such as increasing k value for alumina formation, decreasing martensitic start temperature, or lowering necessary minimum aluminum and chromium for third element effect.

The contour map below, Figure 45, shows where the proposed GA composition lies in terms of its K value, effective energy valence, and free. Using the contour map, it can be seen that the new alloy proposed by GA has a much higher K value than the average experimental composition. This can be attributed to the considerably lower free energy, rather than the effective valence, which in turn increases the K value of the alloy.

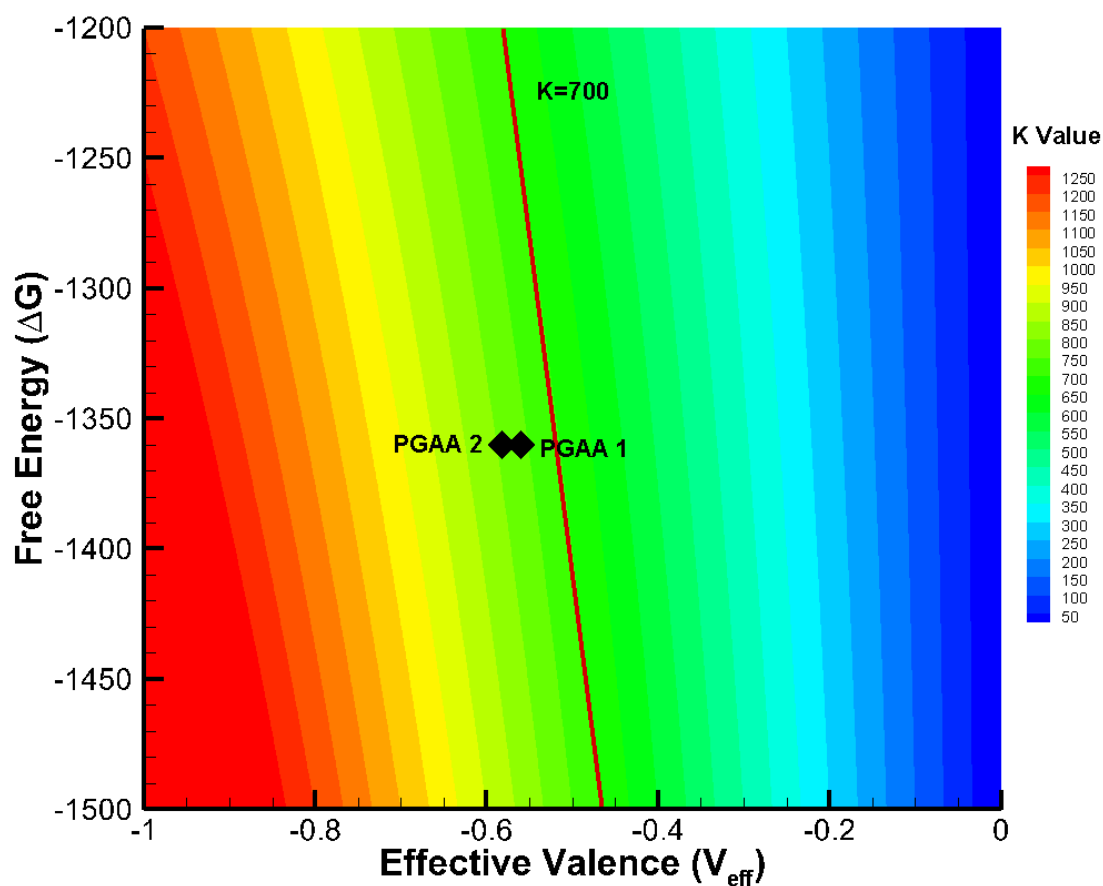


Figure 45 Free Energy, Effective Valence, and K Value of Experimental Alloys

In the third element models seen in Figure 46 and Figure 47, the PGAA alloys 1 and 2 meets the acceptable minimum aluminum and chromium values required for the third element phenomena to favor alumina formation. For both the PGAA alloys, the third element models demonstrated an agreement with the effective valence model. With the combination of both effective valence and third element models showing favorable alumina forming conditions, provided that there are no errors during alloy fabrication, it should be extremely likely for a stable, continuous alumina oxide layer to be formed.

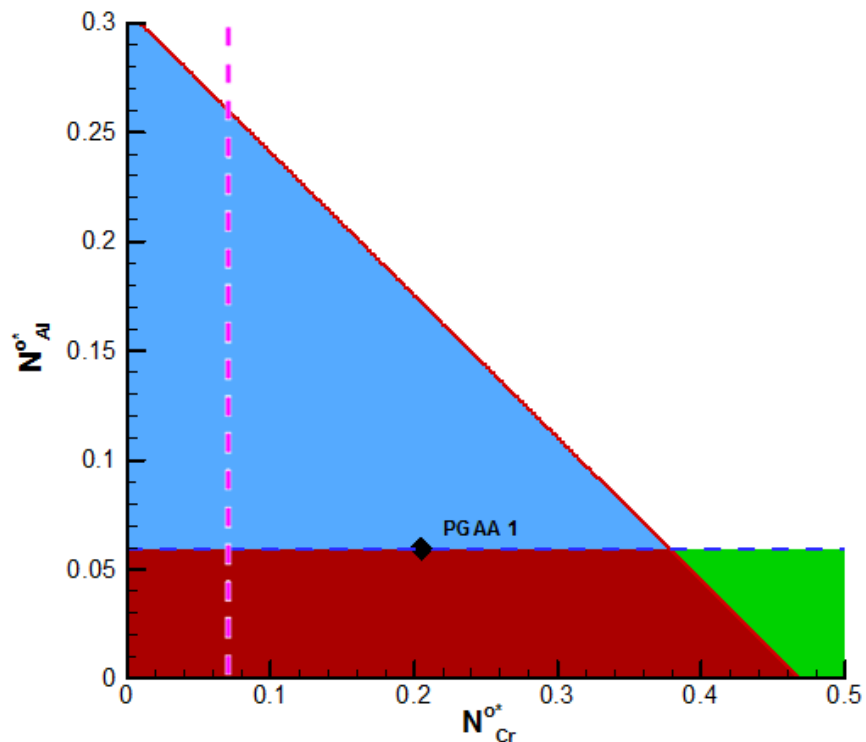


Figure 46 Third Element Effect of PGAA1

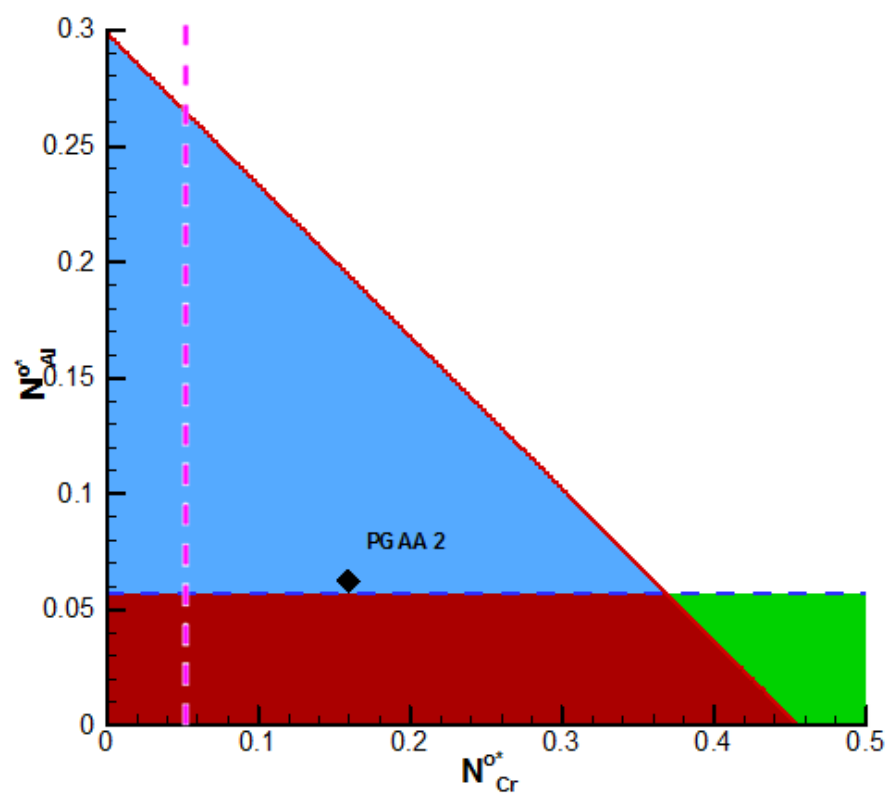


Figure 47 Third Element Effect of PGAA 2

CHAPTER VIII

SUMMARY

In this work, the CALPHAD method is utilized through the implementation of the effective valence and third element models, of which are used to predict alumina formation. In addition to thermodynamics, the commercial code Dictra is used in conjunction with the TCFE7, MOBFE1, and NIST database to accurately predict and model diffusion behavior. Including the kinetic and thermodynamic stability of alumina formation, there are 8 parameters involved in the design process to create and optimize an alloy for peak performance: alloy element composition, austenite formation temperature, martensitic start temperature, phase stability, K value, minimum third element aluminum

In order to predict the state of alumina oxide formation both effective valence and third element models are needed. Although there is a decent trend for alumina formation in both models, there are still inaccuracies within the prediction model; as such, using both models with different prediction methods allows for a better oxide layer calculation where the prediction must agree for both the effective valence and third element phenomena models.

Using the fairly reliable prediction of alumina scale formation, GA is implemented as the next step in the alloy design process. Using GA, it becomes much more computationally affordable for alloy discovery and optimization, both of which are completed through GA's survival of the fittest routine and fitness function.

REFERENCES

- [1] AG EIE. IEA, 2001.
- [2] OECD. OECD/IEA, 2006.
- [3] Kofstad P, et al., vol. 468: Elsevier Applied Science London, 1988.
- [4] Opila EJ. Trans Tech Publ, 2004. p.765.
- [5] Meier GH, Materials and Corrosion, vol. 47, 1996. p.595.
- [6] Yamamoto Y, et al.: Oak Ridge National Laboratory (ORNL); Shared Research Equipment Collaborative Research Center, 2008.
- [7] Kubaschewski O, et al., vol. Oxford: Pergamon, 1967.
- [8] Brady MP, et al., Oxid Met, vol. 75, 2011. p.337.
- [9] Brady MP, et al., Stainless Steel World, vol., 2008. p.1.
- [10] Brady MP, et al., Materials Science Forum, vol. 595, 2008. p.725.
- [11] Brady MP, et al., JOM-Journal of Metals, Minerals, and Materials Society, vol. 60, 2008. p.12.
- [12] Brady MP, et al., Scripta Materialia, vol. 57, 2007. p.1117.
- [13] Pint BA, et al.: American Society of Mechanical Engineers, 2007. p.995.
- [14] Yamamoto Y, et al., Metallurgical and Materials Transactions A, vol. 38, 2007. p.2737.
- [15] Yamamoto Y, et al., Science, vol. 316, 2007. p.433.
- [16] Yamamoto Y, et al., Metallurgical and Materials Transactions A, vol. 42, 2011. p.922.
- [17] Yamamoto Y, et al., Intermetallics, vol. 16, 2008. p.453.
- [18] Nie X, et al., Surface and Coatings Technology, vol. 149, 2002. p.245.

- [19] Peraldi R, et al.: Trans Tech Publ, 2004. p.815.
- [20] Prescott R, et al., Oxid Met, vol. 38, 1992. p.233.
- [21] Saluja R, et al., International Journal of Engineering Science & Technology, vol. 4, 2012.
- [22] Wagner C, Z. Elektrochem, vol. 63, 1959. p.772.
- [23] Kofstad P, et al.: Robert E. Krieger Publ., Malabar, FL.
- [24] Sato A, et al., Acta Materialia, vol. 59, 2011. p.225.
- [25] Crank J, London: Oxford University Press, 1979.
- [26] Gesmundo F, et al., Oxid Met, vol. 50, 1998. p.1.
- [27] Gesmundo F, et al., Oxid Met, vol. 25, 1986. p.269.
- [28] Niu Y, et al., Oxid Met, vol. 62, 2004. p.391.
- [29] Niu Y, et al., Corrosion science, vol. 48, 2006. p.4020.
- [30] Rapp RA, Corrosion, vol. 21, 1965. p.382.
- [31] Sundman B, Journal of Phase Equilibria, vol. 12, 1991. p.127.
- [32] Stott F, et al., Oxid Met, vol. 44, 1995. p.113.
- [33] Tomaszewicz P, et al., Oxid Met, vol. 20, 1983. p.75.
- [34] Niu Y, et al., Corrosion Science, vol. 50, 2008. p.345.
- [35] Goldberg DE, vol. 412: Addison-Wesley Reading Menlo Park, 1989.
- [36] Renner G, et al., Computer-Aided Design, vol. 35, 2003. p.709.
- [37] Ganguly S, et al., Computational Materials Science, vol. 45, 2009. p.158.
- [38] Kulkarni AJ, et al., Materials Science and Engineering: A, vol. 372, 2004. p.213.
- [39] Kuroda M, et al., Materials Science and Engineering: A, vol. 385, 2004. p.235.

- [40] Xu W, et al., *Acta Materialia*, vol. 58, 2010. p.3582.
- [41] Ceder G, et al., *Modelling and Simulation in Materials Science and Engineering*, vol. 8, 2000. p.311.
- [42] Mott N, *Trans. Faraday Soc.*, vol. 35, 1939. p.1175.
- [43] Hagel W, *Corrosion*, vol. 21, 1965. p.316.
- [44] Wood GC, *Oxid Met*, vol. 2, 1970. p.11.
- [45] Anderson J, vol. 1: Elsevier, 2012.
- [46] Furukawa GT, et al., *J Res Nat Bur Stand*, vol. 57, 1956. p.67.
- [47] Lee SK, et al., *Physical Review Letters*, vol. 103, 2009. p.095501.
- [48] Huntz A: Springer, 1989. p.81.
- [49] Lang E, vol.: Springer, 1989.
- [50] Reddy KPR, et al., *Oxid Met*, vol. 17, 1982. p.429.
- [51] Lukas HL, et al., vol. 131: Cambridge University Press Cambridge, 2007.
- [52] Andersson JO, et al., *Journal of applied physics*, vol. 72, 1992. p.1350.
- [53] Balluffi RW, et al., vol.: John Wiley & Sons, 2005.
- [54] Lupis CH, vol. 251: North-Holland New York et al., 1983.
- [55] AL S, *Metal progress*, vol. 106, 1974. p.227.
- [56] Azuma S, et al., *Corrosion Science*, vol. 46, 2004. p.2265.
- [57] Borland J, et al., *British Welding Journal*, vol. 7, 1960. p.22.
- [58] Copson HR, *Interscience*, New York, vol. 247, 1959.
- [59] Cunat P-J, *International Chromium Development Association*, Paris, 2004.
- [60] Korinko P, et al., *Practical Failure Analysis*, vol. 1, 2001. p.61.

- [61] Kyriakongonas A, et al., Analysis and Design of Marine Structures, vol. 1, 2009. p.371.
- [62] Shankar V, et al., Sadhana, vol. 28, 2003. p.359.
- [63] Lippold JC, et al., vol. 1. University of Michigan: Wiley-Interscience, 2005.
- [64] Brady M, et al., Materials Science and Engineering: A, vol. 590, 2014. p.101.
- [65] Ishida K, Journal of Alloys and Compounds, vol. 220, 1995. p.126.
- [66] Lu Q, et al., Acta Materialia, vol. 64, 2014. p.133.
- [67] Chakraborti N, International Materials Reviews, vol. 49, 2004. p.246.
- [68] Deb K, John Wiley & Sons Chichester, 2001.

APPENDIX

Table 3 Experimental Alumina Forming Alloys

	Fe	Ni	Cr	Al	Si	Mn	Mo	Nb	Ti	V	C	B	Cu	W
AFA Alloy 1	Bal.	25.02	14.06	3.06	0.14	2.00	2.00	1.02	0.05	0.05	0.0470	0.0096	0.52	0.96
AFA Alloy 2	Bal.	25.05	13.99	3.03	0.15	2.00	2.00	1.00	0.05	0.05	0.2040	0.0104	0.51	0.96
AFA Alloy 3	Bal.	25.05	14.03	4.13	0.14	2.00	2.00	0.99	0.05	0.05	0.0490	0.0100	0.52	0.96
AFA Alloy 4	Bal.	25.03	13.97	4.11	0.14	2.00	1.99	1.01	0.05	0.05	0.2090	0.0104	0.52	0.96
AFA Alloy 5	Bal.	25.02	13.84	3.06	0.13	1.99	2.00	1.02	0.05	0.05	0.1060	0.0078	0.51	0.96
AFA Alloy 6	Bal.	20.05	13.84	3.07	0.13	2.00	1.99	1.01	0.05	0.05	0.2000	0.0080	0.52	0.97
AFA Alloy 7	Bal.	25.05	13.98	4.17	0.14	1.99	1.98	2.53	0.05	0.05	0.2010	0.0092	0.52	0.97
AFA Alloy 8	Bal.	12.08	13.84	2.52	0.13	4.99	0.15	1.03	0.05	0.05	0.1710	0.0110	3.04	0.15
AFA Alloy 9	Bal.	12.05	13.84	2.52	0.13	6.79	0.15	1.01	0.05	0.05	0.2000	0.0090	3.06	0.15
AFA Alloy 10	Bal.	12.04	13.92	2.52	0.14	9.93	0.15	1.01	0.05	0.05	0.1000	0.0090	3.06	0.14
AFA Alloy 11	Bal.	12.09	13.89	2.54	0.14	9.96	0.15	1.01	0.05	0.05	0.2000	0.0090	3.06	0.15
AFA Alloy 12	Bal.	32.06	18.69	3.10	0.13	6.96	0.15	3.32	0.05	0.05	0.1140	0.0017	0.15	0.14
AFA Alloy 13	Bal.	32.06	18.69	3.10	0.13	0.15	0.15	3.32	0.05	0.05	0.1110	0.0017	0.15	0.14
AFA Alloy 14	Bal.	32.08	18.72	3.08	0.13	0.15	0.15	3.27	0.05	0.05	0.0160	0.0018	0.15	0.14
AFA Alloy Base	Bal.	25.20	14.90	3.00	0.15	1.90	2.00	2.50	0.00	0.00	0.0900	0.0100	0.00	0.00
880-4	Bal.	24.40	9.70	4.80	0.40	0.15	0.00	0.00	0.00	0.00	0.1300	0.0005	0.00	0.00
1.5 Al Trip As	Bal.	0.00	0.00	1.50	0.06	1.55	0.00	0.00	0.00	0.00	0.1100	0.0000	0.00	0.00
HTUPS 2	Bal.	20.00	14.20	2.40	0.15	1.95	2.46	0.14	0.31	0.50	0.0760	0.0110	0.00	0.00
HTUPS 3	Bal.	19.98	14.21	3.67	0.10	1.92	2.46	0.14	0.31	0.49	0.0790	0.0110	0.00	0.00
HTUPS 4	Bal.	19.95	14.19	2.48	0.15	1.95	2.46	0.86	0.00	0.00	0.0750	0.0100	0.00	0.00

Table 4 Proposed GA Alloy List

C	Mn	Ni	Mo	Al	Cr	Si	Tms	Val	ΔG
2.46E-03	9.71E-02	1.52E-01	2.38E-02	2.00E-02	1.92E-01	1.45E-03	-2.35E+02	-6.49E-01	-1.35E+03
2.46E-03	9.56E-02	1.56E-01	2.42E-02	2.00E-02	1.81E-01	1.94E-03	-2.21E+02	-6.28E-01	-1.35E+03
2.46E-03	9.56E-02	1.56E-01	2.39E-02	2.03E-02	1.81E-01	1.53E-03	-2.21E+02	-6.29E-01	-1.35E+03
2.46E-03	9.56E-02	1.56E-01	2.42E-02	2.00E-02	1.81E-01	1.53E-03	-2.21E+02	-6.29E-01	-1.35E+03
2.46E-03	9.50E-02	1.56E-01	2.39E-02	2.02E-02	1.81E-01	1.58E-03	-2.20E+02	-6.28E-01	-1.35E+03
2.46E-03	9.56E-02	1.55E-01	2.42E-02	2.00E-02	1.81E-01	1.53E-03	-2.20E+02	-6.28E-01	-1.35E+03
2.46E-03	9.56E-02	1.56E-01	2.39E-02	2.02E-02	1.79E-01	1.53E-03	-2.19E+02	-6.26E-01	-1.35E+03
2.46E-03	9.56E-02	1.56E-01	2.41E-02	2.06E-02	1.79E-01	1.53E-03	-2.19E+02	-6.26E-01	-1.35E+03
2.46E-03	9.56E-02	1.56E-01	2.39E-02	2.00E-02	1.79E-01	1.53E-03	-2.19E+02	-6.26E-01	-1.35E+03
2.46E-03	9.56E-02	1.56E-01	2.41E-02	2.06E-02	1.79E-01	1.99E-03	-2.18E+02	-6.23E-01	-1.35E+03
2.46E-03	9.50E-02	1.56E-01	2.39E-02	2.00E-02	1.79E-01	1.53E-03	-2.18E+02	-6.25E-01	-1.35E+03
2.46E-03	9.50E-02	1.56E-01	2.39E-02	2.02E-02	1.79E-01	1.53E-03	-2.18E+02	-6.25E-01	-1.35E+03
2.46E-03	9.56E-02	1.56E-01	2.48E-02	2.00E-02	1.78E-01	1.94E-03	-2.17E+02	-6.22E-01	-1.35E+03
2.46E-03	9.56E-02	1.56E-01	2.42E-02	2.00E-02	1.78E-01	1.99E-03	-2.17E+02	-6.21E-01	-1.35E+03
2.46E-03	9.56E-02	1.56E-01	2.48E-02	2.00E-02	1.78E-01	1.94E-03	-2.17E+02	-6.22E-01	-1.35E+03
2.46E-03	9.56E-02	1.55E-01	2.17E-02	2.51E-02	1.80E-01	2.36E-03	-2.17E+02	-6.17E-01	-1.36E+03
2.46E-03	9.56E-02	1.56E-01	2.42E-02	2.00E-02	1.78E-01	1.94E-03	-2.17E+02	-6.21E-01	-1.35E+03
2.46E-03	9.56E-02	1.56E-01	2.42E-02	2.00E-02	1.78E-01	1.94E-03	-2.16E+02	-6.21E-01	-1.35E+03
2.46E-03	9.50E-02	1.56E-01	2.39E-02	2.00E-02	1.76E-01	4.84E-03	-2.15E+02	-6.10E-01	-1.35E+03
2.46E-03	9.56E-02	1.56E-01	2.42E-02	2.00E-02	1.77E-01	1.94E-03	-2.15E+02	-6.20E-01	-1.35E+03
2.46E-03	9.56E-02	1.56E-01	2.42E-02	2.00E-02	1.77E-01	1.84E-03	-2.15E+02	-6.20E-01	-1.35E+03
2.46E-03	9.58E-02	1.56E-01	2.39E-02	2.00E-02	1.76E-01	1.58E-03	-2.15E+02	-6.19E-01	-1.35E+03
2.46E-03	9.50E-02	1.56E-01	2.42E-02	2.01E-02	1.77E-01	3.18E-03	-2.15E+02	-6.16E-01	-1.35E+03
2.46E-03	9.50E-02	1.56E-01	2.42E-02	2.01E-02	1.77E-01	3.08E-03	-2.15E+02	-6.16E-01	-1.35E+03
2.46E-03	9.50E-02	1.56E-01	2.42E-02	2.51E-02	1.77E-01	3.60E-03	-2.14E+02	-6.12E-01	-1.36E+03
2.46E-03	9.50E-02	1.53E-01	2.39E-02	2.06E-02	1.79E-01	1.58E-03	-2.14E+02	-6.22E-01	-1.35E+03
2.25E-03	9.43E-02	1.58E-01	2.22E-02	2.03E-02	1.81E-01	1.63E-03	-2.13E+02	-6.29E-01	-1.35E+03
2.43E-03	8.67E-02	1.56E-01	2.39E-02	2.06E-02	1.89E-01	4.84E-03	-2.13E+02	-6.27E-01	-1.35E+03
2.53E-03	9.82E-02	1.54E-01	2.31E-02	2.34E-02	1.68E-01	7.06E-03	-2.12E+02	-5.85E-01	-1.36E+03
3.01E-03	9.04E-02	1.55E-01	2.31E-02	2.85E-02	1.68E-01	2.72E-03	-2.06E+02	-5.83E-01	-1.36E+03
2.52E-03	8.44E-02	1.53E-01	2.40E-02	2.61E-02	1.84E-01	3.93E-03	-1.98E+02	-6.12E-01	-1.36E+03
2.46E-03	8.52E-02	1.56E-01	2.42E-02	2.51E-02	1.81E-01	2.01E-03	-1.96E+02	-6.14E-01	-1.35E+03
2.46E-03	8.72E-02	1.56E-01	2.30E-02	2.54E-02	1.77E-01	3.54E-03	-1.96E+02	-6.03E-01	-1.36E+03
2.25E-03	8.70E-02	1.58E-01	2.13E-02	2.27E-02	1.81E-01	3.18E-03	-1.96E+02	-6.14E-01	-1.35E+03
2.46E-03	8.65E-02	1.56E-01	2.39E-02	2.00E-02	1.76E-01	4.84E-03	-1.96E+02	-6.02E-01	-1.35E+03
3.03E-03	9.82E-02	1.31E-01	2.31E-02	2.85E-02	1.67E-01	4.68E-03	-1.95E+02	-5.63E-01	-1.36E+03
2.89E-03	8.46E-02	1.58E-01	2.06E-02	2.66E-02	1.68E-01	5.96E-03	-1.95E+02	-5.72E-01	-1.36E+03
2.89E-03	8.46E-02	1.58E-01	2.06E-02	2.66E-02	1.68E-01	5.95E-03	-1.94E+02	-5.72E-01	-1.36E+03
2.25E-03	8.70E-02	1.58E-01	2.13E-02	2.25E-02	1.78E-01	6.90E-03	-1.94E+02	-5.98E-01	-1.35E+03
2.25E-03	8.70E-02	1.58E-01	2.13E-02	2.27E-02	1.78E-01	6.49E-03	-1.94E+02	-5.99E-01	-1.35E+03
3.03E-03	9.82E-02	1.31E-01	2.31E-02	2.85E-02	1.67E-01	3.54E-03	-1.94E+02	-5.65E-01	-1.36E+03
2.85E-03	8.46E-02	1.58E-01	2.06E-02	2.91E-02	1.68E-01	5.95E-03	-1.93E+02	-5.70E-01	-1.36E+03
2.25E-03	8.64E-02	1.58E-01	2.13E-02	2.30E-02	1.78E-01	6.49E-03	-1.93E+02	-5.99E-01	-1.35E+03

Table 4 Continued

C	Mn	Ni	Mo	Al	Cr	Si	Tms	Val	ΔG
2.85E-03	8.46E-02	1.58E-01	2.02E-02	2.91E-02	1.68E-01	5.96E-03	-1.93E+02	-5.70E-01	-1.36E+03
2.25E-03	8.64E-02	1.58E-01	2.13E-02	2.25E-02	1.78E-01	6.49E-03	-1.92E+02	-5.99E-01	-1.35E+03
2.85E-03	8.46E-02	1.57E-01	2.06E-02	2.66E-02	1.68E-01	5.97E-03	-1.92E+02	-5.71E-01	-1.36E+03
2.85E-03	8.46E-02	1.57E-01	2.06E-02	2.66E-02	1.68E-01	5.95E-03	-1.92E+02	-5.71E-01	-1.36E+03
2.85E-03	8.46E-02	1.57E-01	2.02E-02	2.91E-02	1.68E-01	5.95E-03	-1.91E+02	-5.69E-01	-1.36E+03
2.46E-03	8.54E-02	1.56E-01	2.39E-02	2.00E-02	1.76E-01	1.58E-03	-1.91E+02	-6.09E-01	-1.35E+03
2.50E-03	9.66E-02	1.33E-01	2.44E-02	2.13E-02	1.75E-01	3.13E-03	-1.87E+02	-5.91E-01	-1.35E+03
2.81E-03	9.82E-02	1.30E-01	2.31E-02	2.34E-02	1.68E-01	4.37E-03	-1.87E+02	-5.67E-01	-1.36E+03
2.89E-03	8.46E-02	1.51E-01	2.04E-02	2.66E-02	1.68E-01	5.95E-03	-1.85E+02	-5.64E-01	-1.36E+03
2.74E-03	9.82E-02	1.31E-01	2.31E-02	2.85E-02	1.67E-01	3.54E-03	-1.85E+02	-5.67E-01	-1.36E+03
2.50E-03	9.11E-02	1.33E-01	2.48E-02	2.00E-02	1.75E-01	3.08E-03	-1.75E+02	-5.88E-01	-1.35E+03
4.05E-03	4.59E-02	1.60E-01	2.37E-02	3.32E-02	1.85E-01	7.42E-03	-1.72E+02	-5.61E-01	-1.36E+03
1.69E-03	9.37E-02	1.58E-01	2.10E-02	2.13E-02	1.59E-01	7.74E-03	-1.66E+02	-5.70E-01	-1.35E+03
2.22E-03	9.14E-02	1.33E-01	2.22E-02	2.13E-02	1.75E-01	3.49E-03	-1.65E+02	-5.84E-01	-1.35E+03
2.78E-03	8.36E-02	1.33E-01	2.04E-02	2.64E-02	1.69E-01	2.73E-03	-1.55E+02	-5.57E-01	-1.36E+03
1.72E-03	8.64E-02	1.55E-01	2.07E-02	2.63E-02	1.60E-01	1.88E-03	-1.43E+02	-5.73E-01	-1.36E+03
1.72E-03	8.64E-02	1.55E-01	2.07E-02	2.63E-02	1.60E-01	2.01E-03	-1.42E+02	-5.71E-01	-1.36E+03
1.72E-03	8.64E-02	1.54E-01	2.07E-02	2.63E-02	1.60E-01	1.88E-03	-1.42E+02	-5.72E-01	-1.36E+03
1.72E-03	8.64E-02	1.53E-01	2.07E-02	2.63E-02	1.60E-01	1.88E-03	-1.41E+02	-5.71E-01	-1.36E+03
1.72E-03	8.64E-02	1.54E-01	2.07E-02	2.63E-02	1.60E-01	1.90E-03	-1.41E+02	-5.70E-01	-1.36E+03
1.72E-03	8.64E-02	1.53E-01	2.07E-02	2.63E-02	1.60E-01	1.98E-03	-1.40E+02	-5.70E-01	-1.36E+03
1.58E-03	8.64E-02	1.55E-01	2.07E-02	2.63E-02	1.60E-01	1.98E-03	-1.38E+02	-5.74E-01	-1.36E+03
1.58E-03	8.64E-02	1.55E-01	2.07E-02	2.63E-02	1.60E-01	1.88E-03	-1.38E+02	-5.74E-01	-1.36E+03
1.58E-03	8.64E-02	1.55E-01	2.07E-02	2.65E-02	1.60E-01	1.90E-03	-1.38E+02	-5.74E-01	-1.36E+03
1.58E-03	8.64E-02	1.55E-01	2.07E-02	2.65E-02	1.60E-01	1.88E-03	-1.38E+02	-5.73E-01	-1.36E+03
1.62E-03	8.64E-02	1.53E-01	2.07E-02	2.65E-02	1.60E-01	1.90E-03	-1.37E+02	-5.72E-01	-1.36E+03
1.58E-03	8.64E-02	1.54E-01	2.07E-02	2.63E-02	1.60E-01	1.98E-03	-1.36E+02	-5.71E-01	-1.36E+03
1.58E-03	8.64E-02	1.53E-01	2.07E-02	2.63E-02	1.60E-01	1.98E-03	-1.36E+02	-5.72E-01	-1.36E+03
1.58E-03	8.64E-02	1.53E-01	2.07E-02	2.65E-02	1.60E-01	1.98E-03	-1.36E+02	-5.72E-01	-1.36E+03
1.72E-03	8.12E-02	1.56E-01	2.07E-02	2.63E-02	1.60E-01	2.83E-03	-1.33E+02	-5.66E-01	-1.36E+03
1.72E-03	8.12E-02	1.56E-01	2.07E-02	2.63E-02	1.60E-01	2.01E-03	-1.32E+02	-5.68E-01	-1.36E+03
1.41E-03	8.44E-02	1.58E-01	2.40E-02	2.61E-02	1.59E-01	2.23E-03	-1.31E+02	-5.77E-01	-1.36E+03
1.72E-03	8.12E-02	1.56E-01	2.07E-02	2.63E-02	1.60E-01	2.83E-03	-1.31E+02	-5.65E-01	-1.36E+03
1.72E-03	8.12E-02	1.56E-01	2.08E-02	2.63E-02	1.60E-01	2.81E-03	-1.31E+02	-5.65E-01	-1.36E+03
1.72E-03	8.12E-02	1.56E-01	2.07E-02	2.63E-02	1.60E-01	2.01E-03	-1.31E+02	-5.67E-01	-1.36E+03
1.72E-03	8.12E-02	1.56E-01	2.08E-02	2.65E-02	1.60E-01	1.98E-03	-1.31E+02	-5.67E-01	-1.36E+03
1.72E-03	8.12E-02	1.55E-01	2.08E-02	2.63E-02	1.60E-01	2.81E-03	-1.30E+02	-5.64E-01	-1.36E+03
1.72E-03	8.12E-02	1.55E-01	2.08E-02	2.65E-02	1.60E-01	1.98E-03	-1.30E+02	-5.66E-01	-1.36E+03
1.72E-03	8.12E-02	1.54E-01	2.08E-02	2.63E-02	1.60E-01	2.83E-03	-1.29E+02	-5.63E-01	-1.36E+03
1.72E-03	8.12E-02	1.54E-01	2.07E-02	2.63E-02	1.60E-01	2.01E-03	-1.29E+02	-5.65E-01	-1.36E+03
1.72E-03	8.12E-02	1.54E-01	2.08E-02	2.65E-02	1.60E-01	1.98E-03	-1.29E+02	-5.65E-01	-1.36E+03
1.72E-03	8.12E-02	1.53E-01	2.07E-02	2.65E-02	1.60E-01	1.88E-03	-1.28E+02	-5.65E-01	-1.36E+03
1.58E-03	8.12E-02	1.55E-01	2.07E-02	2.63E-02	1.60E-01	3.66E-03	-1.27E+02	-5.64E-01	-1.36E+03

Table 4 Continued

C	Mn	Ni	Mo	Al	Cr	Si	Tms	Val	ΔG
1.62E-03	8.12E-02	1.56E-01	2.07E-02	2.65E-02	1.60E-01	2.01E-03	-1.27E+02	-5.67E-01	-1.36E+03
1.39E-03	8.44E-02	1.53E-01	2.40E-02	2.09E-02	1.59E-01	3.88E-03	-1.27E+02	-5.71E-01	-1.35E+03
1.58E-03	8.12E-02	1.55E-01	2.07E-02	2.63E-02	1.60E-01	2.01E-03	-1.26E+02	-5.68E-01	-1.36E+03
1.58E-03	8.12E-02	1.56E-01	2.07E-02	2.63E-02	1.60E-01	2.01E-03	-1.26E+02	-5.68E-01	-1.36E+03
1.62E-03	8.12E-02	1.53E-01	2.07E-02	2.65E-02	1.60E-01	1.98E-03	-1.25E+02	-5.67E-01	-1.36E+03
1.58E-03	8.12E-02	1.55E-01	2.07E-02	2.65E-02	1.60E-01	2.01E-03	-1.25E+02	-5.67E-01	-1.36E+03
1.58E-03	8.12E-02	1.55E-01	2.07E-02	2.65E-02	1.60E-01	2.21E-03	-1.25E+02	-5.66E-01	-1.36E+03
1.62E-03	8.12E-02	1.54E-01	2.07E-02	2.65E-02	1.60E-01	1.98E-03	-1.25E+02	-5.66E-01	-1.36E+03
1.58E-03	8.12E-02	1.53E-01	2.07E-02	2.63E-02	1.60E-01	2.01E-03	-1.24E+02	-5.67E-01	-1.36E+03
1.58E-03	8.12E-02	1.54E-01	2.07E-02	2.63E-02	1.60E-01	2.01E-03	-1.24E+02	-5.66E-01	-1.36E+03
1.58E-03	8.12E-02	1.54E-01	2.07E-02	2.63E-02	1.60E-01	1.90E-03	-1.24E+02	-5.66E-01	-1.36E+03
1.58E-03	8.12E-02	1.53E-01	2.07E-02	2.65E-02	1.60E-01	2.01E-03	-1.23E+02	-5.65E-01	-1.36E+03
1.39E-03	8.31E-02	1.53E-01	2.46E-02	2.61E-02	1.58E-01	3.93E-03	-1.22E+02	-5.66E-01	-1.36E+03
2.81E-03	3.62E-02	1.59E-01	2.15E-02	2.24E-02	1.97E-01	1.99E-03	-1.22E+02	-5.99E-01	-1.35E+03
2.81E-03	3.62E-02	1.59E-01	2.16E-02	2.74E-02	1.97E-01	1.89E-03	-1.21E+02	-5.96E-01	-1.35E+03
2.81E-03	3.55E-02	1.59E-01	2.15E-02	2.49E-02	1.97E-01	2.92E-03	-1.20E+02	-5.94E-01	-1.35E+03
2.81E-03	3.55E-02	1.59E-01	2.15E-02	2.74E-02	1.97E-01	2.72E-03	-1.19E+02	-5.93E-01	-1.35E+03
1.62E-03	8.12E-02	1.56E-01	2.07E-02	2.65E-02	1.54E-01	2.01E-03	-1.19E+02	-5.56E-01	-1.36E+03
1.58E-03	8.12E-02	1.56E-01	2.07E-02	2.63E-02	1.54E-01	2.83E-03	-1.19E+02	-5.54E-01	-1.36E+03
2.81E-03	3.55E-02	1.59E-01	2.15E-02	2.99E-02	1.97E-01	2.10E-03	-1.19E+02	-5.93E-01	-1.36E+03
1.32E-03	8.54E-02	1.53E-01	2.05E-02	2.52E-02	1.56E-01	1.99E-03	-1.18E+02	-5.63E-01	-1.35E+03
2.80E-03	3.55E-02	1.59E-01	2.22E-02	2.12E-02	1.94E-01	5.38E-03	-1.18E+02	-5.85E-01	-1.35E+03
2.81E-03	3.55E-02	1.59E-01	2.15E-02	2.74E-02	1.97E-01	1.99E-03	-1.18E+02	-5.94E-01	-1.35E+03
2.81E-03	3.55E-02	1.58E-01	2.15E-02	2.74E-02	1.97E-01	1.89E-03	-1.18E+02	-5.95E-01	-1.35E+03
2.81E-03	3.55E-02	1.58E-01	2.15E-02	2.74E-02	1.97E-01	1.89E-03	-1.18E+02	-5.95E-01	-1.35E+03
2.78E-03	3.55E-02	1.59E-01	2.21E-02	2.12E-02	1.94E-01	5.30E-03	-1.18E+02	-5.86E-01	-1.35E+03
2.78E-03	3.55E-02	1.59E-01	2.15E-02	2.12E-02	1.94E-01	6.13E-03	-1.18E+02	-5.82E-01	-1.35E+03
2.78E-03	3.55E-02	1.59E-01	2.21E-02	2.12E-02	1.94E-01	5.30E-03	-1.17E+02	-5.85E-01	-1.35E+03
2.78E-03	3.55E-02	1.59E-01	2.15E-02	2.12E-02	1.94E-01	5.30E-03	-1.17E+02	-5.85E-01	-1.35E+03
2.78E-03	3.55E-02	1.59E-01	2.15E-02	2.12E-02	1.94E-01	5.30E-03	-1.17E+02	-5.85E-01	-1.35E+03
2.37E-03	3.99E-02	1.71E-01	2.13E-02	2.25E-02	1.87E-01	3.08E-03	-1.17E+02	-5.93E-01	-1.35E+03
2.78E-03	3.55E-02	1.59E-01	2.21E-02	2.98E-02	1.94E-01	6.23E-03	-1.16E+02	-5.78E-01	-1.36E+03
2.25E-03	4.54E-02	1.71E-01	2.13E-02	2.30E-02	1.78E-01	6.90E-03	-1.15E+02	-5.70E-01	-1.35E+03
3.15E-03	3.34E-02	1.62E-01	2.38E-02	3.38E-02	1.83E-01	5.65E-03	-1.12E+02	-5.55E-01	-1.36E+03
2.78E-03	3.55E-02	1.59E-01	2.20E-02	2.10E-02	1.88E-01	5.30E-03	-1.09E+02	-5.73E-01	-1.35E+03
2.78E-03	3.55E-02	1.59E-01	2.15E-02	3.10E-02	1.88E-01	5.31E-03	-1.07E+02	-5.66E-01	-1.36E+03
2.23E-03	3.99E-02	1.71E-01	2.13E-02	2.25E-02	1.81E-01	3.08E-03	-1.04E+02	-5.81E-01	-1.35E+03
2.46E-03	4.62E-02	1.56E-01	2.42E-02	2.53E-02	1.78E-01	3.54E-03	-1.04E+02	-5.66E-01	-1.35E+03
2.76E-03	2.51E-02	1.59E-01	2.20E-02	2.10E-02	1.98E-01	5.31E-03	-9.80E+01	-5.83E-01	-1.35E+03
2.04E-03	2.56E-02	1.73E-01	2.46E-02	2.01E-02	1.98E-01	6.35E-03	-9.53E+01	-6.03E-01	-1.35E+03
1.41E-03	4.28E-02	1.70E-01	2.40E-02	2.09E-02	1.84E-01	4.29E-03	-8.90E+01	-5.97E-01	-1.35E+03
2.76E-03	2.51E-02	1.59E-01	2.14E-02	2.12E-02	1.91E-01	5.31E-03	-8.88E+01	-5.69E-01	-1.35E+03
2.04E-03	2.69E-02	1.66E-01	2.40E-02	2.13E-02	1.98E-01	6.14E-03	-8.84E+01	-5.96E-01	-1.35E+03

Table 4 Continued

C	Mn	Ni	Mo	Al	Cr	Si	Tms	Val	ΔG
2.20E-03	3.97E-02	1.58E-01	2.13E-02	2.54E-02	1.81E-01	3.08E-03	-8.54E+01	-5.67E-01	-1.35E+03
2.76E-03	2.51E-02	1.59E-01	2.20E-02	2.12E-02	1.88E-01	6.13E-03	-8.53E+01	-5.62E-01	-1.35E+03
2.76E-03	2.51E-02	1.59E-01	2.14E-02	2.12E-02	1.88E-01	5.30E-03	-8.44E+01	-5.63E-01	-1.35E+03
1.97E-03	3.99E-02	1.66E-01	2.46E-02	3.03E-02	1.73E-01	6.14E-03	-8.04E+01	-5.55E-01	-1.36E+03
2.76E-03	1.99E-02	1.59E-01	2.14E-02	2.10E-02	1.88E-01	6.13E-03	-7.31E+01	-5.56E-01	-1.35E+03
1.25E-03	4.75E-02	1.68E-01	2.28E-02	2.31E-02	1.71E-01	2.05E-03	-7.09E+01	-5.76E-01	-1.35E+03
2.25E-03	2.46E-02	1.71E-01	2.13E-02	3.30E-02	1.81E-01	5.25E-03	-6.89E+01	-5.55E-01	-1.36E+03
1.18E-03	4.62E-02	1.64E-01	2.29E-02	2.06E-02	1.74E-01	2.05E-03	-6.65E+01	-5.81E-01	-1.35E+03
1.25E-03	4.62E-02	1.64E-01	2.26E-02	2.06E-02	1.71E-01	2.05E-03	-6.42E+01	-5.73E-01	-1.35E+03
1.25E-03	4.10E-02	1.68E-01	2.28E-02	2.31E-02	1.66E-01	3.76E-03	-5.03E+01	-5.56E-01	-1.35E+03